TOWARD SUSTAINABLE PRODUCTION OF LIQUID FUELS AND CHEMICALS: IMPROVING AND EXPANDING CHAIN ELONGATION OF WASTE CARBON INTO *N*-CAPROATE AND *N*-CAPRYLATE WITH REACTOR MICROBIOMES

A Thesis

Presented to the Faculty of the Graduate School

of Cornell University

In Partial Fulfillment of the Requirements for the Degree of

Master of Science

by

Leo Alexander Kucek

February 2016

ABSTRACT

Production of *n*-caproate and *n*-caprylate has been described previously in pure cultures of anaerobic bacteria (*e.g.*, *Megasphaera elsdenii*, *Clostridium kluyveri*) and in reactor microbiomes. In two studies, reactor microbiomes were continuously fed either lactate or ethanol, and the volumetric production rates (productivities) of *n*-caproate and *n*-caprylate were systematically improved. In one study, lactate to *n*-caproate conversion was demonstrated in a continuously fed bioreactor for the first time. The maximum *n*-caproate productivity achieved was 6.9 g COD/L-d. In a separate study, an *n*-caprylate productivity of 19.4 g COD/L-d was achieved, with a corresponding *n*-caprylate to *n*-caproate product ratio of 11 g COD/ g COD. Each of these values surpassed the maximum reported in the literature. Several operating parameters were varied, and in-line product recovery was achieved *via* pertraction (membrane-based liquid-liquid extraction). These studies promote the development of resource recovery processes to convert diverse waste carbon into sustainable liquid fuels and chemicals.

BIOGRAPHICAL SKETCH

Leo A. Kucek is a product of the Midwest: his Hoosier parents raised him in Waukesha, Wisconsin, and he grew up in a home that valued kindness, dedication, and resourcefulness. His family embraced deep conversation and creative problem solving; perhaps it is not surprising that a loquacious engineering thesis was in his future. His teachers and community members in Wisconsin encouraged Leo to challenge conventional thinking, to communicate freely and effectively, and to trust that anything can be accomplished with teamwork and collaboration.

When Leo left Wisconsin in 2004, his mission was clear: to prepare for a career in renewable energy. He graduated in 2009 with a Bachelor's of Chemical Engineering and a minor in Political Science from the University of Minnesota. Before graduating, Leo worked as a co-op engineer at Cargill Corn Milling in Eddyville, Iowa, and as a research intern at the Pacific Northwest National Laboratory (PNNL) in Sequim, Washington. At Minnesota, he led a student environmental organization (MPIRG) before leading a multi-disciplinary Engineers Without Borders (EWB) team focused on resource recovery and sanitation systems for a community in Haiti.

Before leaving Minnesota, Leo made an important connection: he met his wife, Lisa Kissing Kucek. They left the Midwest in 2009 to live in Prosser, Washington, and in 2011, they married. For four years, Leo conducted photosynthetic microbial research at PNNL, including an algal resource recovery project from food processing wastewater. PNNL provided Leo a foundation in bioreactor operation and experimental design, and gratitude is especially owed to: Eric Hill; Dr. Matthew Melnicki; Dr. Alex Beliaev; and Dr. Allan Konopka for their guidance. In 2013, Lisa and Leo left Washington State to attend Cornell University in Ithaca, New York.

Following the completion of their degrees, Lisa and Leo will finally return home to the loving arms of the Midwest. In October 2015, Leo joined Applied Technologies, Inc. (ATI) in Brookfield, Wisconsin. He is now a project engineer in their municipal and industrial services divisions, where he is currently focused on enhanced biological phosphorus removal (EBPR), anaerobic treatment systems, and other resource recovery projects. Throughout his career, Leo's goal has remained the same: to develop and implement systems that: 1) restrain environmental pollution; 2) serve and empower all stakeholders, especially marginalized communities; and 3) create renewable fuels and chemicals to meet society's needs. Leo believes that we have a responsibility to clean up after ourselves, to be fair and generous to our global neighbors and future generations, and to establish sustainable systems to deliver the products upon which we all depend. In order to fulfill these responsibilities, Leo left academic research and joined Applied Technologies, Inc. to put innovative resource recovery technologies to work.

DEDICATION

To my community, to my family, and to my love.

ACKNOWLEDGEMENTS

First, I would like to acknowledge the guidance and support from my advisor, Prof. Largus T. Angenent. His expertise in the field of anaerobic reactor microbiomes and resource recovery from wastes drew me to Cornell University, and he generously welcomed me into his laboratory. Research conducted by Lars and his students (especially Dr. Matthew T. Agler) provided the foundation upon which this thesis was built. Lars entrusted me to pick up the baton from their work, and to expand and improve chain elongation within the carboxylate platform. I am grateful for the guidance, resources, and academic independence that Lars provided for me to complete this task. With his upcoming transition to Germany, Lars' leadership will be sorely missed at Cornell University and within the research community of the United States.

Second, I could not have completed this work without another contribution from Lars: the Angenent Lab. Lars built a collaborative, dedicated, intelligent, trustworthy, and remarkably fun team at Cornell, and these individuals provided me so much joy and support throughout the past two years. While all members of the laboratory, past and present, deserve gratitude, I would like to thank the following individuals for their specific contributions to this thesis:

- Juan Guzman — bioreactor construction, RGD analysis
- Lauren Harroff — bioreactor sampling, GC analysis, thesis editing
- Andrew Jin — bioreactor sampling, batch bioreactor experiments
- Dylan Kahlstorf — bioreactor sampling, batch bioreactor experiments
- Mytien Nguyen — co-author, microbial community analysis, HPLC analysis
- Catherine Spirito — co-author, microbial community analysis
- Divya Vasudevan — bioreactor construction
- Dr. Jiajie Xu — bioreactor sampling, figure preparation

Third, I would like to express my appreciation to the many members of the Department of Biological and Environmental Engineering. Department staff including: Jeff Carmichael; Doug Caveney; Debbie Higgins; Brenda Marchewka; and Peggy Stevens deserve special recognition for their contributions that enabled me to complete this thesis. I am also grateful for many members of the Soil and Water Lab, including Erin Menzies, for their critiques, encouragement, and camaraderie. The entire department was always generous to me, and I am thankful for the warm embrace that I received from faculty, staff, and fellow graduate students.

Next, I would like to thank Prof. Jim Gossett (Cornell University). I sincerely appreciate the wonderful course that he taught (CEE 6570, Biological Processes); it provided me a foundation for evaluating diverse wastewater treatment operations, especially using tools from bioenergetics. I would also like to thank Prof. Gossett for serving on my committee, as well as for his careful review of my thesis. I was lucky to learn from Prof. Gossett before his retirement.

Finally, I would like to acknowledge the funding that supported my work. From the Graduate School at Cornell University, I received a departmental fellowship that provided me support in my first year. From the Graduate School, I also received funding to present my research at conferences (National Advanced Biofuels Conference and Expo, Minneapolis, MN, October 2014; and WEFTEC, Chicago, IL, September 2015). From the National Science Foundation (NSF), I was awarded a fellowship from the Graduate Research Fellowship Program (GRFP). Additional funding for this work was awarded to Prof. Lars Angenent, including support from: the NSF SusChEM Program (Award # 1336186); and the U.S. Army Research Laboratory and the U.S. Army Research Office (Contract/Grant number W911NF-12-1-0555).

TABLE OF CONTENTS

LIST OF FIGURES

Chapter 4

LIST OF TABLES

CHAPTER 1

INTRODUCTION, OBJECTIVES, AND ORGANIZATION

1.1 Introduction

To sustain healthy and productive global communities and ecosystems, new processes are required to effectively convert wastes into sustainable liquid fuels and chemicals. Carbon-rich wastes and wastewaters from industry, agriculture, and communities pose ecological risks if left untreated, but these wastes can also be treated by resource recovery processes. For example, many wastes can be converted to methane-rich biogas *via* anaerobic digestion. In another example, the syngas platform can effectively convert recalcitrant lignocellulosic residues from forestry and agriculture into carbon monoxide- and hydrogen-rich syngas. The value of these gaseous products (*i.e.*, biogas and syngas) has been suppressed due to low prices of nonrenewable alternatives, which in turn has limited the adoption of these technologies. Alternatively, waste carbon can be converted into higher-value liquid fuels and chemicals. In this thesis, I present results from anaerobic reactor microbiome experiments that converted waste carbon into medium-chain carboxylate products (*e.g.*, *n*-caproate and *n*-caprylate), from which liquid fuels and chemicals can be sustainably produced.

1.2 Objectives

I approached this research with several objectives. First, I sought to provide the first demonstration of conversion of lactate to *n*-caproate in a continuously fed bioreactor. The choice of lactate was based on its abundance as an intermediate in the breakdown of carbon-rich wastes. Second, in an ethanol-fed system, my focus was to improve the productivity of medium-chain

carboxylates, especially *n*-caprylate. Third, I hoped to better understand how substrate and product concentrations in the bioreactor, bioreactor pH, and in-line product recovery *via* pertraction (membrane-based liquid-liquid extraction) affected medium-chain carboxylate productivity. Finally, I wanted to characterize microbial community changes within the reactor microbiome, and to ultimately link these changes to bioreactor function.

1.3 Organization

In Chapter 2, a literature review of medium-chain carboxylate production is provided. Areas of focus include: 1) substrate diversity (*e.g.,* lactate utilization); 2) bioreactor productivity (*e.g.,* ethanol to *n*-caproate); and 3) reported undissociated carboxylic acid concentrations (*e.g., n*-caproic acid inhibitory concentrations).

In Chapter 3, I present the first demonstration of *n*-caproate production from lactate in a continuously fed bioreactor. *n*-Caproate production from exogenous lactate addition had been observed previously only in batch-fed bioreactors, especially with the type strain *Megasphaera elsdenii*. I achieved sustained *n*-caproate production from a reactor microbiome in which *M. elsdenii* was nearly absent.

In Chapter 4, I describe an ethanol-fed reactor microbiome that achieved a high-rate *n*-caprylate productivity more than four times greater than reported elsewhere. The product ratio of *n*-caprylate to *n*-caproate was greater than 25 during this high-productivity phase. Bioreactor concentrations, rates, and microbiome analyses indicate that overloading occurred at the end of this experiment, and it is likely that increasing the transfer rate *via* pertraction would have further improved bioreactor productivity.

In Chapter 5, research conclusions and suggestions for future work are proposed. Emphasis is placed on carefully determining the impacts of substrate and product concentrations on bioreactor productivity. In addition, our characterization of the reactor microbiomes suggests that unexpected microbial species (*i.e.*, neither the type strains *Megasphaera elsdenii* nor *Clostridium kluyveri*) are responsible for *n*-caproate and *n*-caprylate production. These communities should be closely examined to link relative abundance to metabolic activity and ultimately, bioreactor performance. Finally, to ensure commercial implementation, future selection of substrates, operating parameters, and product recovery strategies should be based on life-cycle and techno-economic analyses.

CHAPTER 2

LITERATURE REVIEW: *N*-CAPROATE AND *N*-CAPRYLATE PRODUCTION SUBSTRATE DIVERSITY, BIOREACTOR CONCENTRATIONS, AND PRODUCTIVITY

Abstract

A literature review of medium-chain carboxylate production was conducted. Areas of focus included: substrate diversity (*e.g.,* lactate utilization); bioreactor productivity (*e.g.,* ethanol to *n*-caproate); and reported undissociated carboxylic acid concentrations (*e.g., n*-caproic acid inhibitory concentrations). *n*-Caproate and *n*-caprylate have both been produced by reactor microbiomes that were fed diverse substrates, and improvements in bioreactor volumetric production rates (productivities) can be made based on understanding how the concentrations of substrates and products in the bioreactor broth affect competing metabolic pathways.

2.1 Introduction and scope

In this chapter, a literature review is presented on microbial production of medium-chain carboxylates (MCCs, ranging from six to twelve carbons). Focus is placed on the chain elongation of short-chain carboxylates (SCCs, ranging from two to five carbons) to *n*-caproate and *n*-caprylate. The types of reduced substrates (electron donors) capable of supporting this chain elongation are reviewed, and are grouped into sections on lactate, carbohydrates, and ethanol. Chemical oxygen demand (COD) is used as a common unit for comparing the energy available in varied substrates and products. Bioreactor productivities and loading rates are included when available, and bioreactor concentrations of undissociated medium-chain carboxylic acids are reported. Medium-chain carboxylate production *via* chain elongation has great potential: productive microbial systems can convert diverse waste carbon into sustainable precursors for energy-dense fuels and hydrophobic chemicals.

2.2 Lactate

2.2.1 n-*Caproate production from lactate*

Production of short-chain carboxylates (*e.g.*, acetate, propionate, *n*-butyrate, *n*-valerate) in bioreactors that were fed lactate has been established in the literature for more than a half century (Elsden and Lewis, 1953, Bhat and Barker, 1947, Diez-Gonzalez et al., 1995). Many of these and subsequent studies utilized pure cultures of bacteria that were isolated from the rumen, but most studies noted the absence of any *n*-caproate production (Prabhu et al., 2012, Hino et al., 1994, Gutierrez et al., 1959). Five studies were conducted in which bioreactors were fed exogenous lactate (as the sole carbon and energy source) and produced *n*-caproate (Elsden et al., 1956, Ladd, 1959, Marounek et al., 1989, Weimer and Moen, 2013, Zhu et al., 2015) (Table 2.1). The first four of these studies demonstrated DL-lactate to *n*-caproate conversion in pure culture batch systems of the type strain of *Megasphaera elsdenii*. The fifth study, which was recently completed by Zhu et al. (2015), was the first to report production of *n*-caproate from a reactor microbiome that was fed exogenous lactate (the isomer of the added lactate was not specified) as the sole carbon and energy source.

Table 2.1: Lactate-fed batch bioreactors resulting in *n*-caproate production. Conversion of exogenous lactate to *n*-caproate was only reported for the five studies listed. For batch studies with the type strain *Megasphaera elsdenii*, bioreactor pH values were all near neutral, leading to micromolar concentrations of undissociated *n*-butyric acid and *n*-caproic acid. The maximum *n*-caproate productivity reported was based on a batch duration of less than an hour (Ladd, 1959), and the highest *n*-caproate concentration, yield, and selectivity (0.5 g COD/L, 27%, and 17%, respectively) were achieved at the lowest initial lactate concentration and loading rate investigated (1.9 g COD/L and 2.3 g COD/L-d, respectively) (Marounek et al., 1989). Increased undissociated concentrations of *n*-caproic acid and sustained productivities of *n*-caproate were reported from the recent microbiome study (Zhu et al., 2015). The fed-batch scheme (several batch additions of substrate, with several days between feeding) yielded the highest concentration of *n*-caproate and *n*-caproic acid, as well as the highest *sustained* productivity of *n*-caproate (*i.e.*, longer than one hour duration). Based on data from: (Elsden et al., 1956, Ladd, 1959, Marounek et al., 1989, Weimer and Moen, 2013, Zhu et al., 2015).

Microbial culture	**Initial substrate**	**Final carboxylate product bioreactor concentrations**					
Strain ID	[DL-Lactate]	[Acetate]	[Propionate]	[*n*-Butyrate]	[*n*-Valerate]	[*n*-Caproate]	**Reference**
	g COD/L (mM)	*g COD/L (mM)*					
M. elsdenii LC-S	12.4 (129)	1.3 (20)	2.7 (24)	3.3 (20)	5.4 (26)	0.4 (1.5)	Elsden *et al.* (1956)
M. elsdenii LC1	2.7 (28)	0.1 (1)	0.1 (1)	0.6 (4)	1.4 (7)	0.3 (1.0)	Ladd (1959)
M. elsdenii J1	1.9 (20)	0.4 (6)	0.7 (6)	1.4 (9)	*N.D.*	0.5 (2.0)	Marounek *et al.* (1989)
M. elsdenii T81	9.4 (98)	1.8 (28)	3.3 (30)	1.6 (10)	1.7 (8)	0.0 (0.1)	Weimer and Moen (2013)
Microbiome	32.1 (333)	1.0 (15)	*N.D.*	2.4 (15)	*N.D.*	27.7 (108)	Zhu *et al.* (2015)
Microbiome	28.5 (296)	0.6 (9)	*N.D.*	1.8 (11)	1.8 (9)	24.3 (95)	Zhu *et al.* (2015)
Microbiome	71.3 (740)	0.6 (9)	*N.D.*	4.9 (31)	1.8 (9)	51.7 (202)	Zhu *et al.* (2015)

Undissociated carboxylic acid concentrations		**Bioreactor conditions**		**Bioreactor productivity**			
[*n*-Butyric Acid]	[*n*-Caproic Acid]	pH	Temperature	Type	Duration	*n*-Caproate	**Reference**
g COD/L (mM)			*°C*		*h*	*g COD/L-d (mM/d)*	
0.01 (0.1)	0.00 (0.01)	7.4	38	Batch	72	0.1 (0.5)	Elsden *et al.* (1956)
0.01 (0.1)	0.01 (0.02)	6.5	37	Batch	0.75	8.5 (33)	Ladd (1959)
0.02 (0.1)	0.01 (0.03)	6.7	39	Batch	20	0.6 (2.4)	Marounek *et al.* (1989)
0.03 (0.2)	0.00 (0.00)	6.5	39	Batch	48	0.0 (0.1)	Weimer and Moen (2013)
0.05-0.15 (0.3-0.9)	0.65-1.95 (2.5-7.6)	6.0-6.5	30	Batch	120	5.5 (22)	Zhu *et al.* (2015)
0.04-0.11 (0.2-0.7)	0.57-1.71 (2.2-6.7)	6.0-6.5	30	Fed-Batch	89	6.5 (26)	Zhu *et al.* (2015)
0.10-0.30 (0.6-1.9)	1.21-3.64 (4.7-14.2)	6.0-6.5	30	Fed-Batch	384	3.2 (13)	Zhu *et al.* (2015)

The microbiome inoculum that was utilized by Zhu and his colleagues was collected from the mud lining of a fermentation pit that was used to convert carbohydrate-rich feedstocks (*e.g.*, wheat, sorghum, and maize) into the fermented precursor ("yellow water") of Chinese strong-flavored liquor (CSFL) (Zhu et al., 2015). Yellow water is a complex carbon-rich mixture composed primarily of ethanol, lactate, and glucose. *n*-Butyrate, *n*-caproate, and ethyl caproate are also abundant and desired products in this fermentation because these constituents give CSFL its distinct flavor (Tao et al., 2014). In a preliminary experiment, yellow water was batch-fed (one feeding per day) to a semi-continuously operated reactor (SCOR), and the resulting concentration of *n*-caproate reached up to 53.0 g COD/L (207 mM) (Zhu et al., 2015). A carbon and energy balance on this fermentation was insufficient to prove that lactate was converted to *n*-caproate in this yellow water-fed SCOR. Therefore, a batch test in which lactate was fed as the sole carbon and energy source was conducted, and this resulted in 27.7 g COD/L (108 mM) *n*-caproate produced from 32.1 g COD/L (333 mM) lactate fed. This batch accumulation of *n*-caproate from lactate lasted five days, corresponding to an *n*-caproate productivity of 5.5 g COD/L-d (Figure 2.1).

A follow-up experiment was then conducted in a batch bioreactor in which lactate was fed, completely consumed, and then batch-fed again intermittently (several days between feeding) upon exhaustion of residual lactate (Zhu et al., 2015). In this fed-batch study, the first phase was marked by a rapid accumulation of *n*-caproate from two additions of lactate over a period of almost four days. The resulting average *n*-caproate productivity from this first phase was 6.5 g COD/L-d, but only 24.3 g COD/L (95 mM) *n*-caproate was accumulated. By the end of the second phase, the cumulative rate of *n*-caproate accumulation had decreased to 3.2 g COD/L-d, but the maximum *n*-caproate concentration accumulated to 51.7 g COD/L (202 mM).

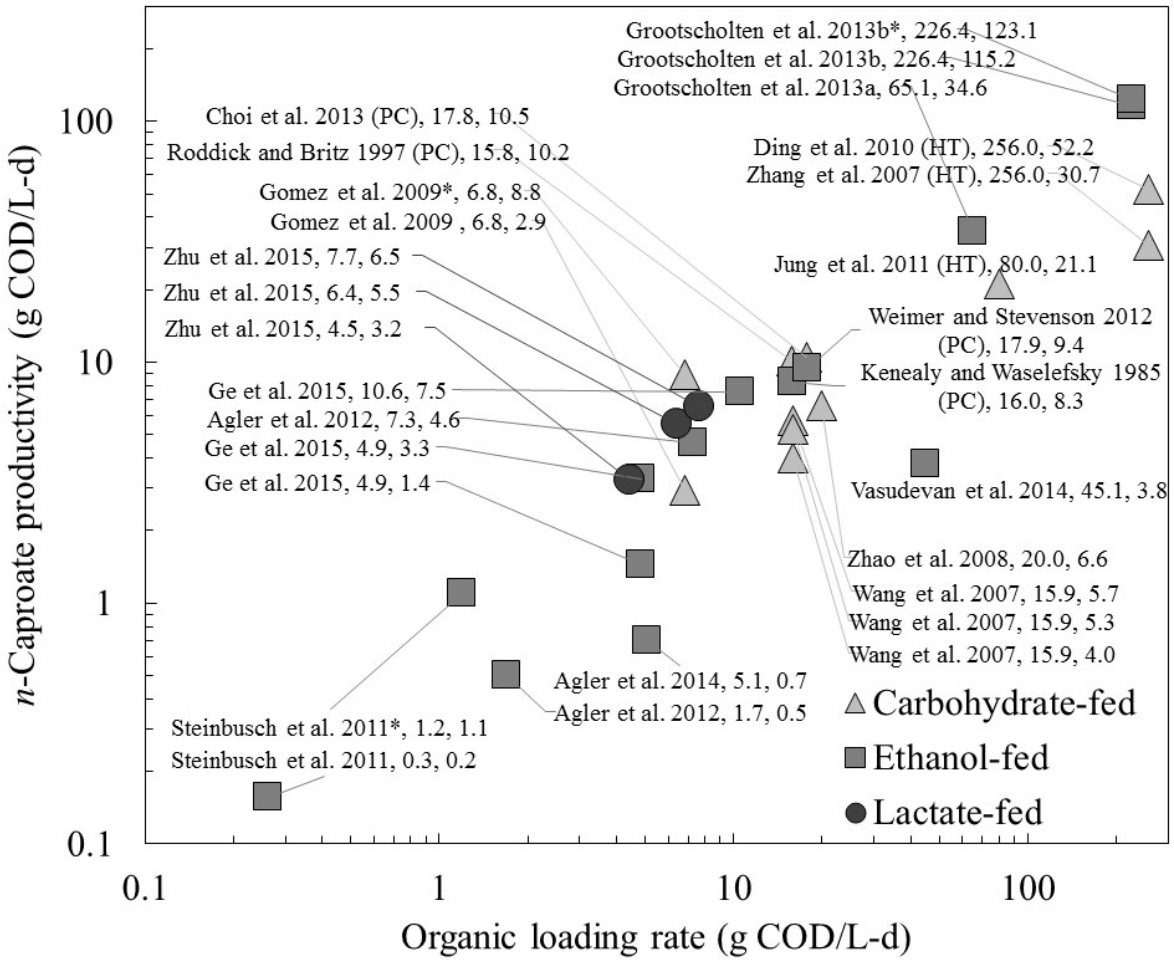

Figure 2.1: *n*-Caproate productivities. Results from 14 studies with high medium-chain carboxylate production performance (*e.g.*, concentrations, productivity) are reported. Indications include: 1) methanogen-suppression *via* heat treatment (HT); 2) use of pure cultures (PC) (*M. elsdenii and C. kluyveri*); and 3) maximum instantaneous values reported (*). The referenced study, the organic loading rate, and the *n*-caproate productivity are listed for each data point. Both *n*-caproate productivity and organic loading rates are presented on logarithmic scales.

Unfortunately, detailed pH data was not provided in this study by Zhu and his colleagues, except for defining the ranges of pH values for each experiment. In the SCOR experiment in which complex carbon-rich yellow water was fed, the pH was maintained between 5.5 and 6.5. The uncertainty in the pH used leads to uncertainty about the hydrophobic *n*-caproic acid concentrations achieved, ranging from 1.2 to 10.3 g COD/L (5 to 40 mM) undissociated *n*-caproic acid. In the batch and two-phase fed-batch study, the pH was defined to be between 6.0 and 6.5. To compare these results to other concentrations of undissociated *n*-caproic acid (Figure 2.2), the average value of this range (pH 6.25) was assumed, and the ranges of undissociated *n*-caproic acid concentrations were calculated. The maximum concentrations of undissociated *n*-caproic acid accumulated were between 0.6 and 2.0 g COD/L (3 and 8 mM) in the batch study and ranged from 1.2 to 3.6 g COD/L (5 to 14 mM) in the fed-batch study.

2.2.2 Production of n-*caproate, but not necessarily due to conversion from lactate*

In some studies, *n*-caproate accumulation was reported, but the authors were unable to prove that the observed consumption of initial or intermediate lactate was responsible for *n*-caproate production. For example, in the yellow water-fed SCOR, lactate was consumed at a rate of 3.6 g COD/L-d and *n*-caproate was produced at a rate of 1.6 g COD/L-d (Zhu et al., 2015). The simultaneous consumption rates of ethanol (1.5 g COD/L-d) and glucose (0.6 g COD/L-d), however, indicated that the carbon and energy balance alone could not preclude the possibility that ethanol and glucose were the precursors for *n*-caproate. In a study of *Eubacterium pyruvativorans*, the amount of DL-lactate consumed was insufficient to provide the energy or carbon present in the observed *n*-caproate accumulated (Wallace et al., 2003), and peptide-rich pancreatic casein hydrolysate (PCH), rather than DL-lactate, was later proven to be the primary carbon and energy source for *n*-caproate production in *E. pyruvativorans* (Wallace et al., 2004).

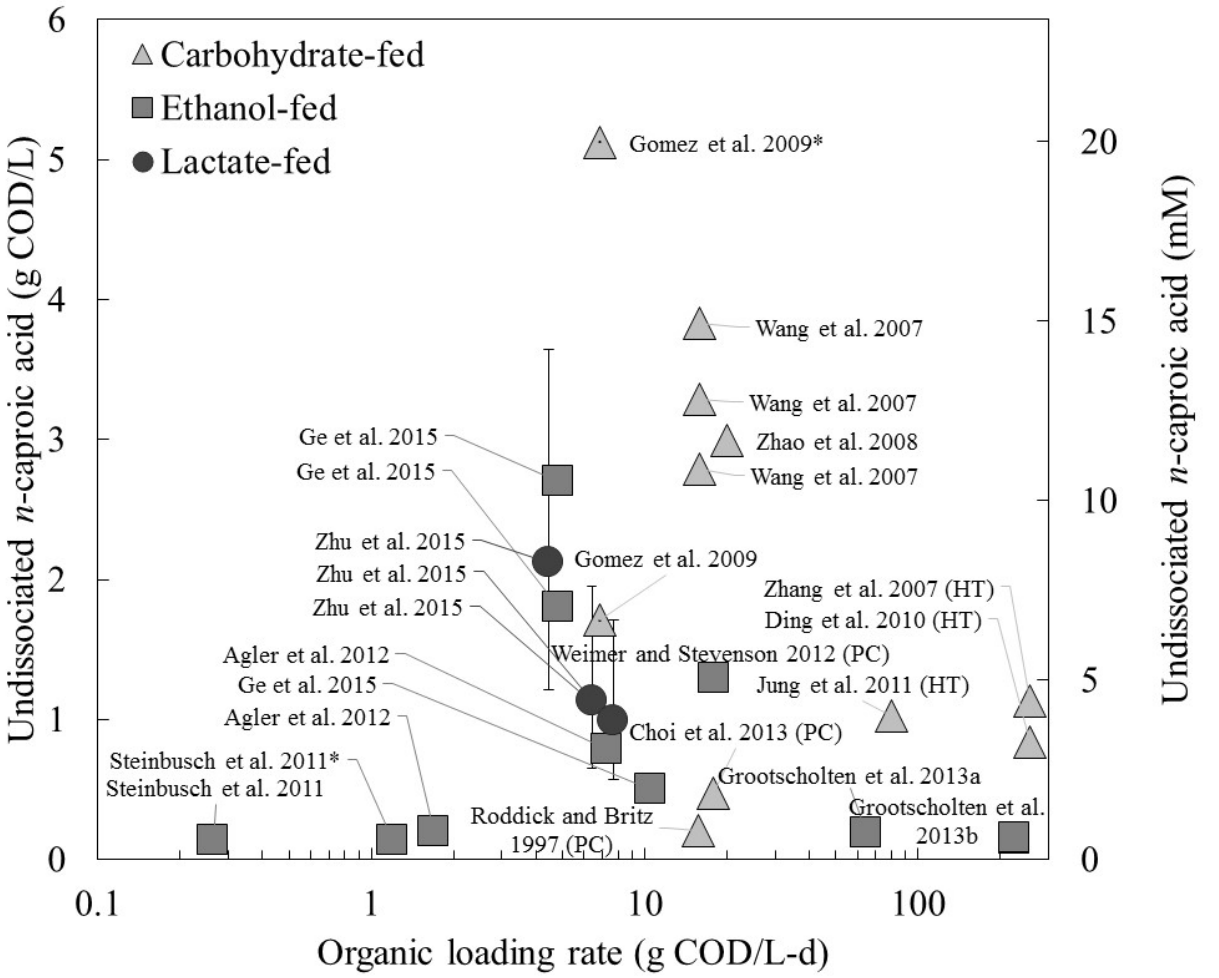

Figure 2.2: Bioreactor concentrations of undissociated *n*-caproic acid. Results from 13 studies with high medium-chain carboxylate production performance (*e.g.*, concentrations, productivity) are reported. Uncertainty for the values from Zhu et al., 2015 is based on the wide range of bioreactor pH values reported (pH 6.0-6.5). Indications include: 1) methanogen-suppression *via* heat treatment (HT); 2) use of pure cultures (PC) (*M. elsdenii* or *C. kluyveri*); and 3) maximum instantaneous values reported (*). Organic loading rates are presented on a logarithmic scale. Undissociated *n*-caproic acid concentration data was not available for Agler et al., 2014.

In a final instance, observations suggested that intermediate lactate consumption was correlated with *n*-caproate accumulation in a reactor microbiome (Agler et al., 2012b). Specifically, in a bioreactor that was fed complex carbohydrates (*i.e.*, maize fiber hydrolysate), lactate accumulated to approximately 0.2 g COD/L (1.6 mM) before it was completely consumed (Agler et al., 2012b). No exogenous lactate was fed to this bioreactor, but *n*-caproate began to accumulate in the bioreactor broth immediately after intermediate lactate was observed. Furthermore, *n*-caproate production ceased immediately after the residual lactate concentration was exhausted. Similar observations were made by Sträuber et al. (Sträuber et al., 2012, Sträuber et al., 2015). All of these experiments in which lactate was consumed when *n*-caproate was produced suggested that lactate could be converted to *n*-caproate, but they were unable to provide unambiguous proof.

2.2.3 Lactate conversion pathways

One of the main differences between lactate-fed systems and ethanol-fed systems is the prevalence of competing pathways for production of odd-numbered short-chain carboxylates (SCCs, *e.g.*, propionate, *n*-valerate) (Weimer and Moen, 2013). In ethanol-fed systems, even-numbered products (*e.g.*, acetate, *n*-butyrate) are the predominant SCC products produced *via* the reverse β-oxidation pathway (Spirito et al., 2014). Lactate-fed systems, however, often produce propionate (and sometimes *n*-valerate) in addition to (or at the expense of) acetate and *n*-butyrate (Marounek et al., 1989). While several authors have examined this phenomenon of propionate production from lactate, a study by Hino and Kuroda (Hino and Kuroda, 1993) was among the first to provide a pathway that explained how two competing pathways in the type strain *M. elsdenii* could convert L-lactate to either *n*-butyrate (and *n*-caproate) or to propionate (Figure 2.3).

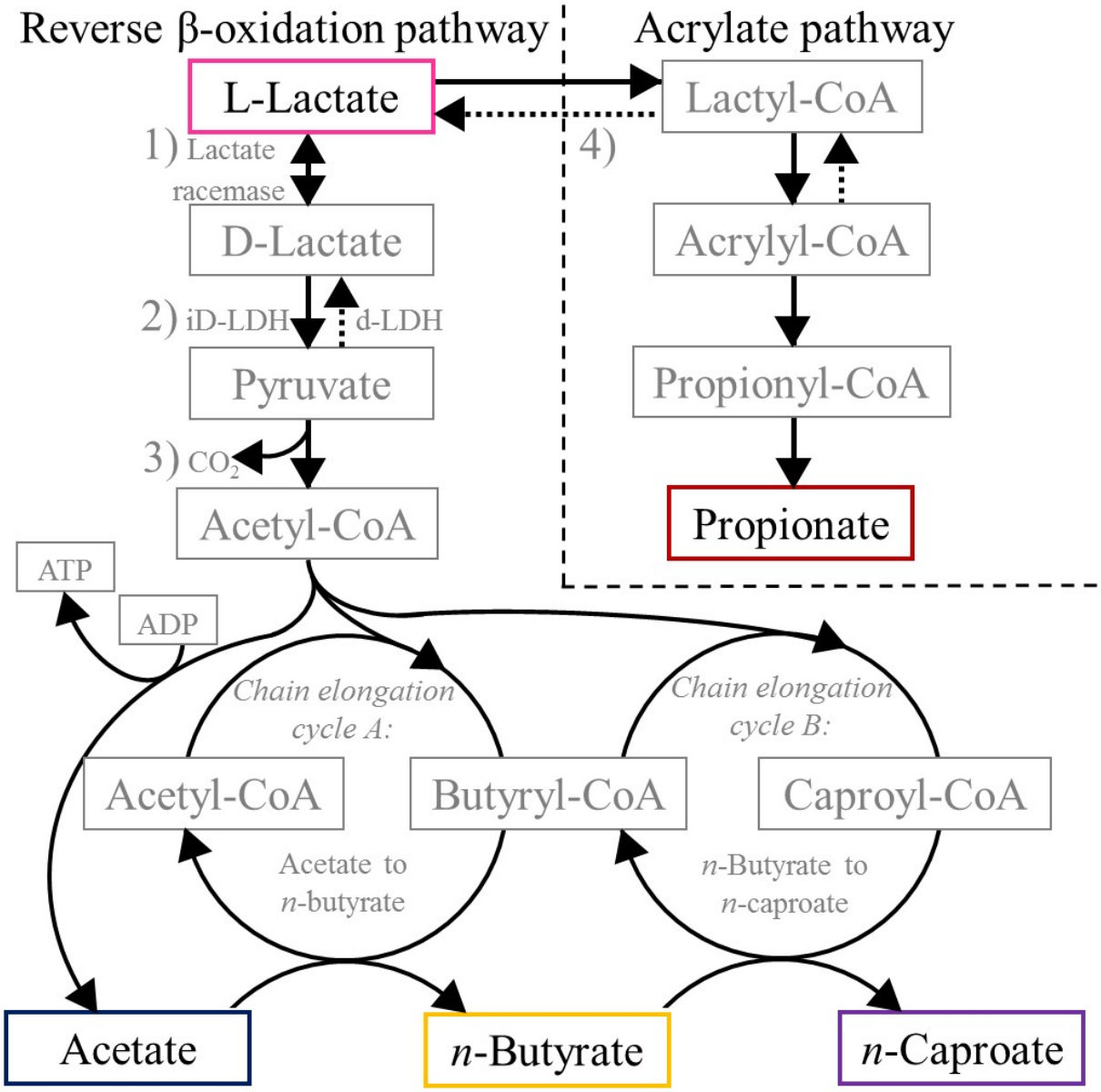

Figure 2.3: Lactate conversion pathways. DL-Lactate can proceed to either *n*-caproate or propionate *via* the reverse β-oxidation pathway or the acrylate pathway, respectively. Based on (Spirito et al., 2014) and (Hino and Kuroda, 1993).

L-lactate can be converted to *n*-caproate *via* the reverse β-oxidation pathway through three steps. First, lactate racemase (LR) is an enzyme that catalyzes isomerization between D-lactate and L-lactate (Figure 2.3, Step 1). LR is induced by the presence of either D- or L-lactate, but not by the presence of, for example, glucose (Hino and Kuroda, 1993). The LR reaction appears to be readily reversible (Hino and Kuroda, 1993), but has also been described as potentially rate-limiting in the conversion of L-lactate to D-lactate (Hino and Kuroda, 1993). In glucose-fed batch bioreactors, or in cultures that were continuously fed exogenous DL-lactate (Prabhu et al., 2012), it was suggested that the low concentrations of residual lactate present in the bioreactor broth would fail to induce LR (Hino and Kuroda, 1993). Several experiments have been conducted in bioreactors that were fed either DL-lactate or substrates which yield D-lactate (*e.g.*, glucose), and their results support this explanation. If L-lactate were fed continuously to a bioreactor, however, it is unclear if low residual lactate concentrations would fail to induce LR, and if these low residual concentrations of lactate would affect the isomerization of L-lactate to D-lactate before its conversion to pyruvate.

In a second step from L-lactate to *n*-caproate, lactate dehydrogenases catalyze conversion between D-lactate and pyruvate (Figure 2.3, Step 2). Pyruvate is a central metabolic intermediate in the chain elongation of D-lactate to *n*-butyrate *via* reverse β-oxidation (Spirito et al., 2014). Only the D-lactate isomer can be converted directly to pyruvate; L-lactate would first need to be isomerized *via* lactate racemase (LR). To convert between D-lactate and pyruvate, two types of lactate dehydrogenases are present in *M. elsdenii* (Hino and Kuroda, 1993). First, the NAD-independent D-lactate dehydrogenase (iD-LDH) can convert D-lactate to pyruvate in a predominantly favorable and irreversible reaction (Hino and Kuroda, 1993). Alternatively, a NAD-dependent lactate dehydrogenase (d-LDH) is capable of the reverse reaction (Hino and

Kuroda, 1993). When the proportion of pyruvate to D-lactate increases, the equilibrium behavior promotes further conversion of pyruvate to D-lactate and activity of the d-LDH (Hino and Kuroda, 1993). This 'pyruvate bottleneck' or 'D-lactate deficit' would result in decreased carbon flux towards reverse β-oxidation products and increased flux towards propionate.

In a final step from L-lactate to *n*-caproate, acetyl-CoA can be generated from pyruvate (Figure 2.3, Step 3). The two carbon atoms derived from the generated acetyl-CoA molecule can then chain elongate SCCs to MCCs (*e.g.*, *n*-caproate) *via* reverse β-oxidation. When acetate is the dominant SCC, the prevailing chain elongation progression is towards even-numbered carboxylates such as *n*-butyrate and *n*-caproate (Spirito et al., 2014). When propionate is present, however, it can be chain elongated *via* the reverse β-oxidation pathway to *n*-valerate and *n*-enanthate (Grootscholten et al., 2013c).

In the competing acrylate pathway, L-lactate can be converted to propionate (Figure 2.3, Step 4). Under L-lactate-rich conditions, lactyl-CoA forms as an intermediate. When this occurs, a subsequent state to achieve redox balance perpetually generates propionyl-CoA (Prabhu et al., 2012). Consequently, available L-lactate would be continually directed toward propionate production (Prabhu et al., 2012). This explanation suggests that once residual L-lactate concentrations accumulate and induce lactyl-CoA formation, it may be difficult to direct lactate-carbon flux toward pyruvate and even-numbered chain elongation products (*e.g.*, *n*-caproate). Finally, the addition of exogenous acrylate is also known to increase the carbon flux towards propionate and has been thoroughly studied (Ladd and Walker, 1959, Elsden et al., 1956, Prabhu et al., 2012, Hetzel et al., 2003, Diez-Gonzalez et al., 1995, Hino and Kuroda, 1993); a more detailed review of this topic is outside the scope of this study.

Surprisingly, in the first reactor microbiome study in which exogenous lactate was converted into *n*-caproate, no propionate production was reported (Zhu et al., 2015). Their batch-fed systems were operated with lactate constantly in excess, which I expected would induce the acrylate pathway. It is possible that microbes with the competing acrylate pathway had disappeared or were outcompeted based on the unique environmental selection process employed (Tao et al., 2014). However, propionate production from lactate is ubiquitous among anaerobic bacteria (Thauer et al., 1977). Therefore, the lack of propionate production in the study by Zhu et al. (2015) appears to be atypical for most anaerobic reactor microbiomes

2.2.4 Bioreactor pH and concentrations of undissociated carboxylic acids

Investigations focused specifically on how bioreactor pH affects the conversion of lactate to *n*-caproate have not been conducted. Nevertheless, observations from bioreactor studies that fed lactate and operated at varied pH values remain instructive. Most studies in which lactate was fed were conducted at pH values near or slightly below neutral (Table 2.1). In a bioreactor of *M. elsdenii* that was operated at pH 6.7 and continuously-fed DL-lactate, *n*-butyrate production was dominant, and neither propionate nor *n*-caproate were produced (Prabhu et al., 2012). In another study focused on several rumen bacteria capable of utilizing lactate, it was observed that maximum growth rates occurred between pH 6.0 to 6.5 for most bacteria evaluated (Counotte and Prins, 1981). Of the bacteria evaluated, *M. elsdenii* was distinguished by its unique capability to grow and utilize DL-lactate below a pH of 5.5, and it could grow in bioreactor conditions as low as approximately pH 4.7. Unfortunately, *n*-caproate accumulation was not measured in this study (Counotte and Prins, 1981). In one study, however, L-lactate was fed under low pH conditions, and *n*-caproate production was assessed. In batch bioreactors, L-lactate was added at 1.5 and 3.0 g COD/L (15 and 30 mM) to a reactor microbiome operated at pH 5.5

(Agler et al., 2012b). Production of *n*-caproate was investigated but not observed. Although the results from the literature were inconclusive, they provided a foundation for an area of research: if L-lactate were fed continuously to a bioreactor operated at a suppressed pH, it is unclear whether the predominant carbon flux could be directed towards reverse β-oxidation products (*e.g.*, *n*-butyrate, *n*-caproate) as opposed to towards propionate *via* the acrylate pathway.

2.3 Carbohydrates

2.3.1 Several intermediates exist in the conversion of carbohydrates to n-*caproate*

While lactate is present in many wastewaters, the majority of COD in most wastewaters is derived from proteins, carbohydrates, and fats. Of these constituents, carbohydrates (including sugars, starches, and cellulose) comprise from approximately 18% of the COD in municipal wastewaters (Raunkjær et al., 1994) up to approximately 70% of the COD in some food processing wastewaters (Arslan et al., 2013, Gómez et al., 2009). To design effective microbial systems capable of converting COD from these carbohydrate-rich streams into products such as *n*-caproate, the conversion pathways and intermediate processes employed must be understood.

Lactate is one common intermediate in the anaerobic breakdown of carbohydrates (Kleerebezem and van Loosdrecht, 2007), and it has been observed in bioreactors that produced *n*-caproate when carbohydrates were fed (Agler et al., 2012b, Sträuber et al., 2012, Sträuber et al., 2015). Pyruvate and ethanol are also key intermediates (Agler et al., 2011, Spirito et al., 2014) through which carbohydrates can be converted to *n*-butyrate and *n*-caproate within pure cultures (Weimer and Moen, 2013) and reactor microbiomes (Temudo et al., 2008). Although residual concentrations of these intermediates in the bioreactor broth are sometimes below detection limits, large carbon fluxes can pass from carbohydrate substrates through these three

intermediates to generate acetyl-CoA, and ultimately, desired products such as *n*-caproate (Agler et al., 2011).

2.3.2 Undissociated n*-caproic acid concentrations were highest in carbohydrate-fed systems*

Accumulation of undissociated medium-chain carboxylic acids in the bioreactor broth can cause product inhibition (Grootscholten et al., 2013a). Understanding the levels at which product inhibition and toxicity occur are important areas for continued research. Carbohydrate-fed anaerobic reactor microbiomes (without heat treatments) have accumulated undissociated *n*-caproic acid (but not *n*-caprylic acid) at the highest concentrations reported in the literature (Figure 2.2) (Wang et al., 2007, Zhao et al., 2008, Gómez et al., 2009)

In two studies led by Wang and Zhao, the pH of an anaerobic reactor microbiome was maintained below 4, the hydraulic retention times (HRTs) ranged from 12 to 17 h, and the organic loading rates (OLRs) were between 15.9 and 20.0 g COD/L-d (Wang et al., 2007, Zhao et al., 2008). These two studies achieved maximum concentrations of undissociated *n*-caproic acid ranging from 2.8 to 3.8 g COD/L (11 to 15 mM) and *n*-caproate productivities from 4.0 to 6.6 g COD/L-d (Figure 2.1). In a subsequent study, Gomez and his colleagues operated an anaerobic reactor microbiome at pH 5.5 with an HRT of 3 d and an average OLR of 6.8 g COD/L-d (Gómez et al., 2009). They achieved steady and instantaneous concentrations of undissociated *n*-caproic acid of 1.7 and 5.1 g COD/L (7 and 20 mM), respectively, along with *n*-caproate productivities of 2.9 and 8.8 g COD/L-d, respectively. Ranging from 1.7 to 5.1 g COD/L (7 to 20 mM) undissociated *n*-caproic acid, these four maximum concentrations correspond to approximately 7-22% of the solubility limit of undissociated *n*-caproic acid (23.8 g COD/L, 93 mM) (Xu et al., 2015).

Another unique reactor microbiome study deserves mention. In this study, the concentration of undissociated *n*-caproic acid was determined to reach up to 12.2 g COD/L (48 mM) (Tao et al., 2014). This unusually high value was calculated based on a total (undissociated plus dissociated) *n*-caproate concentration of 12.8 g COD/L (50 mM) at a reported pH of 3.6. In this solid-state fermentation system, it is possible that a pH gradient may have existed in the heterogenous media, leading to the possibility of lower *n*-caproic acid levels. If the pH and *n*-caproate concentrations were uniform throughout the slurry, however, these values would correspond to an undissociated *n*-caproic acid concentration of 51% of the solubility limit (Tao et al., 2014). To achieve these levels, carbohydrate-rich feedstocks (*e.g.*, wheat, sorghum, and maize) were fermented for one year in pit mud to produce the precursor for Chinese strong-flavored liquour (CSFL). Consequently, as this study was not conducted as a conventional anaerobic reactor experiment, parameters such as organic loading rates were not available. Regardless, this data suggests that microbial systems are capable of accumulating extremely high concentrations of undissociated *n*-caproic acids, especially when fed carbohydrates.

As a comparison, for ethanol-fed systems, the highest level of undissociated *n*-caproic acid achieved was only 2.7 g COD/L (10.5 mM) (Figure 2.2) (Ge et al., 2015). Furthermore, Ge and his colleagues suggested that concentrations of undissociated *n*-caproic acid were inhibitory near 1.9 g COD/L (7.5 mM) (Ge et al., 2015). This proposed inhibition level (1.9 g COD/L, 7.5 mM) is lower than the undissociated *n*-caproic acid concentrations achieved (from 1.7 to 5.1 g COD/L, 7 to 20 mM) in several studies in which carbohydrates were fed (Figure 2.2). Therefore, while the rate of *n*-caproate production may have been inhibited at an undissociated *n*-caproic acid concentration of 1.9 g COD/L (7.5 mM), it is likely that the level of toxicity for undissociated *n*-caproic acid is higher.

2.3.3 n-*Caproate productivities achieved from carbohydrate-fed bioreactors were moderate*

In addition to accumulating exceptionally high concentrations of undissociated *n*-caproic acid, some carbohydrate-fed bioreactors have also demonstrated considerable *n*-caproate productivities (Figure 2.1). Many of these carbohydrate-fed bioreactors were actually designed to produce hydrogen, and all of the following highly productive bioreactors used heat treatments to suppress hydrogenotrophic methanogens within their microbial communities. For example, two separate studies fed glucose at an OLR of 256.0 g COD/L-d. The first reported an *n*-caproate productivity up to 30.7 g COD/L-d in a bioreactor operated at pH 4.0 (Zhang et al., 2007), and the second bioreactor produced *n*-caproate at a rate of 52.2 g COD/L-d when operated at pH 5.5 (Ding et al., 2010). These two bioreactors were operated at very short HRTs of 1 and 2 h, respectively. Finally, a subsequent investigator fed a carbohydrate-rich waste at an OLR of 80.0 g COD/L-d and HRT of 6 h, and reported an *n*-caproate productivity of 21.1 g COD/L-d at pH 5.5 (Jung et al., 2011). The corresponding *n*-caproate yields were low (12%, 20%, and 26%, respectively). Low yields are not surprising because these systems were designed to produce hydrogen; optimal loading rates for *n*-caproate production are unlikely to be the same.

Finally, carbohydrate-fed pure cultures of *M. elsdenii* designed for *n*-caproate recovery have resulted in competitive production and yields. In a glucose-fed system, an *n*-caproate productivity and yield up to 10.2 g COD/L-d and 65% were observed at an OLR of 15.8 g COD/L-d (Roddick and Britz, 1997). Similarly, in a sucrose-fed system loaded at 17.8 g COD/L-d, an *n*-caproate productivity and yield up to 10.5 g COD/L-d and 59% were reported (Choi et al., 2013). Although competitive *n*-caproate productivities and yields are clearly possible from carbohydrates, carbohydrate-fed systems (without exogenous ethanol) have not yet shown *n*-caprylate generation.

2.4 Ethanol

2.4.1 Maximum n-*caproate and* n-*caprylate productivities were achieved from ethanol*

n-Caproate has been produced at productivities up to 123.1 g COD/L-d (Figure 2.1) (Grootscholten et al., 2013d), and limited *n*-caprylate productivity has been reported (Figure 2.4). When *n*-caprylate production within reactor microbiomes was first reported, the maximum *n*-caprylate productivities observed were lower than 0.14 g COD/L-d (Steinbusch et al., 2011). Subsequent authors (Agler et al., 2012a, Agler et al., 2014, Ge et al., 2015) reported some improvements in *n*-caprylate productivity, but substantial improvements were reported by Grootscholten and his colleagues (Grootscholten et al., 2013b, Grootscholten et al., 2013d). In a continuously fed upflow anaerobic filter operated at short hydraulic retention times and at neutral pH, they observed *n*-caprylate productivities up to 4.4 g COD/L-d (Grootscholten et al., 2013d).

2.4.2 Product inhibition can limit bioreactor productivities of n-*caprylate and* n-*caproate*

Product inhibition is a central challenge for MCC production *via* fermentation systems because undissociated medium-chain carboxylic acids (MCCAs) can inhibit microbial activity (Desbois, 2012). Undissociated MCCAs (*e.g.*, *n*-caproic acid, *n*-caprylic acid) are hydrophobic, and hydrophobicity increases for MCCAs with longer carbon chains (Steinbusch et al., 2011). These MCCAs can therefore: penetrate the hydrophobic lipid membranes of microbial cells; dissociate into corresponding MCCs and protons; and exhaust cellular efforts of expelling excess protons to maintain a neutral pH in the cytoplasm (Skrivanova et al., 2006). In MCC-producing bioreactor systems, accumulated MCCAs can therefore stall bioreactor productivity through product inhibition.

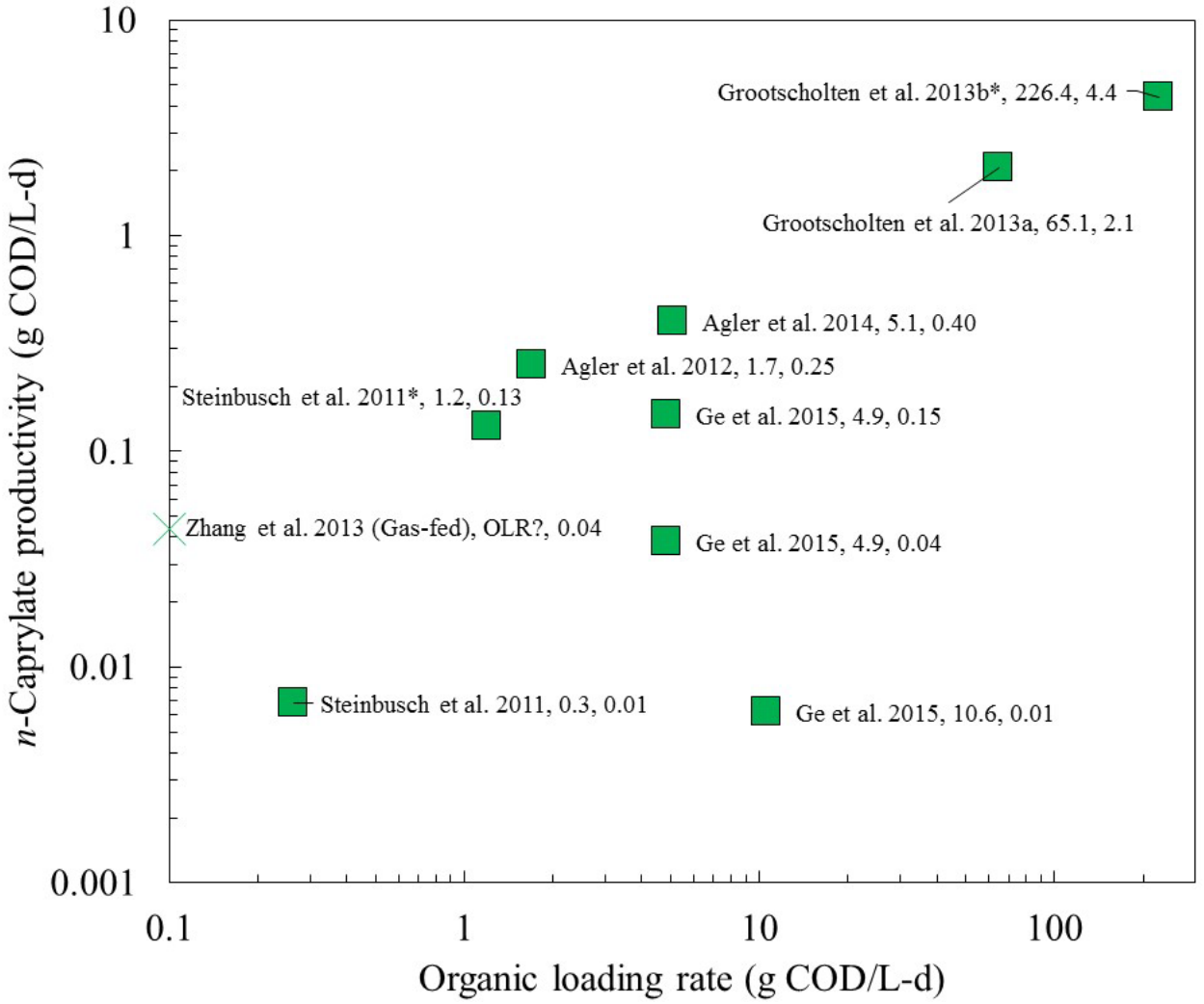

Figure 2.4: *n*-Caprylate productivities in ethanol-fed or gas-fed bioreactors. Results are from seven studies in which *n*-caprylate production was reported. Maximum instantaneous values reported are indicated (*). The referenced study, the organic loading rate, and the *n*-caprylate productivity are listed. Both *n*-caprylate productivities and organic loading rates are presented on logarithmic scales. One study (Zhang et al., 2013, X) produced *n*-caprylate in a bioreactor in which gas composed of carbon dioxide and hydrogen was fed; they did not present organic loading rates, so this marker was placed at an organic loading rate near the sum of the total carboxylate volumetric production rates.

Two approaches have emerged to overcome product inhibition and increase MCC bioreactor productivity: 1) a neutral pH system with inhibition of methanogens *via* chemical addition (Steinbusch et al., 2011) or very short HRTs (Grootscholten et al., 2013d); and 2) a low pH system with in-line product recovery (Agler et al., 2012a). In the second approach, the overall product recovery (transfer) rate for an individual MCC (*e.g.*, g *n*-caprylate-COD/d) is proportional to the concentration of an individual undissociated MCCA in the bioreactor broth (*e.g.*, g *n*-caprylic acid-COD/L). Therefore, increased residual MCCA concentrations in the bioreactor broth would lead to higher MCC product recovery and total production rates, unless the increased concentrations also lead to product inhibition.

2.4.3 Minimum inhibitory concentrations of n*-caprylic acid are unknown*

Little is currently known about the minimum inhibitory concentrations at which undissociated MCCAs will inhibit microbial activity. The highest reported concentration of undissociated *n*-caprylic acid was less than 0.08 g COD/L (0.21 mM) (Figure 2.5), and this value was achieved in a batch fixed-film system operated at pH 6.0 in which a gas composed of carbon dioxide and hydrogen was continuously fed (Zhang et al., 2013). For ethanol-fed systems, the highest concentration of *n*-caprylic acid accumulated was even lower (0.05 g COD/L, 0.14 mM) (Ge et al., 2015). These maximum *n*-caprylic acid concentrations range from 3 to 4% of the solubility limit of undissociated *n*-caprylic acid (1.7 g COD/L, 4.7 mM) (Xu et al., 2015). One study reported that *n*-caprylic acid is inhibitory (to *E. coli*) at 1.6 g COD/L (4.4 mM) (Skrivanova et al., 2006), but this concentration was nearly equal to the solubility limit, and was thus probably excessive. No product inhibition studies have been conducted to specifically relate MCC productivity to concentrations of undissociated MCCAs in the bioreactor broth.

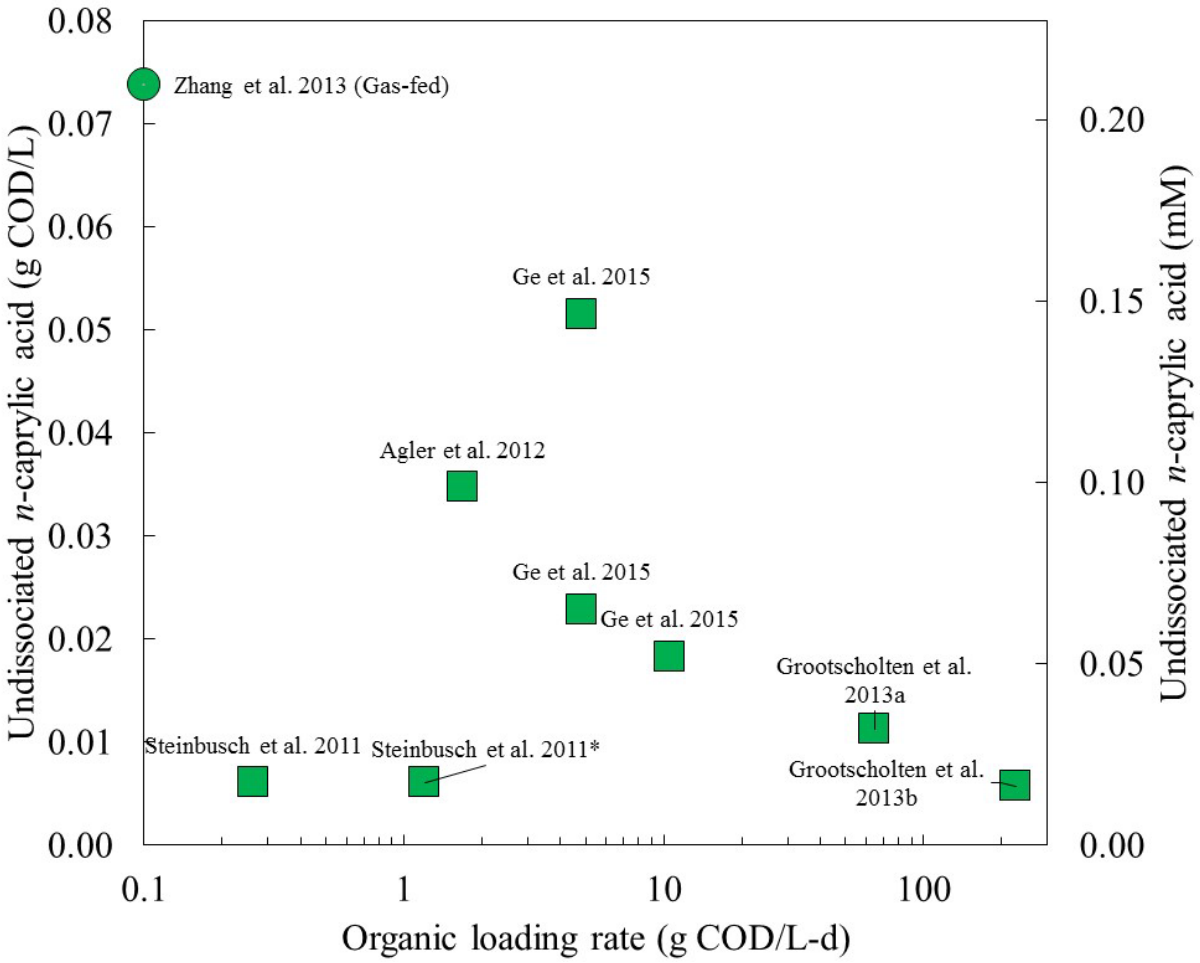

Figure 2.5: Undissociated *n*-caprylic acid concentrations in ethanol-fed or gas-fed bioreactors. Results are from six studies in which *n*-caprylate production was reported. Maximum instantaneous values reported are indicated (*). Organic loading rates are presented on logarithmic scales. One study (Zhang et al. 2013, circle) produced *n*-caprylate in a bioreactor in which gas composed of carbon dioxide and hydrogen was fed; they did not present organic loading rates, so this marker was placed at an organic loading rate near the sum of the total carboxylate volumetric production rates. Undissociated *n*-caprylic acid concentration data was not available for Agler et al. 2014.

2.4.4 The reported product ratios of n-*caprylate to* n-*caproate were consistently low*

The ratio of *n*-caprylate to *n*-caproate production has remained low (Figure 2.6). The highest reported product ratio of *n*-caprylate to *n*-caproate was less than 1.5 (g COD/g COD) (Zhang et al., 2013). This ratio was observed in a fixed-film batch system operated at pH 6.0 with very low MCC productivity (0.07 g COD/L-d) in which carbon dioxide and hydrogen were continuously fed. For all ethanol-fed systems, *n*-caprylate to *n*-caproate product ratios were less than 0.6 (Agler et al., 2014), and systems that produced *n*-caprylate at rates higher than 1 g COD/L-d were marked by product ratios less than 0.06 (Grootscholten et al., 2013b). Ultimately, *n*-caprylate will remain a minor product unless rates and proportions of *n*-caprylate production increase to the same order of magnitude as high-rate *n*-caproate productivity (~10-100 g COD/L-d) (Grootscholten et al., 2013d, Grootscholten et al., 2013b).

2.4.5 Substrate ratios and levels affected the product ratios of n-*caproate to* n-*butyrate*

To explain what may affect *n*-caprylate to *n*-caproate product ratios, it is instructive to review early literature that documented increased product ratios of *n*-caproate to *n*-butyrate in the type strain *Clostridium kluyveri*. Batch studies of *C. kluyveri* demonstrated that increased substrate ratios of ethanol to acetate led to increased product ratios of *n*-caproate to *n*-butyrate (Bornstein and Barker, 1948, Weimer and Stevenson, 2012). This trend occurred even when the initial concentration of ethanol was fixed and the initial acetate concentration was increased (Figure 2.7, A-B). In addition, when the initial concentration of acetate was fixed and the initial concentration of ethanol was increased, the product ratio of *n*-caproate to *n*-butyrate and the total *n*-caproate production increased until the initial ethanol concentration was 44 g COD/L and the initial ethanol to acetate substrate ratio was 6 (g COD/g COD) (Figure 2.7C) (Weimer and Stevenson, 2012). This suggested that ethanol inhibition occurred near 44 g COD/L (460 mM).

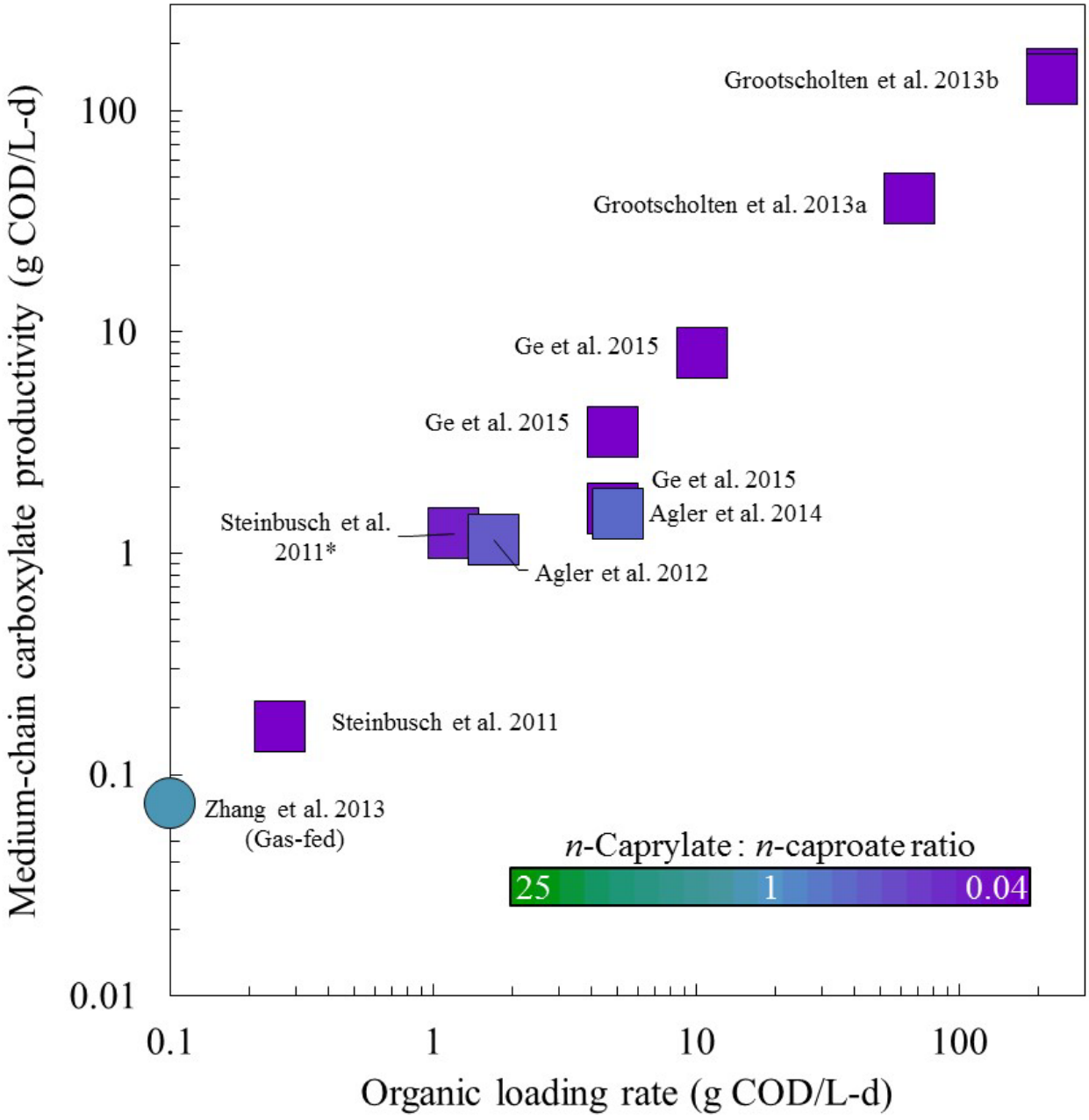

Figure 2.6: Medium-chain carboxylate productivity and product ratios of *n*-caprylate : *n*-caproate from ethanol-fed or gas-fed bioreactors. Results are from seven studies in which *n*-caprylate production was reported. Indications include maximum instantaneous values reported (*). A color gradient was used to show the product ratio of *n*-caprylate (green) to *n*-caproate (purple). Blue represents a mixture of these two products. Both medium-chain carboxylate productivities and organic loading rates are presented on logarithmic scales. One study (Zhang et al. 2013, circle) produced *n*-caprylate from carbon dioxide- and hydrogen-gas; they did not present organic loading rates, so this marker was placed at an organic loading rate near the sum of the total carboxylate productivities. The following studies reported *n*-caprylate to *n*-caproate product ratios greater than 0.04: Ge et al. 2015 (0.05); Grootscholten et al. 2013a (0.06); Steinbusch et al. 2011* (0.12); Agler et al. 2012 (0.50); Agler et al. 2014 (0.57); and Zhang et al. 2013 (1.47).

Continuously fed bioreactor studies of the type strain *C. kluyveri* provided additional evidence that increased ethanol to acetate substrate ratios led to increased *n*-caproate to *n*-butyrate product ratios. Ethanol and acetate were fed at either ethanol-limited or excess ethanol substrate ratios (Figure 2.7D), and the HRT was varied to evaluate the effect of different total organic loading rates (OLRs, 8 to 71 g COD/L-d) (Kenealy and Waselefsky, 1985). For several equivalent total organic loading rates, the ethanol-limited substrate ratio led to lower *n*-caproate to *n*-butyrate product ratios than the excess ethanol substrate ratios (~0.6 vs. ~0.8, respectively). Moreover, when the substrate ratios were fixed but the total organic loading rates were increased, the *n*-caproate productivity decreased at the highest loadings for each ratio, indicating substrate inhibition (overloading). Furthermore, when *n*-caproate productivity decreased because of substrate inhibition at these high organic loading rates, *n*-butyrate productivity simultaneously increased. This led to decreased product ratios of *n*-caproate to *n*-butyrate, and batch studies with substrate inhibition yielded similar results (Figure 2.7, A-B). From these findings, it can be hypothesized that increased product ratios of *n*-caprylate to *n*-caproate could be achieved with increased substrate ratios of ethanol to acetate. However, these results also serve as a harbinger: excessive ethanol concentrations and loadings must be avoided to prevent substrate inhibition.

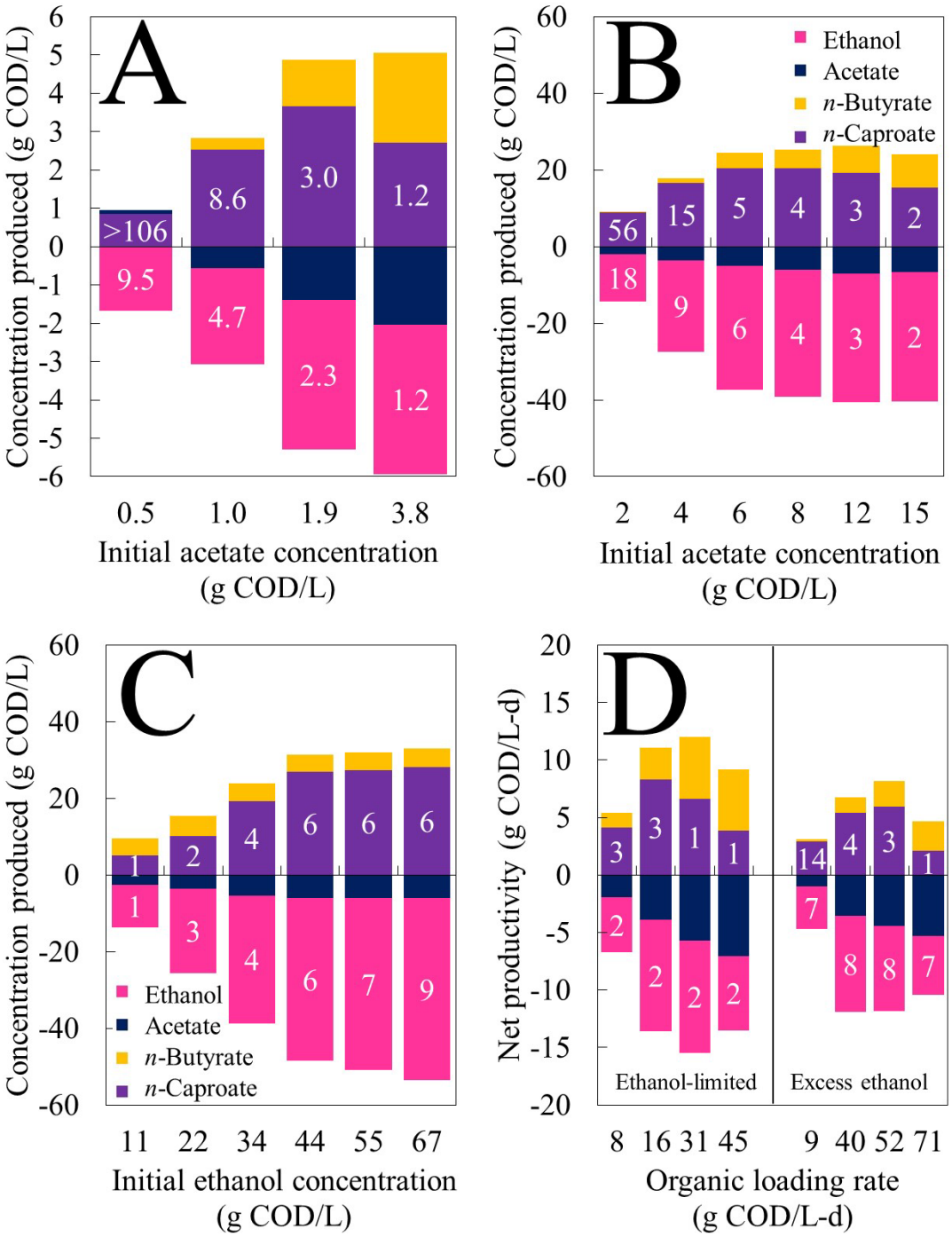

Figure 2.7: Substrate ratios and concentrations affected carboxylate product ratios and concentrations in batch and continuously fed bioreactors of *C. kluyveri*. For (A)-(C), the concentrations of ethanol and carboxylates that were either produced (positive values) or consumed (negative values) are shown for batch bioreactor experiments of *Clostridium kluyveri*. For (D), the net volumetric production rate (productivity) of ethanol and carboxylates that were either produced (positive values) or consumed (negative values) are shown for a continuously fed bioreactor of *C. kluyveri*. In all experiments, ethanol and acetate were fed. The initial substrate ratio (ethanol to acetate) for each treatment is displayed upon the concentration of the ethanol consumed. Additionally, the product ratio (*n*-caproate to *n*-butyrate) for each treatment is displayed upon the concentration of the *n*-caproate produced.

(A) From Bornstein and Barker, 1948: in this batch study, the initial concentration of ethanol was fixed (4.5 g COD/L, 47 mM) and the initial concentration of acetate was varied. The bioreactor temperature was 30°C, the pH was 7, and the duration was 12 d. When the initial concentration of acetate was increased, the ratio of *n*-caproate to *n*-butyrate produced decreased. At the maximum initial concentration of acetate fed, the produced *n*-caproate concentration decreased.

(B) From Weimer and Stevenson, 2012: in this batch study, the initial concentration of ethanol was fixed (33.6 g COD/L, 350 mM) and the initial concentration of acetate was varied. The bioreactor temperature was 39°C, the initial pH was 6.8, and the duration was 3 d. When the initial concentration of acetate was increased, the ratio of *n*-caproate to *n*-butyrate produced decreased. At the maximum initial concentration of acetate fed, the produced *n*-caproate concentration decreased.

(C) From Weimer and Stevenson, 2012: in this batch study, the initial concentration of acetate was fixed (7.7 g COD/L, 120 mM) and the initial concentration of ethanol was varied. The bioreactor temperature was 39°C, the initial pH was 6.8, and the duration was 3 d. When the initial concentration of ethanol was increased, the ratio of *n*-caproate to *n*-butyrate produced increased until the initial concentration of ethanol was 44 g COD/L (460 mM); higher initial levels of ethanol led to substrate inhibition and decreased ethanol utilization.

(D) From Kenealy and Waselefsky, 1985: in this continuously fed bioreactor study, the substrate ratio of ethanol to acetate was either ethanol-limited or had excess ethanol (2 or ~7 g COD/g COD, respectively). Increased substrate ratios and decreased substrate concentrations led to increased product ratios.

CHAPTER 3

CONVERSION OF L-LACTATE INTO *N*-CAPROATE BY A CONTINUOUSLY FED REACTOR MICROBIOME

Adapted from a manuscript by Leo A. Kucek, Mytien Nguyen, and Largus T. Angenent

(Submitted to Water Research)

Abstract

Conversion of lactate to *n*-caproate had been described for the type strain *Megasphaera elsdenii* in batch systems. Recently, investigators have also described production of *n*-caproate from endogenous or exogenous lactate with batch-fed reactor microbiomes. However, no reports exist of lactate to *n*-caproate conversion within a continuously fed bioreactor. Since continuously fed systems are advantageous for biotechnology production platforms, my objective was to develop such a system. Here, continuous lactate to *n*-caproate conversion was demonstrated for more than 165 days. The volumetric *n*-caproate production rate (productivity) was improved when I decreased the operating pH from 5.5 to 5.0, and was again improved when an in-line product recovery *via* pertraction (membrane-based liquid-liquid extraction) was utilized. I observed a maximum *n*-caproate productivity of 6.9 g COD/L-d for a period of 17 days at an L-lactate loading rate of 9.1 g COD/L-d, representing the highest sustained lactate to *n*-caproate conversion rate ever reported. Two competing lactate conversion pathways required careful management: 1) the reverse β-oxidation pathway to *n*-caproate; and 2) the acrylate pathway to propionate. Maintaining a low residual lactate concentration in the bioreactor broth was necessary to direct lactate conversion towards *n*-caproate instead of propionate. These findings provide a foundation for the development of new resource recovery processes to produce higher-value liquid products (*e.g.*, *n*-caproate) from carbon-rich wastewaters containing lactate or lactate precursors (*e.g.*, carbohydrates).

3.1 Introduction

To sustain healthy communities and ecosystems, a new paradigm of resource recovery from wastewater is required (Guest et al., 2009). Carbon-rich wastewaters with high chemical oxygen demand (COD) pose ecological risks if left untreated, but these wastes can be converted into fuels and chemicals *via* the carboxylate platform (Angenent et al., 2004, Agler et al., 2011). In the carboxylate platform, anaerobic reactor microbiomes (open cultures of microbial consortia) are used to convert complex wastes into intermediate short-chain carboxylates (SCCs, ranging from two to five carbons) (Agler et al., 2012b). Throughout this text, mixtures of both dissociated carboxylates and their corresponding undissociated carboxylic acids are referred to as carboxylates. These intermediate SCCs can be converted into methane-rich biogas *via* anaerobic digestion, which is a carboxylate platform technology. Using similar reactor microbiomes, however, intermediate SCCs can also be chain-elongated to medium-chain carboxylates (MCCs, ranging from six to twelve carbons) (Xu et al., 2015) *via* the reverse β-oxidation pathway (Spirito et al., 2014) to create higher-value liquid fuels and chemicals (Agler et al., 2011).

The reverse β-oxidation pathway was established from bioreactor studies in which ethanol (as an energy and carbon source) was converted into *n*-caproate (Spirito et al., 2014). *n*-Caproate is a six-carbon MCC that has a variety of uses, including use as an antimicrobial to replace antibiotics in agriculture (Desbois, 2012). *n*-Caproate also has emerging applications as a chemical precursor for products ranging from flavors (Kenealy et al., 1995) to aviation fuels (Harvey and Meylemans, 2014). Besides ethanol (Grootscholten et al., 2013d), other reduced substrates have also been utilized for production of *n*-caproate, including: carbohydrates (Gómez et al., 2009); polyols (Jeon et al., 2013); and lactate (Elsden et al., 1956).

Lactate is an important intermediate in the anaerobic breakdown of carbohydrates (Kleerebezem and van Loosdrecht, 2007). Carbohydrates comprise ~18% of the COD in municipal wastewaters (Raunkjær et al., 1994) and up to ~70% of the COD in some food processing wastewaters (Arslan et al., 2013, Gómez et al., 2009). Lactate to *n*-caproate conversion has been proposed to proceed similarly to the reverse β-oxidation pathway used for the conversion of ethanol to *n*-caproate: lactate (a three-carbon SCC) is converted to acetyl-CoA, which then enters the reverse β-oxidation cycle (Spirito et al., 2014, Zhu et al., 2015). Until recently, *n*-caproate production from exogenous lactate had only been clearly demonstrated in pure-culture studies using *Megasphaera elsdenii* in batch systems (Elsden et al., 1956, Ladd, 1959, Marounek et al., 1989, Weimer and Moen, 2013). *M. elsdenii* is a bacterium isolated from the rumen that was found to be uniquely tolerant of pH values below 5.5, metabolizing DL-lactate even at pH values as low at 4.7 (Counotte and Prins, 1981).

Recently, Zhu et al. (Zhu et al., 2015) produced *n*-caproate from exogenous lactate with a reactor microbiome for the first time. *Clostridium IV*, within the family Ruminococcaceae, dominated this microbiome, while *M. elsdenii* was not observed. The inoculum was collected from a pit mud that was used to convert carbohydrate-rich feedstocks (*e.g.*, wheat, sorghum, and maize) into the fermented precursor "yellow water" for Chinese strong-flavored liquor production. In batch bioreactors operated between pH 6.0 and 6.5, exogenous lactate was fed as the sole carbon and energy source. From these batch periods of less than four days, a maximum volumetric *n*-caproate production rate (productivity) of 6.5 g COD/L-d was reported. Others had already described that the conversion of lactate to *n*-caproate in reactor microbiomes was likely after finding endogenous lactate consumption and simultaneous *n*-caproate accumulation in batch-fed systems with reactor microbiomes (Agler et al., 2012b, Sträuber et al., 2012, Sträuber

et al., 2015). However, proof was missing because other intermediates from the hydrolysis and acidification of the complex organic substrates (*e.g.*, maize fiber hydrolysate, maize silage) were present in addition to lactate. Similarly to Zhu et al. (2015), Sträuber et al. (2015) observed an abundance of *Clostridium IV* and the absence of *M. elsdenii* in periods when endogenous lactate was consumed and *n*-caproate was simultaneously produced.

In ethanol-fed systems, even-numbered carboxylates (*e.g.*, *n*-butyrate, *n*-caproate) are the predominant products produced *via* the reverse β-oxidation pathway (Spirito et al., 2014). In lactate-fed systems, the even-numbered reverse β-oxidation products are accompanied by odd-numbered SCCs (*e.g.*, propionate, *n*-valerate) (Weimer and Moen, 2013), which are derived from the competing acrylate pathway that converts lactate into propionate (Hino and Kuroda, 1993). In one of the few bioreactor studies in which DL-lactate was fed continuously to a pure culture of the type strain *M. elsdenii*, the presence of these competing metabolic pathways was confirmed, but no *n*-caproate was produced (Prabhu et al., 2012). Others had already found that anaerobic conversion of lactate typically leads to propionate accumulation when lactate is abundant (Sträuber et al., 2015). This is in stark contrast to the recent pit mud reactor microbiome study (Zhu et al., 2015), in which no propionate accumulation was reported, indicating that the competing acrylate pathway was not active.

n-Caproate production from ethanol has been demonstrated using both batch-fed (Steinbusch et al., 2011, Agler et al., 2012a) and continuously fed bioreactors (Grootscholten et al., 2013d). However, I found no reports of *n*-caproate production in bioreactors that were continuously fed exogenous lactate as the sole carbon and energy source. The most successful biotechnology production platforms for anaerobic treatment are continuously fed systems such as upflow anaerobic sludge blanket reactors (Lettinga, 1995). To translate chain elongation with

lactate into real anaerobic treatment systems, I had several experimental objectives: 1) to provide the first demonstration of sustained conversion of lactate to *n*-caproate in a continuously fed reactor microbiome; 2) to evaluate the effects of lactate loading rates and residual lactate concentrations on the production of *n*-caproate and other carboxylates *via* the competing reverse β-oxidation and acrylate pathways; and 3) to characterize microbial community changes within the reactor microbiome corresponding to periods of increased *n*-caproate productivity.

3.2 Materials and methods

3.2.1 Growth medium and inoculum

The basal medium was based on a previous batch study in which lactate was converted to *n*-caproate (Weimer and Moen, 2013), and it contained nutrients and yeast extract (1.25 g/L, 1.6 g COD/L) with modifications as described previously (Vasudevan et al., 2014). L-Lactate and *n*-butyrate were added at varied substrate concentrations to achieve desired loading rates. The medium pH was adjusted with 5 M sodium hydroxide to the operating pH of the bioreactor. The inoculum was derived from a well-characterized reactor microbiome that was fed ethanol-rich yeast fermentation beer (Agler et al., 2012a). This reactor microbiome had been batch-fed semi-continuously (once every two days) throughout an operating period of more than three years at the time of inoculation (Ge et al., 2015). The inoculum was triple-washed in basal media, and approximately 100 mL of this inoculum was added to the bioreactor.

3.2.2 Bioreactor system

An upflow anaerobic filter with was employed with constant bioreactor broth recycling through an in-line pertraction system (membrane-based liquid-liquid extraction) for product extraction (Figure 3.1). The bioreactor was constructed as a vertically oriented cylinder, which was made of Plexiglas®, with an inner diameter of 6 cm. The total volume was 0.70 L, but Kaldnes K1 packing material (Evolution Aqua, Wigan, United Kingdom) was added, resulting in a working volume of 0.55 L. The bioreactor was wrapped with tubing in which hot water from a heating bath (VWR Scientific Model 1104, Radnor, PA, USA) was recirculated for temperature control, resulting in a constant temperature of 34±1°C inside the bioreactor. A pH probe (Mettler 405-DPAS SC K85, Columbus, OH, USA) was mounted at the top of the bioreactor. Automated pH control of the bioreactor broth was maintained with a controller (Eutech Instruments alpha-pH800, Vernon Hills, IL, USA) and a corresponding acid addition pump (Mityflex 913, Bradenton, FL, USA). Hydrochloric acid (0.5 M) was added to the well-mixed feed and recycle inlet at the base of the bioreactor. Fresh media containing L-lactate and *n*-butyrate was continuously fed from a refrigerated vessel (4°C) into the base of the bioreactor using a peristaltic feed pump (Cole Parmer L/S Digital Economy Drive, Vernon Hills, IL, USA) at an average rate of approximately 0.37 L/d and a hydraulic retention time (HRT) of 1.5 d (Figure 3.1). The effluent continuously exited the bioreactor *via* an overflow line connected to the top of the bioreactor. The exit of the overflow line was submerged within a secondary effluent reservoir. An inverted funnel was used to collect the produced gas within the bioreactor and was connected to a flow meter (Ritter MGC-1, Bochum, Germany) (Figure 3.1). In addition, a gas-sample septum and a bubbler were placed in the gas collection system. A sampling port for biomass samples was placed halfway up the vertically oriented bioreactor.

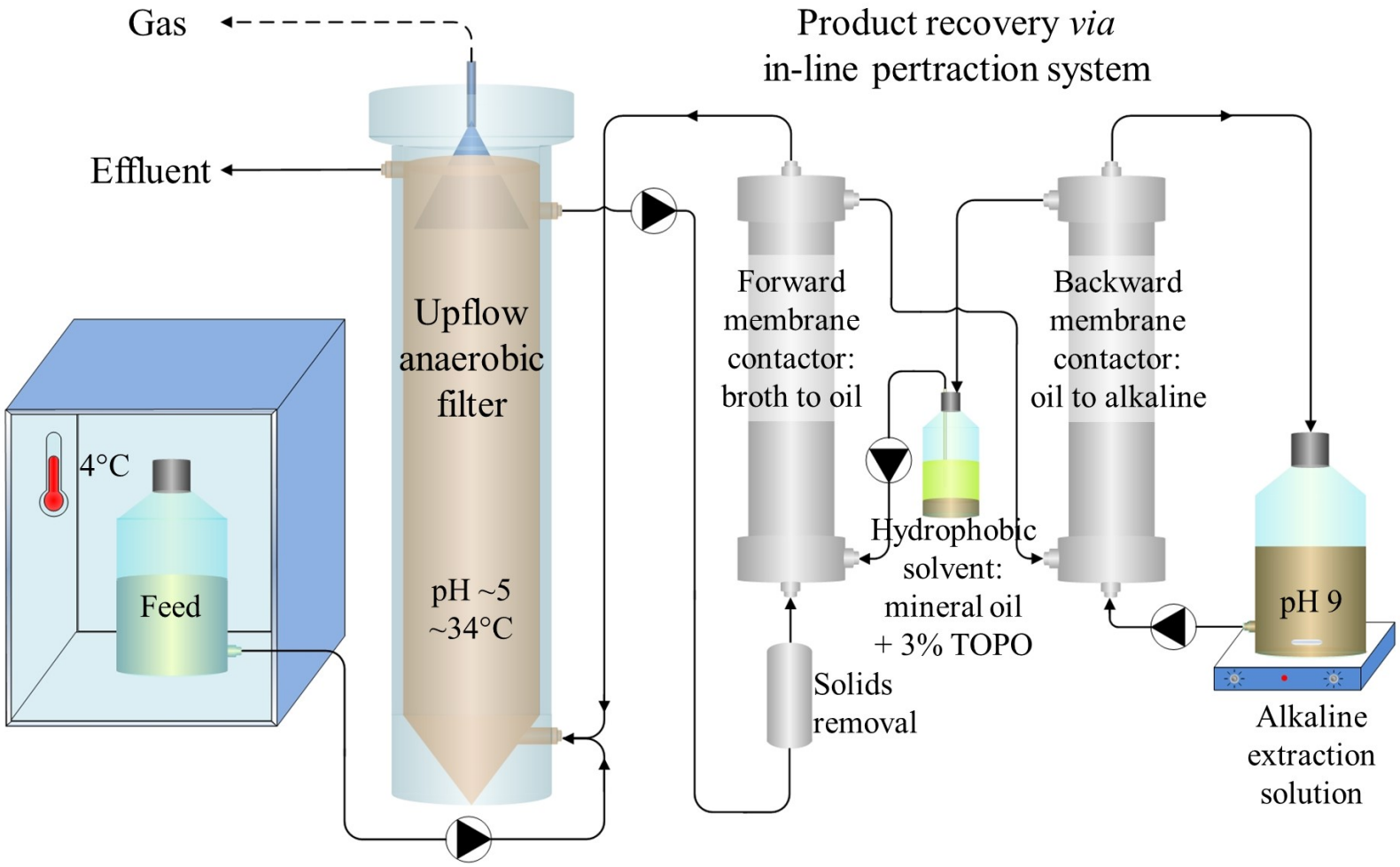

Figure 3.1: **Bioreactor system schematic**. An upflow anaerobic filter was continuously fed basal media containing L-lactate and *n*-butyrate. In-line pertraction (membrane-based liquid-liquid extraction) was used to continuously recover hydrophobic, undissociated medium-chain carboxylic acids (MCCAs) (*e.g.*, *n*-caproic acid) from a bioreactor broth recycle flow. After intermediary recovery in a mineral oil solvent, MCCAs were then transferred across a second membrane contactor to an alkaline extraction solution. Through automatic base addition to the alkaline extraction solution, the pH gradient was maintained, and these carboxylic acids accumulated in the alkaline extraction solution as medium-chain carboxylates (MCCs).

3.2.3 Pertraction system

Product recovery was accomplished with a pertraction system (Figure 3.1) similar to those used in previous reports (Agler et al., 2012a, Ge et al., 2015). One forward and one backward membrane contactor (1.4 m^2 each, Membrana Liqui-Cel 2.5x8, X50 membrane, Charlotte, NC, USA) were used. The hydrophobic solvent was circulated continuously in the lumen of the hydrophobic hollow-fiber membrane modules; the solvent consisted of mineral oil with 30 g/L tri-*n*-octylphosphine oxide (TOPO) (Sigma Aldrich, St. Louis, MO, USA). The stirred alkaline extraction solution was initially buffered with 0.3 M sodium borate and was maintained at pH 9 with automated addition of 5 M sodium hydroxide using a controller (Eutech Instruments alpha-pH800, Vernon Hills, IL, USA) and a corresponding base pump (Mityflex 913, Bradenton, FL, USA). A constant bioreactor broth recycle flow of 60 L/d was maintained using a peristaltic pump (ColeParmer 7553-30, Vernon Hills, IL, USA). To prevent fouling or solids accumulation in the forward membrane contactor, bioreactor broth was drawn from the top of the anaerobic filter and was then pumped through a custom-built, 1.6-mm stainless-steel strainer (Danco 88886, Shorewood, IL, USA), a 65-µm filter (McMaster-Carr 44205K21, Elmhurst, IL, USA), and a subsequent 5-µm filter (Pentek GS-6 SED/5, Upper Saddle River, NJ, USA). A peristaltic pump (ColeParmer 7553-30, Vernon Hills, IL, USA) equipped with two pump heads provided continuous recycle flows of 10 and 58 L/d for the mineral oil solvent and alkaline extraction solution, respectively.

3.2.4 Operating strategy and calculations

This bioreactor experiment was divided into four phases: I) batch phase; II) start-up phase with continuous feeding (with the pertraction system off or on); III) high *n*-caproate productivity phase (with continuous feeding and the pertraction system on); and IV) post-lactate

overloading phase (with continuous feeding and the pertraction system on). Each phase was then divided into several distinct operating periods. For each period, several operating parameters were held constant, including the: organic loading rate (OLR); HRT; bioreactor pH; and operation with or without pertraction. Each operating period was operated for at least five HRT periods, and average bioreactor loading rates and concentrations were reported.

Carboxylate productivities were also calculated as average values for each operating period. Herein, the average bioreactor effluent production rate (g COD/d) *plus* the average transfer rate *via* pertraction (g COD/d) were summed to yield the total production rate (g COD/d). Effluent production rates were calculated as the average bioreactor broth concentration divided by the average HRT for each period. Average transfer rates were calculated by first plotting the increasing amounts of individual carboxylates in the alkaline extraction solution against time. Least squares methods were then used to determine the slope and the sample standard deviation (LINEST function, Microsoft Excel). Production rates were divided by the working bioreactor volume to determine the total volumetric production rates (productivities) (g COD/L-d). All concentrations, rates, and yields were converted to a g COD basis. Feed flow rates were determined volumetrically; effluent rates were determined gravimetrically. Uncertainty was represented by 95% confidence intervals: the standard error was first calculated as the quotient of the sample standard deviation divided by the square root of the number of samples; then, the standard error was multiplied by a t-value corresponding to the degrees of freedom (based on the number of samples). Uncertainty was propagated through calculations, and 95% confidence intervals were included with reported data (*e.g.*, productivities).

3.2.5 Liquid and gas analysis

Liquid samples (1.5 mL) were collected from the bioreactor and the alkaline extraction solution every other day or daily. Bioreactor broth samples were collected from the broth recycle line between the 5-µm filter and the forward membrane contactor. Alkaline extraction solution samples were collected from the well-mixed reservoir (~3 L). Concentrations of most carboxylates were determined with gas chromatography (GC) (Usack and Angenent, 2015). Concentrations of lactate were quantified with high performance liquid chromatography (HPLC). Lactate samples were filtered through a sterile Acrodisc 0.22-µm pore size polyvinylidine fluoride membrane syringe filter (Pall Life Sciences, Port Washington, NY, USA) prior to analysis to remove possible biological and particulate contaminants. Lactate was separated from other compounds on an Aminex HPX-87H 300 mm x 7.8 mm cation-exchange column for carboxylate analysis (Bio-Rad Laboratories Inc., Hercules, CA, USA) at 60°C with 5 mM sulfuric acid as the mobile phase at a flow rate of 0.6 mL/min. HPLC analysis was conducted with the Waters 600E system controller, 717Plus autosampler, and the 410 refractive index detector (Waters Corp, Milford, MA, USA). Data were recorded and analyzed with the PeakSimple Chromatography Data System SRI Model 302, and PeakSimple software v4.44 (Schemback, Germany). The concentrations of methane, carbon dioxide, and hydrogen gases (>2000 ppm) were measured using a GC system (Usack and Angenent, 2015). Furthermore, the concentration of hydrogen gas (<2000 ppm) was determined using a reduction gas detector (RGD) (Trace Analytical RGD, Menlo Park, CA, USA). The RGD inlet was connected to a packed column (Restek, ShinCarbon ST 80/100, Bellefonte, PA, USA) for peak separation, which was installed in a GC system (Gow Mac 580, Bethlehem, PA, USA).

3.2.6 Microbial community analysis: biomass samples, DNA extraction, PCR, sequencing, and data analysis

I collected biomass samples from the bioreactor broth at 18 time points throughout the experiment, as well as one sample from the inoculum. The bioreactor broth was thoroughly mixed by quickly withdrawing and refilling a 60 mL syringe ten times. During this sampling, settled flocculent biomass was resuspended. The sample was collected in 2-mL Eppendorf tubes. These 2-mL samples were then centrifuged at 16,873 x *g* for 4 min and the supernatants were discarded. Concentrations of wet solids in these pelleted biomass samples ranged from 23 to 76 mg/L. These pelleted biomass samples were stored at -80°C until further processing.

Genomic DNA was extracted using the PowerSoil DNA isolation kit (MO BIO Laboratories Inc., Carlsbad, CA). Modifications to the protocol include utilization of custom bead tubes containing a mixture of 300 mg of 0.1-mm diameter and 100 mg of 0.5-mm diameter silica/zirconia beads (Hospodsky et al., 2010), and physical cell lysis with bead-beating at 3450 oscillations/min for 45 s. The DNA amplification protocol was described previously (Regueiro et al., 2015) with the following exceptions: 1) Mag-Bind RxnPure Plus magnetic beads solution (Omega Biotek, Norcross, GA, USA) were used instead of Mag-Bind E-Z Pure; 2) only 20 ng DNA per sample were pooled instead of 100 ng. QIITA (qiita.microbio.me) was used for initial processing of the sequencing data. The sortmerna method was used to bin sequences into operational taxonomic units (OTUs) at 97% identity. Taxonomy was assigned for representative sequences selected for each OTU using the Greengenes v13.8 database from August 2013 (McDonald et al., 2012). The remaining analyses were performed in QIIME v1.9 (Caporaso et al., 2010). Singleton OTUs were removed from the dataset.

Community analysis, including beta diversity and unconstrained ordination, was performed as described previously (Regueiro et al., 2015) with the following exceptions: 1) the alpha diversity was calculated using the Shannon diversity index (Shannon, 1948) rather than Chao1; 2) the Pearson correlation coefficient was calculated for samples collected during Phase III with the functions cor and cor.test in the R stats package (Team, 2014). At a significance level of $p<0.05$ and $n = 11$, the relative abundance of an OTU would be positively correlated with *n*-caproate productivity if the Pearson r was greater than 0.602. Heatmaps were created to represent OTU relative abundances during bioreactor operation *via* the gplots package in R (Warnes et al., 2015).

3.3 Results and discussion

3.3.1 Conversion of L-lactate into n*-caproate was demonstrated in a continuously fed bioreactor for the first time*

In an upflow anaerobic filter, which was continuously fed L-lactate, the maximum *n*-caproate productivity achieved was 6.9 g COD/L-d (Figure 3.2). This maximum productivity was sustained for 17 days (Table 3.1) at an HRT of 1.9 d (Table 3.2) (Phase III, Period 12, Days 176-193). The corresponding L-lactate loading rate was 9.1 g COD/L-d, and the total organic loading rate (OLR) was 17.7 g COD/L-d (Table 3.2). Both L-lactate and *n*-butyrate were fed to the bioreactor, since I had anticipated that *n*-butyrate would be chain-elongated to *n*-caproate by the L-lactate-derived acetyl-CoA. However, addition of *n*-butyrate was unnecessary for *n*-caproate production: a net positive production of *n*-butyrate was observed (Table 3.2) from the chain elongation of endogenous acetate (0.4-2.0 g COD/L, 6-31 mM) with lactate (Figure 3.3).

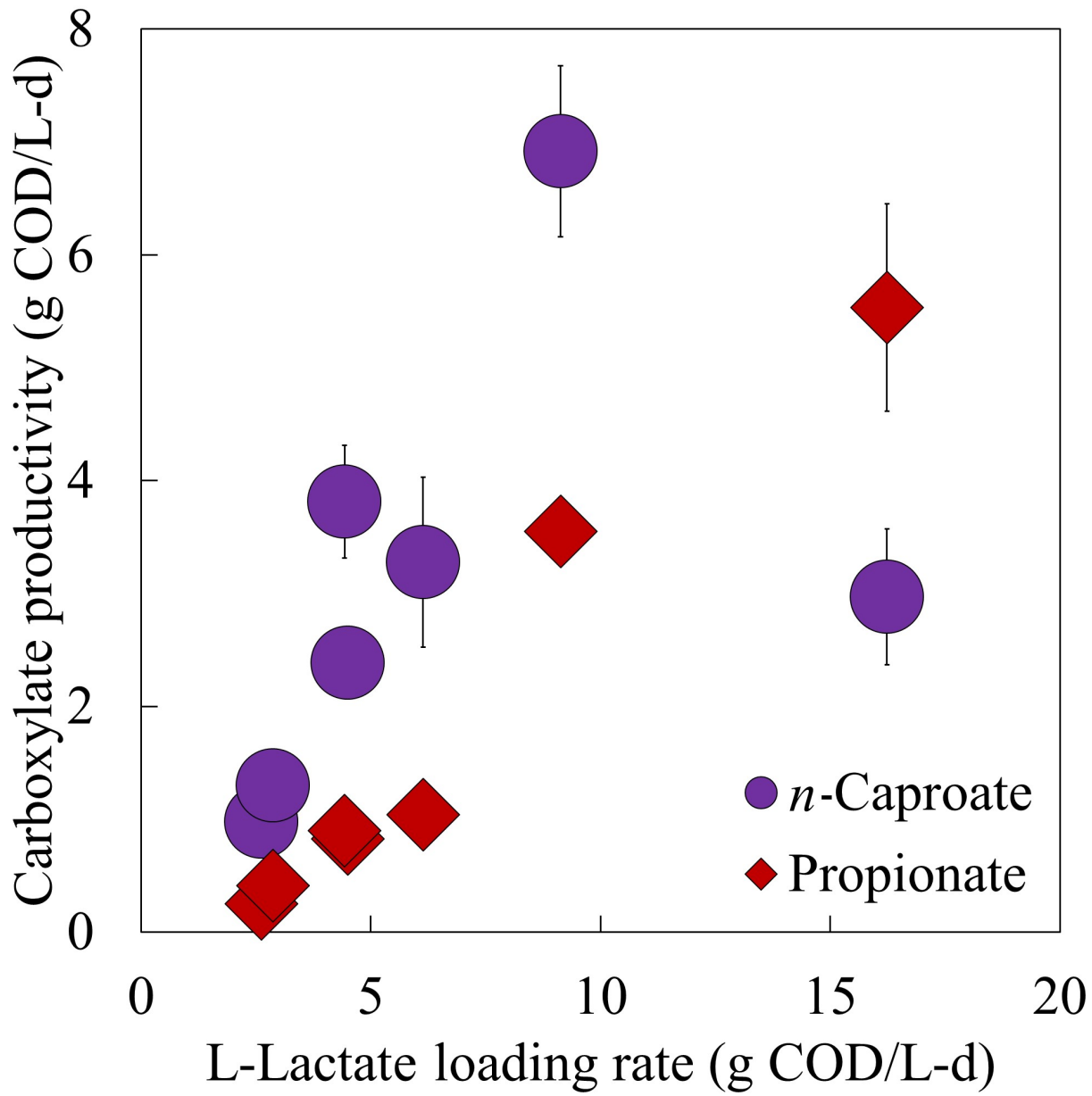

Figure 3.2: *n*-Caproate and propionate productivities are functions of the L-lactate loading rate. *n*-Caproate productivities increased up to 6.9 g COD/L-d when L-lactate loading rates were increased to 9.1 g COD/L-d. After the L-lactate loading rate was increased to 16.2 g COD/L-d, the *n*-caproate productivity decreased to 3.0 g COD/L-d. At this maximum loading rate, the propionate productivity increased to 5.5 g COD/L-d. Error bars represent 95% confidence intervals of average productivities. Data shown are from Phase III only.

Table 3.1: **Average bioreactor broth concentrations**. Average substrate and product concentrations in the bioreactor broth are reported for each operating period. A major disturbance was experienced on Day 166 (Phase III, Period 11), leading to large variability in average bioreactor concentrations. Detection limits were approximately 0.02 g COD/L (0.2 mM) for lactate and approximately 0.02 g COD/L (~0.1 mM) for other carboxylates. The following conversion factors (g COD/mol) were used to convert molar carboxylate concentrations to a g COD-basis: lactate, 96; acetate, 64; propionate, 112; *n*-butyrate, 160; *n*-valerate, 208; *n*-caproate, 256; *n*-heptanoate, 304; *n*-caprylate, 352. B.D.: below detection; N/A: not available (*i.e.*, no replicates). Uncertainty is represented by 95% confidence intervals.

Operating conditions					**Average bioreactor broth concentrations**				
Phase #	Period #	Pertraction + / -	Start - End *d*	Bioreactor pH	[Lactate]	[*n*-Caproate]	[*n*-Butyrate]	[Propionate]	[Other SCC]
					g COD/L				
I	1	-	0 - 22	5.6 ± *0.4*	8.85 ± *21.29*	0.03 ± *0.08*	5.37 ± *2.75*	0.89 ± *0.36*	0.20 ± *1.23*
	2	-	22 - 30	5.5 ± *0.3*	3.07 ± *10.26*	0.19 ± *0.25*	1.62 ± *1.09*	0.21 ± *0.12*	0.93 ± *1.00*
II	3	-	30 - 33	5.6 ± *0.3*	*B.D.*	0.13 ± *0.29*	3.36 ± *7.60*	0.05 ± *0.06*	0.91 ± *1.41*
	4	+	33 - 59	5.3 ± *0.1*	1.52 ± *3.27*	*B.D.*	0.40 ± *0.19*	0.03 ± *0.02*	0.44 ± *0.11*
	5	-	59 - 76	5.4 ± *0.1*	0.02 ± *0.02*	0.15 ± *0.09*	4.45 ± *0.70*	0.16 ± *0.02*	1.33 ± *0.30*
	6	-	76 - 84	5.0 ± *0.2*	0.04 ± *N/A*	0.91 ± *0.94*	3.69 ± *0.49*	0.49 ± *0.14*	1.59 ± *0.10*
III	7	+	84 - 112	5.0 ± *0.0*	0.01 ± *0.01*	0.20 ± *0.30*	0.56 ± *0.46*	0.08 ± *0.04*	0.63 ± *0.14*
	8	+	112 - 120	4.9 ± *0.2*	*B.D.*	0.05 ± *0.01*	0.17 ± *0.02*	0.05 ± *0.01*	0.61 ± *0.03*
	9	+	120 - 146	4.8 ± *0.1*	*B.D.*	0.04 ± *0.01*	0.17 ± *0.02*	0.21 ± *0.02*	0.57 ± *0.05*
	10	+	146 - 162	4.8 ± *0.0*	*B.D.*	0.06 ± *0.02*	0.27 ± *0.02*	0.19 ± *0.03*	0.57 ± *0.06*
	11	+	162 - 176	4.7 ± *0.2*	0.49 ± *1.19*	0.32 ± *0.30*	0.75 ± *0.37*	0.34 ± *0.16*	0.85 ± *0.19*
	12	+	176 - 193	4.8 ± *0.0*	*B.D.*	0.06 ± *0.05*	0.89 ± *0.08*	0.90 ± *0.09*	0.99 ± *0.13*
	13	+	193 - 204	4.8 ± *0.1*	0.14 ± *0.10*	0.05 ± *0.03*	2.81 ± *0.72*	2.85 ± *0.72*	1.60 ± *0.32*
IV	14	+	204 - 213	4.9 ± *0.0*	0.02 ± *0.03*	0.03 ± *0.02*	0.87 ± *0.26*	1.78 ± *0.24*	1.22 ± *0.15*
	15	+	213 - 225	4.9 ± *0.0*	*B.D.*	*B.D.*	0.47 ± *0.02*	1.33 ± *0.07*	0.74 ± *0.07*

Table 3.2: **Average loading rates and carboxylate productivities.** Average productivities of *n*-caproate and several short-chain carboxylates (SCCs) are reported for each operating period. These total productivities were calculated as the sum of average bioreactor effluent production rates plus average transfer rates *via* pertraction for each operating period, normalized to the bioreactor working volume. *n*-Butyrate was fed continuously to the bioreactor; positive rates indicate net production of *n*-butyrate. A major disturbance was experienced in Period 11, leading to net consumption of *n*-butyrate. Total organic loading rates (OLRs) include loading from L-lactate, *n*-butyrate, and yeast extract. To vary the L-lactate and total organic loading rates, the concentrations of L-lactate and *n*-butyrate in the basal medium were changed (instead of the HRT); for each operating period, the concentrations of L-lactate and total organics (g COD/L) in the continuously fed basal medium can be calculated by multiplying the reported average L-lactate and total organic loading rates (g COD/L-d) by the corresponding average HRT (d). The yeast extract concentration in the media was consistently 1.6 g COD/L (1.25 g/L), and the corresponding yeast extract loading rate was approximately 1.1±0.1 g COD/L-d throughout continuous operation (HRT = 1.5±0.1 d). Phase I was in batch operation; thus, continuous loading and production rates were not reported. Uncertainty is represented by 95% confidence intervals.

Operating conditions				**Loading rates**		**Average carboxylate productivities**			
Phase #	Period #	Pertraction + / -	HRT *d*	Total OLR	L-Lactate	*n*-Caproate	Net *n*-Butyrate	Propionate	Other SCC
				g COD/L-d		*g COD/L-d*			
I	1	-	*N/A*	*N/A*		*N/A*			
	2	-	*N/A*	*N/A*		*N/A*			
II	3	-	0.7 ± *0.7*	13.9 ± *10.8*	4.7 ± *3.7*	0.2 ± *0.1*	-1.7 ± *5.2*	0.1 ± *0.1*	1.1 ± *1.2*
	4	+	1.4 ± *0.2*	6.8 ± *1.0*	2.3 ± *0.4*	0.0 ± *0.0*	1.8 ± *0.8*	0.0 ± *0.0*	0.4 ± *0.2*
	5	-	1.6 ± *0.1*	6.0 ± *0.7*	2.0 ± *0.2*	0.1 ± *0.1*	0.0 ± *0.6*	0.1 ± *0.0*	0.9 ± *0.2*
	6	-	1.6 ± *0.1*	5.7 ± *0.9*	2.6 ± *0.4*	0.6 ± *0.6*	0.2 ± *0.5*	0.3 ± *0.1*	1.0 ± *0.1*
III	7	+	1.6 ± *0.0*	5.9 ± *0.8*	2.6 ± *0.3*	1.0 ± *0.2*	1.4 ± *0.3*	0.2 ± *0.0*	0.7 ± *0.1*
	8	+	1.6 ± *0.1*	6.4 ± *0.4*	2.9 ± *0.2*	1.3 ± *0.1*	1.4 ± *1.2*	0.4 ± *0.1*	1.6 ± *0.1*
	9	+	1.5 ± *0.1*	7.9 ± *0.6*	4.5 ± *0.4*	2.4 ± *0.1*	0.5 ± *0.3*	0.8 ± *0.0*	0.9 ± *0.1*
	10	+	1.6 ± *0.1*	9.2 ± *0.7*	4.4 ± *0.4*	3.8 ± *0.5*	0.5 ± *0.9*	0.9 ± *0.1*	1.3 ± *0.1*
	11	+	1.4 ± *0.3*	12.4 ± *1.9*	6.1 ± *0.9*	3.3 ± *0.8*	-1.9 ± *1.1*	1.0 ± *0.1*	2.5 ± *0.3*
	12	+	1.9 ± *0.4*	17.7 ± *1.7*	9.1 ± *0.9*	6.9 ± *0.8*	4.8 ± *2.8*	3.6 ± *0.3*	1.4 ± *0.2*
	13	+	1.3 ± *0.4*	30.8 ± *5.9*	16.2 ± *3.1*	3.0 ± *0.6*	4.7 ± *1.3*	5.5 ± *0.9*	2.3 ± *0.5*
IV	14	+	1.2 ± *0.0*	14.1 ± *1.4*	10.1 ± *1.0*	4.2 ± *1.0*	6.7 ± *1.9*	7.1 ± *0.6*	5.1 ± *0.3*
	15	+	1.3 ± *0.0*	12.1 ± *0.6*	10.1 ± *0.5*	1.5 ± *0.5*	4.0 ± *0.5*	4.5 ± *0.2*	1.7 ± *0.2*

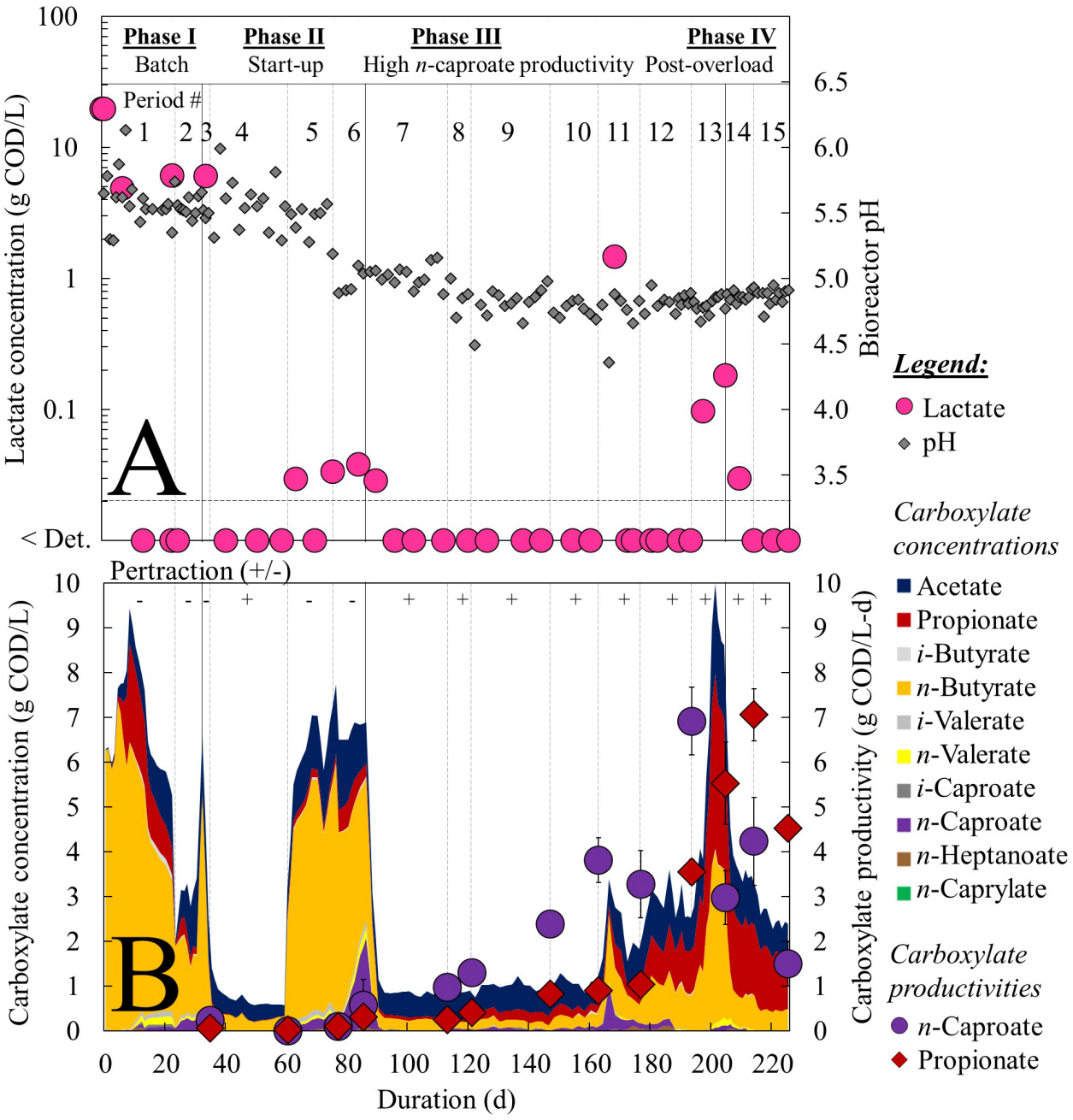

Figure 3.3: **Bioreactor broth concentrations, pH, and carboxylate productivities.** Concentrations of lactate (A) and other carboxylates (B) in the bioreactor broth were determined from samples collected every other day or daily. Bioreactor pH (A) and average productivities of *n*-caproate and propionate (B) were also determined. Operating phases, operating periods, and presence (+) or absence (-) of product recovery *via* in-line pertraction are indicated. Detection limits were 0.02 g COD/L (0.2 mM) for lactate and approximately 0.02 g COD/L (~0.1 mM) for other carboxylates.

Continuous *n*-caproate production for over 165 days was observed in this study (Figure 3.3). Importantly, in-line pertraction was used throughout Phase III, and more than 95% of the *n*-caproate produced was recovered *via* pertraction. To my knowledge, this is the first demonstration of lactate to *n*-caproate conversion in a continuously fed bioreactor, while it is the second demonstration of *n*-caproate production with exogenous lactate in a reactor microbiome (Zhu et al., 2015). In a very early batch study with *M. elsdenii*, the reported productivity of *n*-caproate from lactate was 8.5 g COD/L-d, but the duration of fermentation for which this productivity was calculated was only 45 min (Ladd, 1959). Therefore, the maximum *n*-caproate productivity of 6.9 g COD/L-d that I achieved represents the highest sustained conversion rate of lactate to *n*-caproate. However, this maximum rate remains lower than the *n*-caproate productivities (123.1 g COD/L-d) from bioreactors that were continuously fed ethanol (Grootscholten et al., 2013d).

3.3.2 L-Lactate was converted to n-*caproate during startup, but* n-*caproate productivity was low*

Before reaching the maximum *n*-caproate productivity in Phase III (Period 12), the bioreactor was operated in a sequence of operating phases and periods. In Phase I, the bioreactor was batch-fed and pertraction was not used. The initial L-lactate concentrations for the batches in Phase I (Periods 1 and 2) were 19.7 and 6.1 g COD/L (205 and 64 mM), respectively, and the operating pH was maintained at 5.5 (Figure 3.3A). The second of these two batch periods (Phase I, Period 2, Days 22-30) led to some *n*-caproate accumulation (0.2 g COD/L, 1 mM) (Figure 3.3B). This result indicated that microbial conversion of L-lactate to *n*-caproate was active; therefore, I initiated continuous feeding of media containing L-lactate and *n*-butyrate during Phase II.

The initial continuous feeding rate was high for the first four days of Phase II, corresponding to a short HRT of 0.7 d (Phase II, Period 3, Days 30-33) (Table 3.2). Soon thereafter, the media feed rate was decreased to provide a longer HRT of 1.4 d (Phase II, Period 4, Days 33-59), and the HRT was maintained at an average of 1.5±0.1 d throughout the remainder of the experiment. Consequently, to vary the L-lactate loading rate and the total OLR without varying the HRT, the concentrations of L-lactate (3-24 g COD/L, 30-250 mM) and *n*-butyrate (1-20 g COD/L, 8-125 mM) in the basal media were adjusted (Table 3.2). The concentration of yeast extract in the media was consistently 1.6 g COD/L (1.25 g/L), corresponding to an average yeast extract loading rate of 1.1 g COD/L-d. This yeast extract loading was fed in excess. For commercial applications, optimization to determine the minimum required yeast extract loading rate (or replacement with nutrients contained in complex waste substrates) would be necessary.

Once the HRT was increased from 0.7 to 1.4 d during Phase II, the initial L-lactate loading rate was 2.3 g COD/L-d (Phase II, Period 4, Days 33-59) (Table 3.2). After pertraction was initiated on Day 33 (Phase II, Period 4), the residual lactate was consumed to levels below the detection limit (<0.02 g COD/L, <0.2 mM) (Figure 3.3A). The carboxylate concentrations in the bioreactor broth also declined, and consisted primarily of acetate and *n*-butyrate (Figure 3.3B). However, these 26 days of the operating period (Phase II, Period 4) were marked by failure to produce *n*-caproate: the concentration of *n*-caproate in the bioreactor broth diminished to below the detection limit (<0.02 g COD/L, <0.1 mM); the pertraction system did not recover *n*-caproate and its productivity declined to zero. Due to the lack of *n*-caproate production, the pertraction system was turned off in Period 5. In Period 5, the L-lactate and total organic loading rates were maintained at similar levels as those in Period 4, and residual lactate concentrations in

the bioreactor increased slightly above the detection limit to 0.03 g COD/L (0.3 mM) (Figure 3.3A) (Phase II, Period 5, Days 60-75). The concentrations of all carboxylates in the bioreactor broth increased once pertraction was turned off, and *n*-butyrate was the dominant carboxylate observed (Figure 3.3B). However, some *n*-caproate was also observed in the bioreactor broth, corresponding to an *n*-caproate productivity of 0.1 g COD/L-d.

3.3.3 Lowering the pH led to increased n-*caproate productivities*

The *n*-caproate productivity increased considerably once the operating pH was decreased from 5.5 to 5.0 (Figure 3.3) (Phase II, Period 6, Days 76-84). The impetus for this change was based on the low productivities that had been reached thus far, and the rationale for decreasing the pH was based on observations from the literature. In a previous study of rumen bacteria, only *M. elsdenii* was able to grow and continue to utilize lactate at pH values below 5.5, growing even at pH values as low as 4.7 (Counotte and Prins, 1981). Moreover, in another study of *M. elsdenii*, the absence of *n*-caproate production was reported for a bioreactor operated at pH 6.5 and continuously fed DL-lactate at a lactate loading rate of 10.1 g COD/L-d (Prabhu et al., 2012). It was hypothesized that if I lowered the pH to 5.0, perhaps bacteria such as *M. elsdenii*, which at the time was the only known microbe capable of converting lactate into *n*-caproate, would be able to outcompete other lactate-utilizing microbes and direct its metabolism to increase *n*-caproate productivity.

This strategy worked: when I decreased the pH from 5.5 to 5.0 (Figure 3.3A), the average *n*-caproate productivity increased from 0.1 to 0.6 g COD/L-d (Figure 3.3B) (Phase II, Period 6, Days 76-84). The net productivities of other carboxylates (*e.g.*, *n*-butyrate, propionate) remained consistent with the rates achieved at similar OLRs during Period 5, and the residual lactate concentrations (0.04 g COD/L, 0.4 mM) were also similar. The marginal differences in loading

rates were insufficient to explain this 6x increase in *n*-caproate productivity. The *n*-caproate concentration in the bioreactor broth accumulated to ~2 g COD/L (8 mM), corresponding to an undissociated *n*-caproic acid concentration of less than ~1 g COD/L (3 mM). This concentration of undissociated *n*-caproic acid was lower than concentrations previously hypothesized to induce product inhibition (1.8 g COD/L, 7 mM) (Ge et al., 2015). To prevent *n*-caproic acid concentrations from subsequently increasing to inhibitory levels, the pertraction system was turned on to start Phase III.

3.3.4 Use of pertraction increased n-*caproate productivity*

Before using pertraction, *n*-caproate productivity was observed at rates up to 0.6 g COD/L-d (Figure 3.3B, Phase II, Period 6, Days 76-84). When the pertraction system was turned on, the *n*-caproate productivity increased from 0.6 to 1.0 g COD/L-d at an equivalent L-lactate loading rate (2.6 g COD/L-d) (Phase III, Period 7, Days 84-112). This indicates that although pertraction was not required for *n*-caproate production, the use of pertraction improved productivity considerably. In previous work, this in-line product recovery system had decreased the impacts of product toxicity (Agler et al., 2012a), especially at operating pH values at and below 5.5, and had consistently improved *n*-caproate productivity (Ge et al., 2015). Furthermore, residual concentrations of lactate and total carboxylates decreased in the bioreactor broth once pertraction was turned on (Figure 3.3). However, for a system with in-line product recovery, lower concentrations of products do not necessarily correspond to lower production rates (Figure 3.3B). For example, although average *n*-caproate concentrations decreased from 0.91 to 0.20 to 0.05 g COD/L (4 mM to 1 mM to 0 mM) (Figure 3.3B, Table 3.1) from Period 6 to Period 7 to Period 8, respectively, the *n*-caproate productivities increased from 0.6 to 1.0 to 1.3 g COD/L-d (Figure 3.3B, Table 3.2) (Phase II, Period 6 to Phase III, Period 8, Days 76-120).

3.3.5 Increased L-lactate loading rates led to linear increases in n-*caproate productivities*

During Phase III, when the L-lactate loading rate was steadily increased from 2.6 g COD/L-d to 9.1 g COD/L-d, the *n*-caproate productivity increased linearly (Figure 3.2). Overall, steady operating conditions were experienced for most of Phase III. One key exception was due to a large disturbance on Day 166 (Figure 3.3) (Phase III, Period 11). This anomaly was caused by an air intrusion upstream of the bioreactor recycle pump, which evacuated the bioreactor and pertraction system of liquid and largely filled the system with air. The perturbations led to reduced bioreactor volumes and temporarily increased concentrations of lactate (Figure 3.3A) and other carboxylates (Figure 3.3B). The bioreactor pH was upset to a temporary value of ~3.9, but the system recovered to steady operating conditions within one HRT period.

During steady operating conditions, gas production was observed, and the concentrations of carbon dioxide and methane increased steadily with increasing loading rates (Figure 3.4). In the conversion of lactate to *n*-caproate, the intermediate three-carbon pyruvate is converted to the two-carbon acetyl-CoA, releasing an equimolar amount of carbon dioxide (Figure 3.5). The carbon dioxide observed was probably from the added lactate (62 to 505 mM/d) instead of from the sodium carbonate added (0.2 mM/d). The hydrogen gas concentration in the headspace (typically below 10 ppm) was likely maintained at low levels by hydrogenotrophic methanogens. The pH was maintained near 5.0 for most of this study, which would have inhibited acetoclastic methanogens. Finally, unsubstantial production of *n*-heptanoate and iso-carboxylates was observed. Production of *n*-caprylate or longer-chain carboxylates was not observed. Some *n*-valerate, which is a chain elongation product from propionate, was produced, especially during periods when propionate production and residual lactate concentrations were high (Figure 3.3).

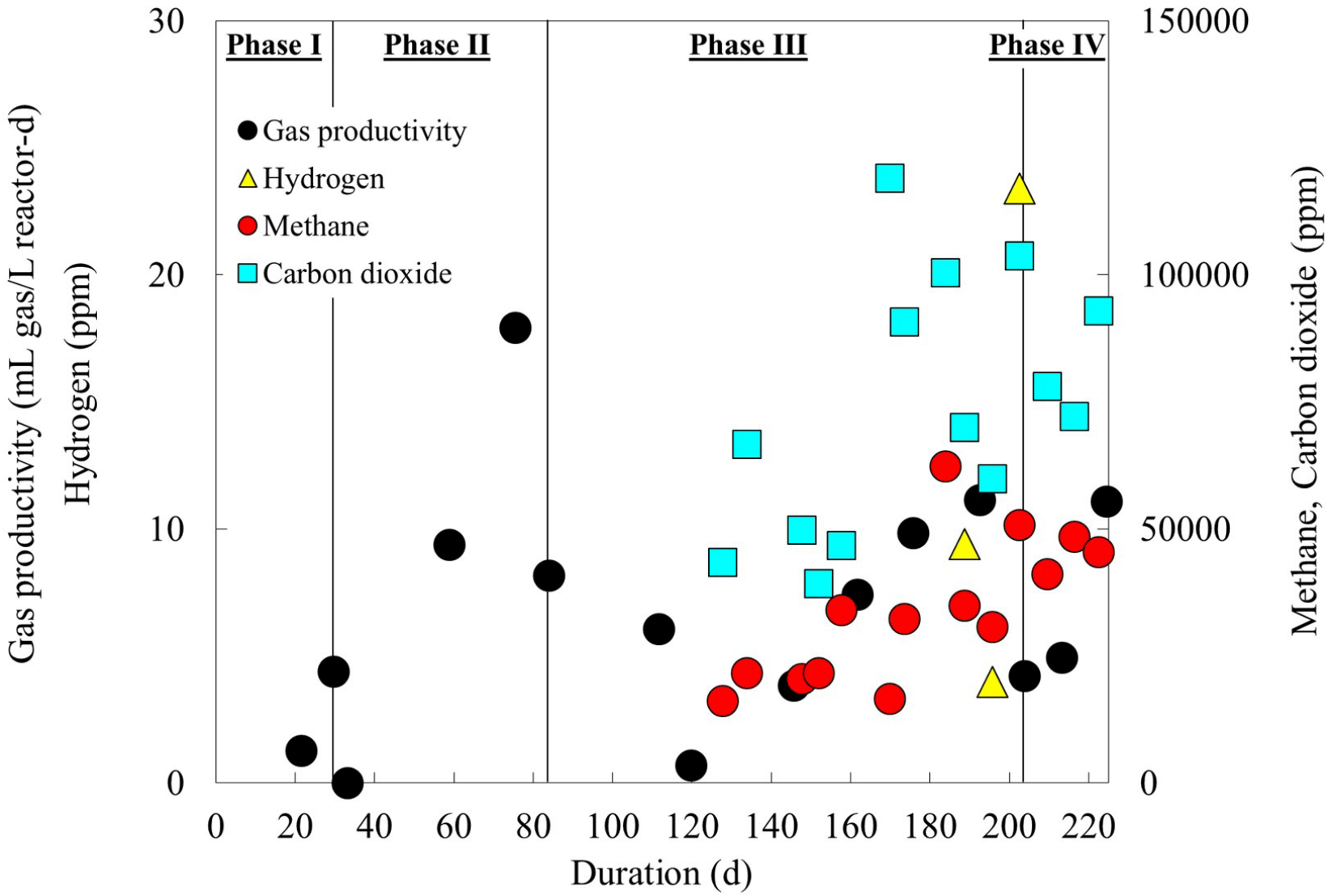

Figure 3.4: Gas productivity and composition throughout operation. Gas productivity along with gas concentrations were determined throughout bioreactor operation. Hydrogen gas concentrations were quantified using the reduced gas detector.

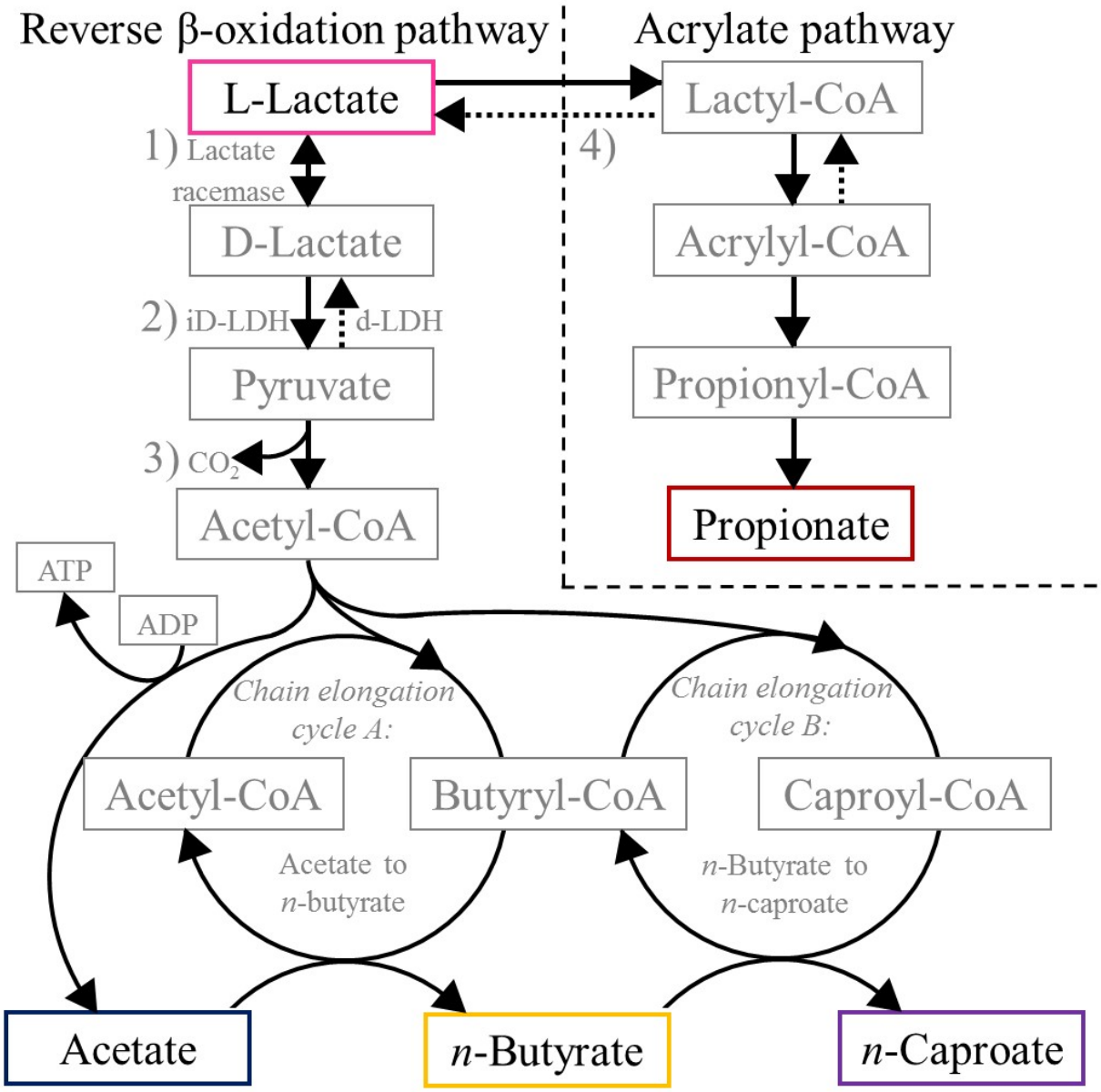

Figure 3.5: Lactate conversion pathways. DL-Lactate can proceed to either *n*-caproate or propionate *via* the reverse β-oxidation pathway or the acrylate pathway, respectively. Based on (Spirito et al., 2014) and (Hino and Kuroda, 1993). [Note: Figure 3.5 is identical to Figure 2.1, but it is replicated here for the convenience of the reader.]

3.3.6 Residual lactate led to production of propionate, but not n*-caproate*

The highest *n*-caproate productivity (6.9 g COD/L-d) was observed when the L-lactate loading rate was 9.1 g COD/L-d. When the L-lactate loading rate was subsequently increased to 16.2 g COD/L-d, the resulting *n*-caproate productivity decreased to 3.0 g COD/L-d (Figure 3.2) (Phase III, Period 13, Days 193-204). To recover from this overloading event, I lowered the L-lactate loading rate from 16.2 to 10.1 g COD/L-d (Phase IV, Period 14, Days 204-213), but the *n*-caproate productivity never recovered (Figure 3.3B). While *n*-caproate productivity decreased following this overloading event, the corresponding propionate productivity reached its highest rate (5.5 g COD/L-d) in Period 13, concluding a linear trend of steady increases with increased L-lactate loading rates throughout Phase III. Propionate productivity increased when *n*-caproate productivity declined due to one key factor: the residual concentration of lactate in the bioreactor broth had increased. The residual lactate concentration began to increase steadily (Figure 3.3A) from below detection to 0.2 g COD/L (2 mM) (Phase III, Period 13, Days 193-204).

Other studies concluded that a low residual concentration of lactate would be necessary to prevent production of propionate *via* the acrylate pathway (Prabhu et al., 2012) (Figure 3.5). Accordingly, L-lactate can then be converted to *n*-caproate *via* the reverse β-oxidation pathway through three steps: 1) L-lactate is first isomerized to D-lactate *via* lactate racemase, which is a reversible and lactate-induced enzyme (Figure 3.5, Step 1); 2) D-lactate is then converted to pyruvate *via* the NAD-independent D-lactate dehydrogenase (iD-LDH), which is a favorable and irreversible reaction as long as pyruvate is consumed in subsequent reactions (Figure. 3.5, Step 2) (Hino and Kuroda, 1993); and 3) pyruvate is converted to acetyl-CoA (Figure 3.5, Step 3), which enters the reverse β–oxidation pathway to chain elongate available SCCs (*e.g.*, acetate) into even-numbered chain elongation products (*e.g.*, *n*-butyrate, *n*-caproate) (Spirito et al., 2014).

In the competing acrylate pathway, L-lactate is converted to propionate (Figure 3.5, Step 4). Under L-lactate-rich conditions, lactyl-CoA forms as an intermediate. When this occurs, a subsequent state to achieve redox balance perpetually generates propionyl-CoA (Prabhu et al., 2012). Consequently, available L-lactate would be continually directed toward propionate production (Prabhu et al., 2012). This explanation suggests that once residual L-lactate concentrations accumulate and induce lactyl-CoA formation, it may be difficult to direct lactate-carbon flux toward pyruvate and even-numbered chain elongation products (*e.g.*, *n*-caproate). Indeed, increased propionate productivity and decreased *n*-caproate productivity were observed *during* and *after* the overloading event in which L-lactate accumulated and induced the acrylate pathway (Phase III, Period 13, Days 193-204). The results of Phase IV (post-overload), thus, confirm that once the acrylate pathway is activated, it is difficult to return to reverse β-oxidation. In addition, these results explain why most batch studies with high initial lactate concentrations do not result in promising *n*-caproate productivities.

Surprisingly, in the first reactor microbiome study in which exogenous lactate was converted into *n*-caproate, no propionate production was reported (Zhu et al., 2015). Their batch-fed systems were operated with lactate constantly in excess, which I expected would induce the acrylate pathway. It is possible that microbes with the competing acrylate pathway had disappeared or were outcompeted based on the unique environmental selection process they employed, but I anticipate that the lack of propionate production is atypical for most lactate-fed reactor microbiome systems. For open-culture bioreactor systems (*e.g.*, wastewater treatment) in which substrate flow consistently introduces diverse bacteria to the reactor microbiome, these results suggest that the acrylate pathway would persist as an important competing pathway that would need to be carefully managed.

3.3.7 Reactor microbiome analyses revealed a surprising absence of M. elsdenii

Reactor microbiome dynamics were also investigated throughout the experiment. Among all samples collected, 1,584 operational taxonomic units (OTUs) were found from high-quality sequence reads. The number of sequences per sample ranged from 35,367 to 139,674 sequences, with a median sequence count of 63,726. 49 OTUs each comprised at least 1% of the relative OTU abundance for one or more samples (Figure 3.6), and these comprised between 84.0 and 94.8% of the total high-quality sequence reads for each sample. The highest observed relative abundance of a single OTU was 63.3% for a Rhodocyclaceae *K82* spp. (Phase I, Period 2, Day 30). During the phase of high *n*-caproate productivity, an *Acinetobacter* spp. was dominant at a relative abundance of 62.9% (Phase III, Period 9, Day 140) (Figure 3.7). While *M. elsdenii* was previously known as the only type strain for which lactate conversion to *n*-caproate had been demonstrated in pure culture, the highest relative abundance observed for *M. elsdenii* was less than 0.01% (Phase III, Period 12, Day 184). Several OTUs with phylogenetic similarities to *M. elsdenii* were detected, including species of *Ruminococcus*, *Oscillospira*, *Clostridium*, and genera from the families Veillonellaceae, Ruminococcaceae, and Clostridiales (Figure 3.6). Of the OTUs detected above 1% relative abundance, an unknown OTU from the family Veillonellaceae was most similar to *M. elsdenii*. Moreover, during the phase of high *n*-caproate productivity (Phase III), the abundance of this OTU was positively correlated with *n*-caproate productivity ($p = 0.005$) (Figure 3.8). Two other OTUs were also positively correlated with *n*-caproate productivity: *Bacteroides* spp. ($p = 0.042$); and *Comamonas* spp. ($p = 0.040$). In the other reactor microbiome study with conversion of exogenous lactate into *n*-caproate, *M. elsdenii* was also scarce or not present (Zhu et al., 2015).

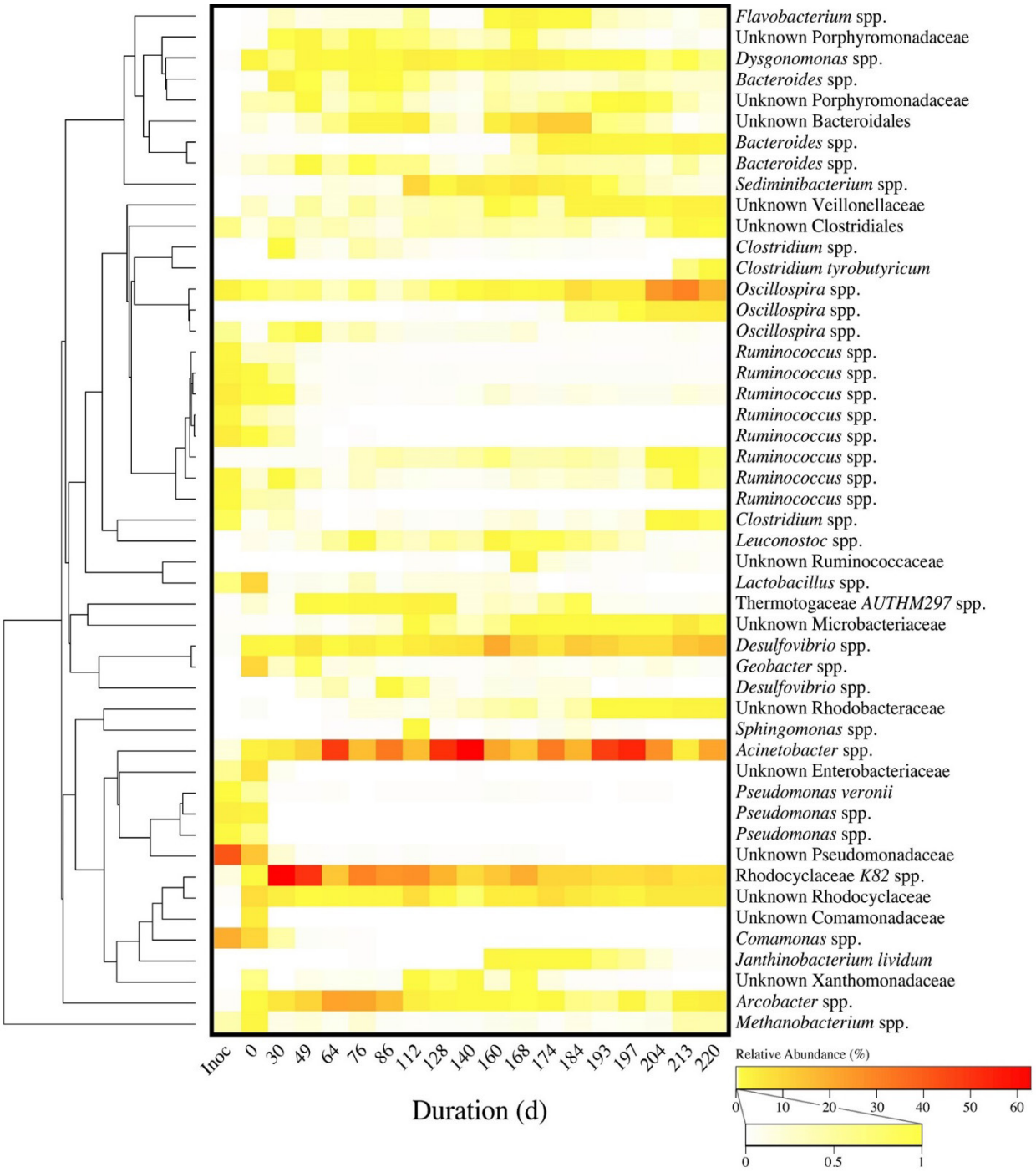

Figure 3.6: OTU relative abundances throughout bioreactor operation. Relative abundances of operational taxonomic units (OTUs) varied throughout bioreactor operation. Each of the 49 OTUs listed comprised at least one percent of the relative abundance for one or more of the samples collected during bioreactor operation, as well as the inoculum. A Rhodocyclaceae *K82* spp. and an *Acinetobacter* spp. were dominant, each comprising up to approximately 63% of the relative abundance. Phylogenetic similarity is indicated.

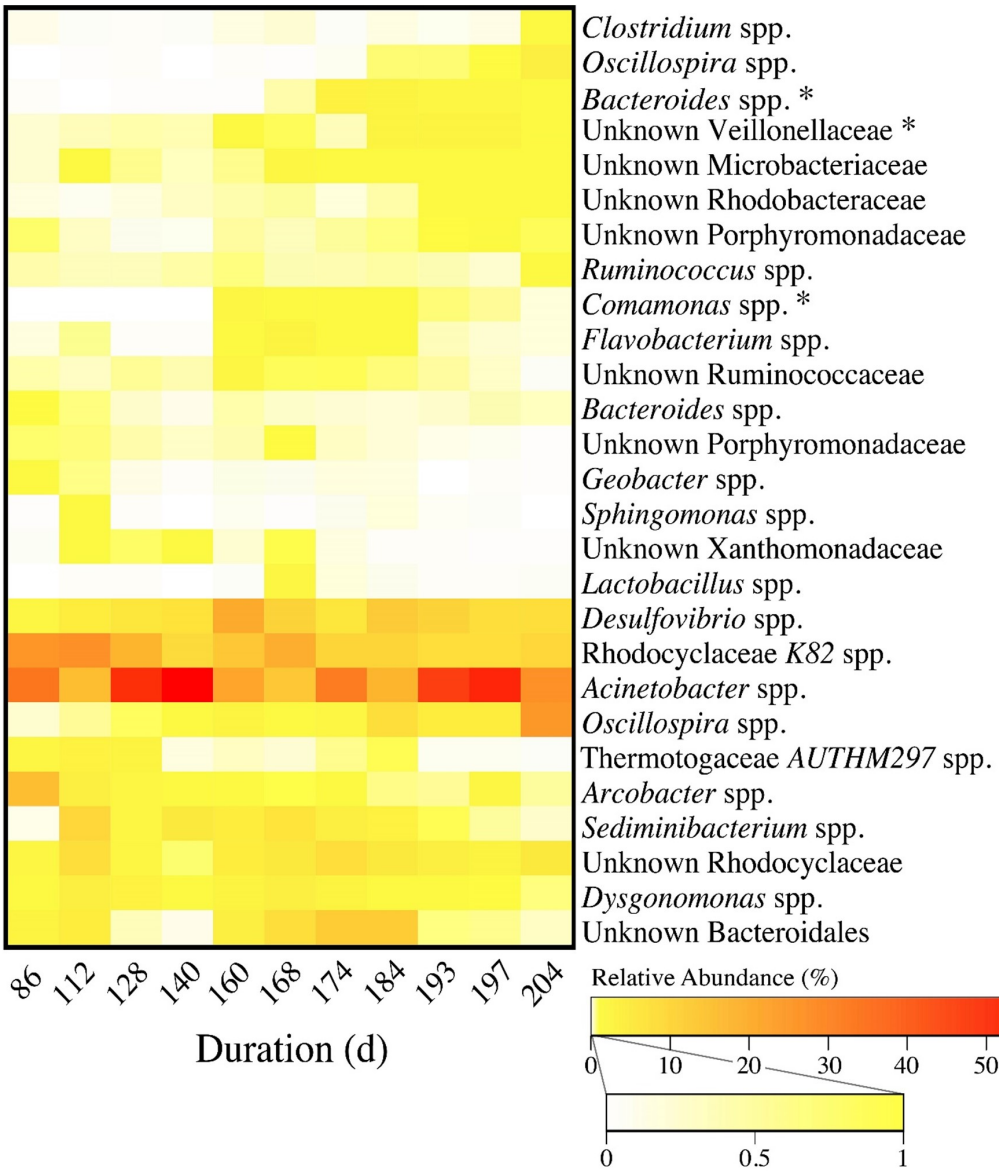

Figure 3.7: **OTU relative abundances during the phase of high *n*-caproate productivity (Phase III).** Relative abundances of operational taxonomic units (OTUs) varied during the phase of high *n*-caproate productivity (Phase III). Each of the 27 OTUs listed comprised at least one percent of the relative abundance for one or more of the samples collected from this phase. OTUs were clustered hierarchically (average linkage) based on the Bray-Curtis dissimilarity index. OTUs were grouped together based on both the average relative abundance and abundance profile throughout the duration of Phase III. This resulted in the localization of OTUs with lower abundances in the top half, and OTUs with higher abundances in the bottom half. Within lower abundant OTUs, several OTUs increased in relative abundance over time, as indicated in the first cluster on top. However, within high abundant OTUs, relative abundance profiles did not indicate any significant trend over time. In Phase III, an *Acinetobacter* spp. was dominant, comprising up to 62.9% of the relative abundance. The relative abundances of three OTUs (marked with asterisks) were correlated ($p<0.05$) with *n*-caproate productivity. Data shown are from Phase III only.

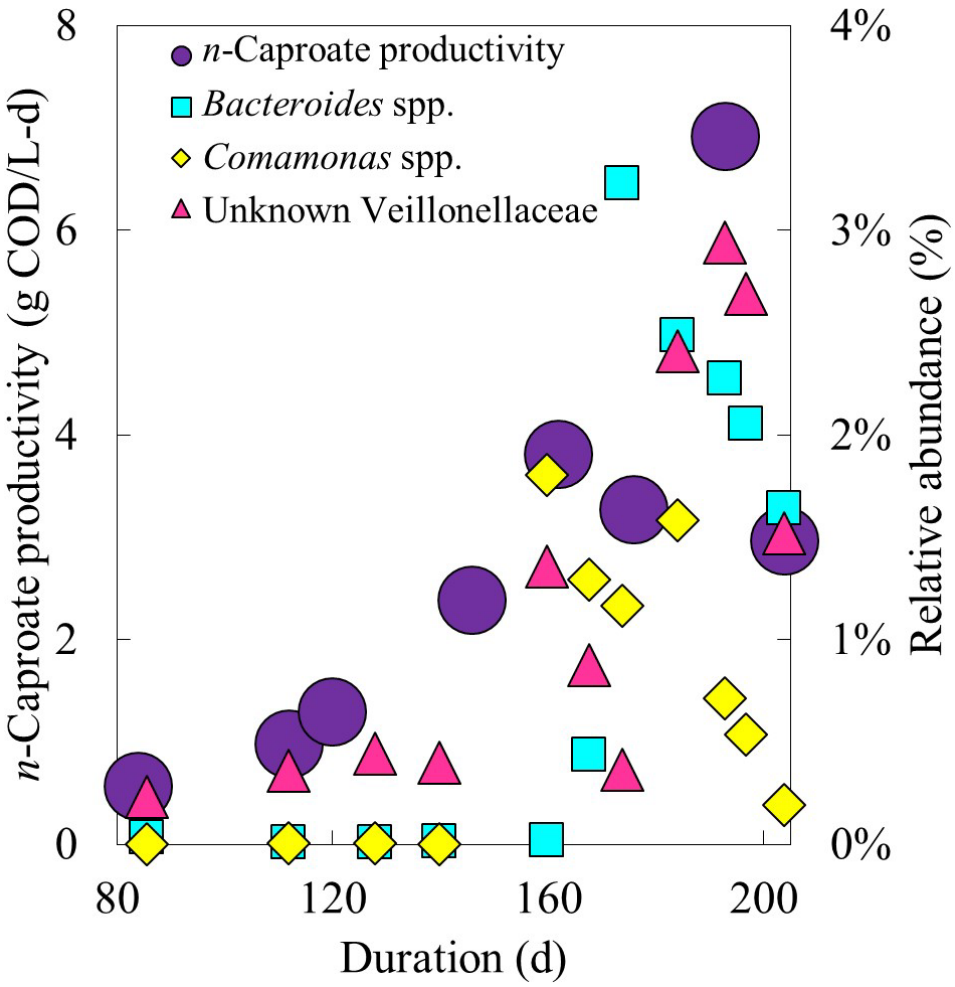

Figure 3.8: Correlation between OTUs and *n*-caproate productivities. Three OTUs (Figure 3.7) were shown to correlate significantly ($p<0.05$) with *n*-caproate productivity.

In this study, no clear trends in alpha diversity were apparent from the Shannon diversity index, suggesting that the richness and evenness of the microbial community at each sampling point remained similar (Figure 3.9). The beta diversity, or dissimilarity of OTU composition between samples, showed that at the onset of overloading, the communities of the final three samples (darkest circles) were distinctly different from early community samples from the bioreactor (light circles) (Figure 3.10). Constrained ordination did not find a correlation between microbial community composition and operating parameters, environmental conditions, or bioreactor performance at significant levels ($p<0.05$).

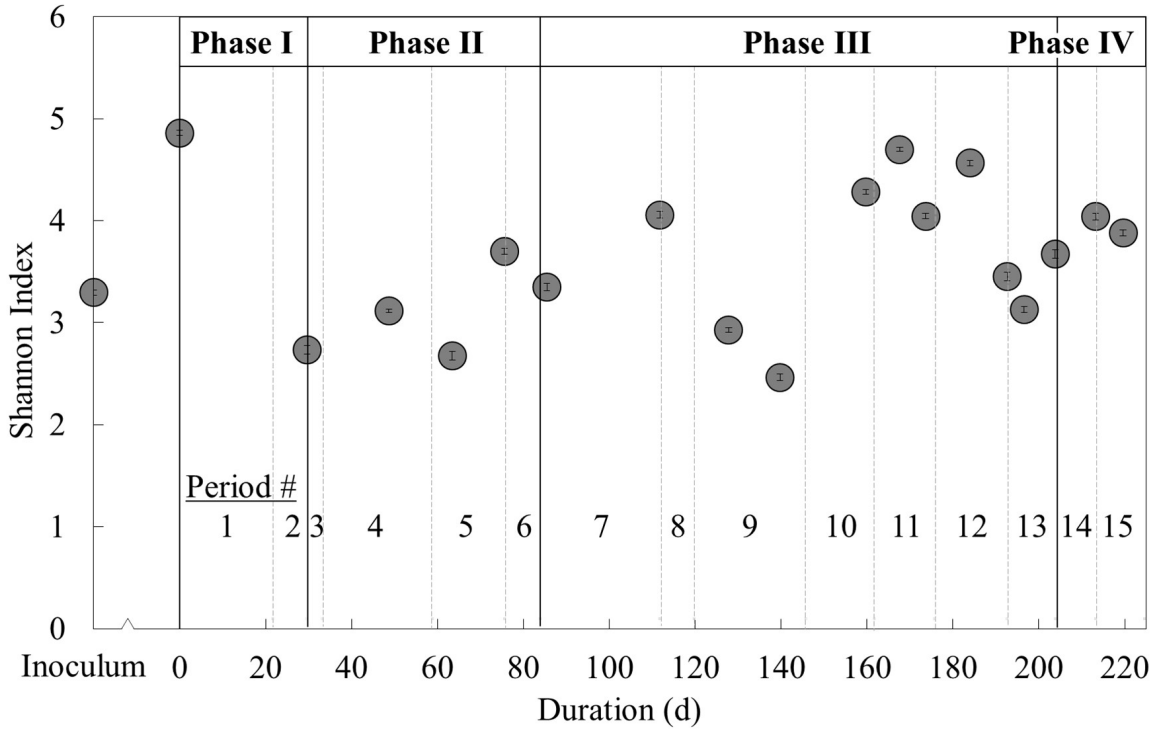

Figure 3.9: Alpha diversity of the reactor microbiome throughout operation. The Shannon index was used to determine the evenness and richness for the 18 samples collected throughout the duration of bioreactor operation, as well as the inoculum sample. Uncertainty is represented by 95% confidence intervals based on ten independent rarefactions.

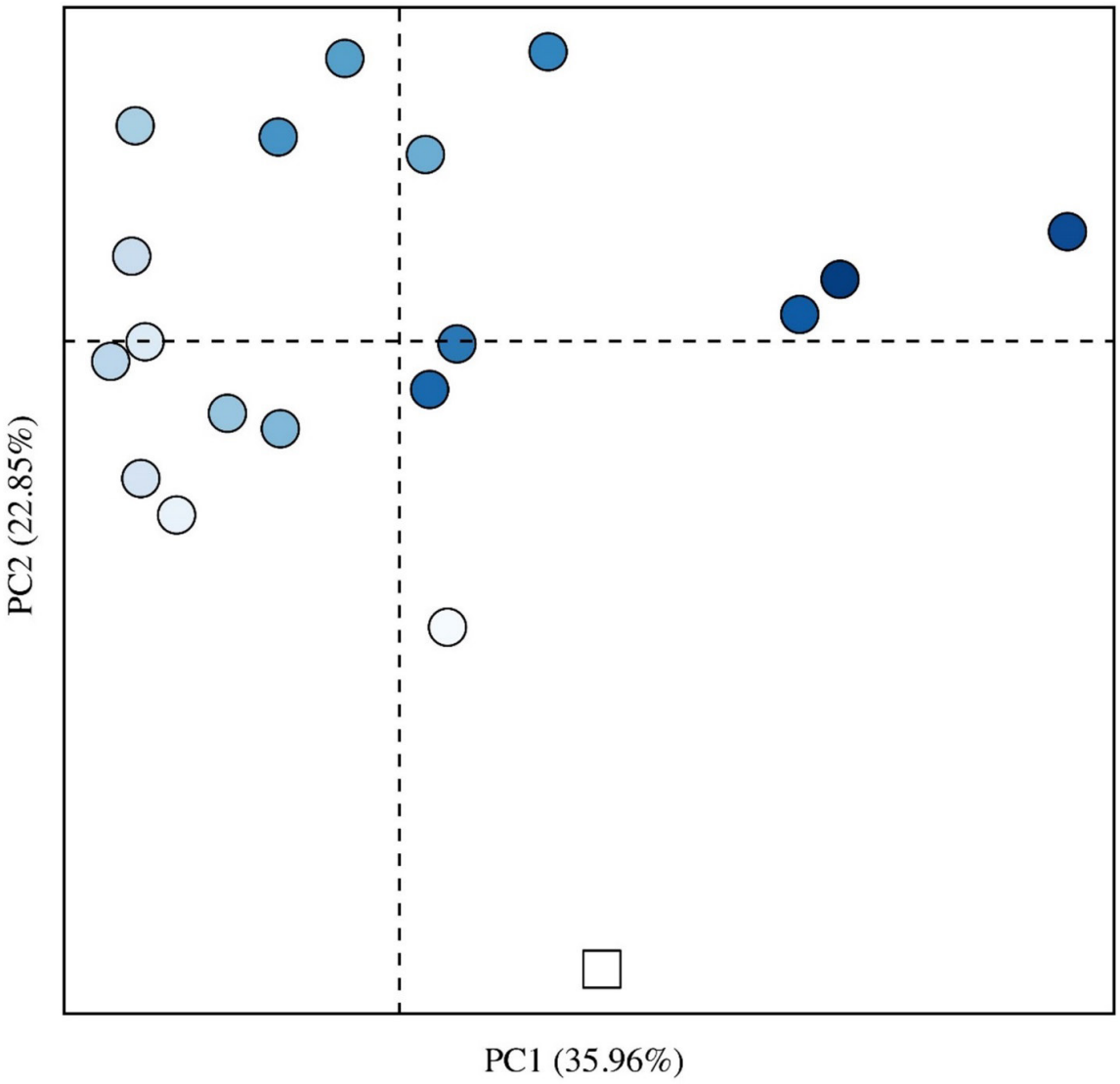

Figure 3.10: Beta diversity of the reactor microbiome throughout operation. Principal coordinates analysis was used to determine the dissimilarity between community samples taken throughout bioreactor operation based on the weighted UniFrac metric. The first two principal coordinate (PC) axes are shown. PC1 explains 36% of the overall phylogenetic variation, while PC2 explains 23%. Darker circles represent samples taken later in bioreactor operation; lighter circles represent earlier samples. The white square represents the inoculum.

3.3.8 Strategy and suggestions for future work

Based on these experimental results, a simplified model is proposed to explain how to direct a lactate-fed system toward improved *n*-caproate productivities (Figure 3.11). First, it was necessary to maintain residual lactate concentrations near zero. Under these conditions, robust *n*-caproate production and restrained propionate production were observed (Figure 3.3, Phase III, Periods 7-12, Days 84-193). Second, these results suggest that operating at pH values near 5.0 may be necessary for conversion of lactate into *n*-caproate in most reactor microbiomes. Specifically, when I decreased the operating pH from 5.5 to 5.0, the *n*-caproate productivity increased from approximately 0.1 to 0.6 g COD/L-d (Phase II, Period 6, Days 76-84). Finally, the use of pertraction increased the *n*-caproate productivity with all other parameters held constant. At longer HRTs, the importance of this pertraction system would be increasingly essential because of the lower dilution rates of the inhibiting undissociated carboxylic acids.

When L-lactate was fed continuously to a bioreactor, the L-lactate-derived carbon flux was primarily towards reverse β-oxidation products (*e.g.*, *n*-butyrate, *n*-caproate). If I had fed D-lactate or DL-lactate at an equivalent lactate loading rate, the *n*-caproate productivity would have probably been at least equal, if not superior, to those observed with L-lactate. This is because the extra metabolic step from L-lactate to D-lactate *via* lactate racemase would not have been required, and also because lactate racemase has been described as potentially rate-limiting in the conversion of L-lactate to D-lactate (Hino and Kuroda, 1993).

Finally, this research supports future efforts using real wastes as substrates. Specifically, wastes containing high lactate concentrations (*e.g.,* fermented food processing wastes) or with high concentrations of precursors to lactate (*e.g.,* carbohydrate-rich food processing wastes) should be evaluated. The upflow anaerobic filter is designed primarily for low-solids substrates;

initial efforts could focus on waste effluents with high loading from dissolved lactate or carbohydrates. Waste carbon can be directed towards *n*-caproate instead of lower-value products by applying the findings of this study. Consequently, new applications are now possible for chain elongation technologies within the carboxylate platform to promote effective resource recovery.

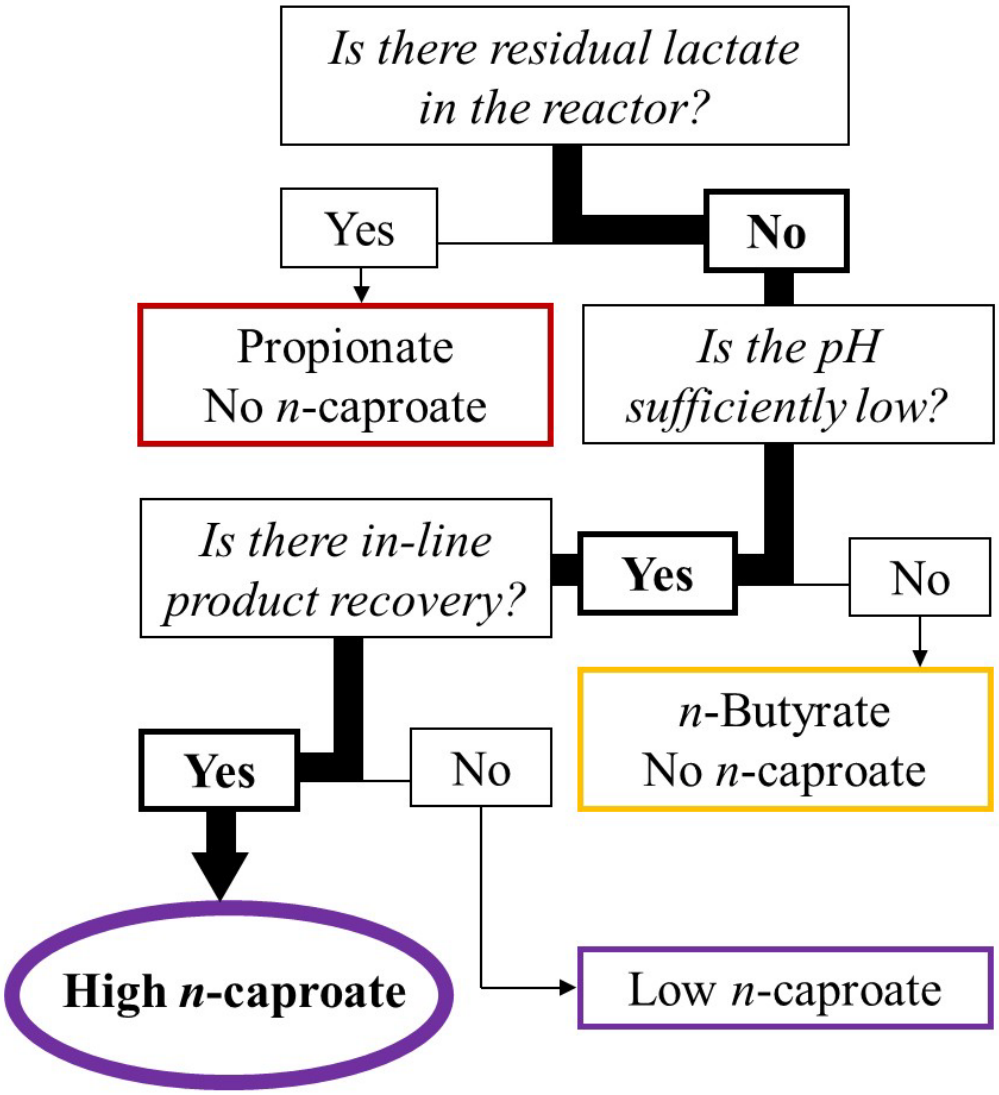

Figure 3.11: Lactate to *n*-caproate decision tree. A simplified model is presented to evaluate if operating conditions are favorable for conversion of lactate to *n*-caproate. For high-rate *n*-caproate productivity, the experimental results suggest the following conditions: 1) low residual lactate concentrations (<0.02 g COD/L, <0.2 mM); 2) low bioreactor pH (<5); and 3) sufficient *n*-caproate recovery (>95% recovery). Lactate-utilizing chain-elongating microbes must also be functional and abundant.

3.4 Conclusions

- *n*-Caproate production from lactate was demonstrated in a continuously fed bioreactor.
- The maximum *n*-caproate productivity of 6.9 g COD/L-d was achieved with a reactor microbiome.
- Low residual lactate concentrations in the bioreactor broth, a bioreactor broth pH of 5, and the use of pertraction were all key operating parameters for effective conversion of L-lactate to *n*-caproate.
- The reactor microbiome was diverse and showed an *Acinetobacter* spp. to be abundant during periods of high *n*-caproate productivity while the type strain *M. elsdenii* was nearly absent.
- This study promotes consideration of real waste streams for use in the carboxylate platform to produce MCCs, including those rich in lactate or lactate-precursors (*e.g.*, carbohydrates).

3.5 Acknowledgements

16S rRNA sequence data and metadata are available on QIITA (http://qiita.microbio.me; study ID 10281) and the EBI database (www.ebi.ack.uk, accession number: in submission). This work was supported by the NSF SusChEM Program (Award # 1336186), as well as by the U.S. Army Research Laboratory and the U.S. Army Research Office (Contract/Grant number W911NF-12-1-0555), which were awarded to L.T.A. L.A.K. was supported by the NSF through the Graduate Research Fellowship Program (GRFP), and by Cornell University's graduate school. M.N. was supported by the Sloan Foundation. The authors wish to thank Prof. Jim Gossett (Cornell University) for his careful review of the manuscript. Gratitude is also expressed for assistance from Divya Vasudevan, Catherine Spirito, Lauren Harroff, and Dr. Jiajie Xu.

CHAPTER 4

N-CAPRYLATE PRODUCTION FROM DILUTE ETHANOL AND ACETATE USING REACTOR MICROBIOMES: INTEGRATION OF THE CARBOXYLATE AND SYNGAS PLATFORMS

Adapted from a manuscript by Leo A. Kucek, Catherine M. Spirito, and Largus T. Angenent

(In preparation for submission to Energy and Environmental Science)

Abstract

The carboxylate and syngas platforms can be integrated to convert diverse waste carbon into valuable liquid products, including *n*-caproate and *n*-caprylate. Production of *n*-caprylate was demonstrated in bioreactors previously, but the reported *n*-caprylate volumetric production rates (productivities) and product ratios of *n*-caprylate to *n*-caproate were consistently low, which relegated *n*-caprylate to merely a by-product of *n*-caproate production. *n*-Caprylate is more valuable than *n*-caproate due to its longer carbon chain, which is advantageous for the production of energy-dense and hydrophobic liquid fuels and chemicals. The hydrophobicity of undissociated *n*-caprylic acid can also inhibit its production. In the present study, *n*-caprylate production was sustained in a continuously fed reactor microbiome. The *n*-caprylate productivity increased to 19.4 g COD/L-d, and the corresponding product ratio of *n*-caprylate to *n*-caproate reached 11 g COD/g COD. When the organic loading rate was increased beyond 34.7 g COD/L-d, the concentration of residual undissociated *n*-caprylic acid increased to an inhibitory level of 0.22 g COD/L (0.6 mM). The productivity, product ratio, and undissociated concentration that were achieved were higher than previous reports in the literature. Improved *n*-caprylate production was based on the utilized substrate levels and in-line product recovery (*i.e.*, pertraction) system. This study promotes the development of resource recovery processes that integrate the syngas and carboxylate platforms.

4.1 Introduction

Sustainable production of liquid fuels and chemicals is one of the great challenges of the 21st century (Chu and Majumdar, 2012). Innovations in renewable power utilization are expected to offset gasoline consumption for personal vehicles, but replacement of diesel and aviation fuels will require energy-dense hydrophobic liquids (Vennestrøm et al., 2011). Furthermore, sustainable hydrophobic chemicals will be necessary substitutes for conventional petrochemicals (Tuck et al., 2012). Utilizing wastes as feedstocks for these products can reduce the ecological, social, and economic costs associated with first-generation renewable fuels and chemicals (Hill et al., 2006). Therefore, new resource recovery processes should be developed to convert wastes into sustainable liquid fuels and chemicals (Bond et al., 2014).

4.1.1 Integration of the carboxylate and syngas platforms

Several platforms, including the carboxylate and syngas platforms, already exist to convert complex wastes into sustainable gaseous fuels and chemicals. In the carboxylate platform, complex organic material is converted into carboxylate intermediates from which final fuel and chemical products are derived (Agler et al., 2011). The most common example of a carboxylate platform technology is anaerobic digestion. Herein, reactor microbiomes (Agler et al., 2012b) (open cultures of microbial consortia) ultimately convert wastes with high chemical oxygen demand (COD) into methane-rich biogas (Zhang et al., 2014). The relatively low value of biogas often delays economic payback (Angenent and Kleerebezem, 2011), however, and recalcitrant wastes such as forestry residues are difficult to digest (Buffiere et al., 2006).

The syngas platform converts diverse feedstocks, including forestry residues and other recalcitrant wastes, into carbon monoxide- and hydrogen-rich syngas *via* thermochemical processes (Laird et al., 2009). Some industrial flue gasses, such as those from steel processing,

can also serve as sources of syngas (Köpke et al., 2011). Syngas can be converted into liquid products (*e.g.*, ethanol, acetate) *via* microbial fermentation (Richter et al., 2013), but conventional product recovery using energy-intensive distillation can be cost-prohibitive for recovery of dilute ethanol. Alternatively, integration of the syngas and carboxylate platforms could upgrade dilute ethanol and acetate from syngas fermentation effluent to higher-value liquid products, such as medium-chain carboxylates (Vasudevan et al., 2014) (Figure 4.1).

4.1.2 Production of n-*caproate and* n-*caprylate* via *the reverse β-oxidation pathway*

Medium-chain carboxylates (MCCs, ranging from six to twelve carbons) (Xu et al., 2015) can be produced within the carboxylate platform by chain-elongating short-chain carboxylates (SCCs, ranging from two to five carbons), such as acetate, *via* the reverse β–oxidation pathway (Spirito et al., 2014) (Figure 4.2). Throughout the text, I use the term carboxylates to refer generally to the combination of dissociated carboxylates and the corresponding undissociated carboxylic acids. To provide the energy required for this chain elongation, addition of an electron donor is necessary. Several electron donors have been used to produce *n*-caproate, including ethanol (Grootscholten et al., 2013d); carbohydrates (Ding et al., 2010); polyols (Jeon et al., 2013); and lactate (Zhu et al., 2015). Ethanol-fed bioreactors have achieved the highest volumetric production rates (productivities) reported (Figure 2.1) (Grootscholten et al., 2013d). Although MCC production from ethanol-rich crop processing streams has already been demonstrated (Agler et al., 2012a), waste-derived syngas fermentation effluent provides an emerging source of dilute ethanol for the sustainable production of MCCs (Vasudevan et al., 2014).

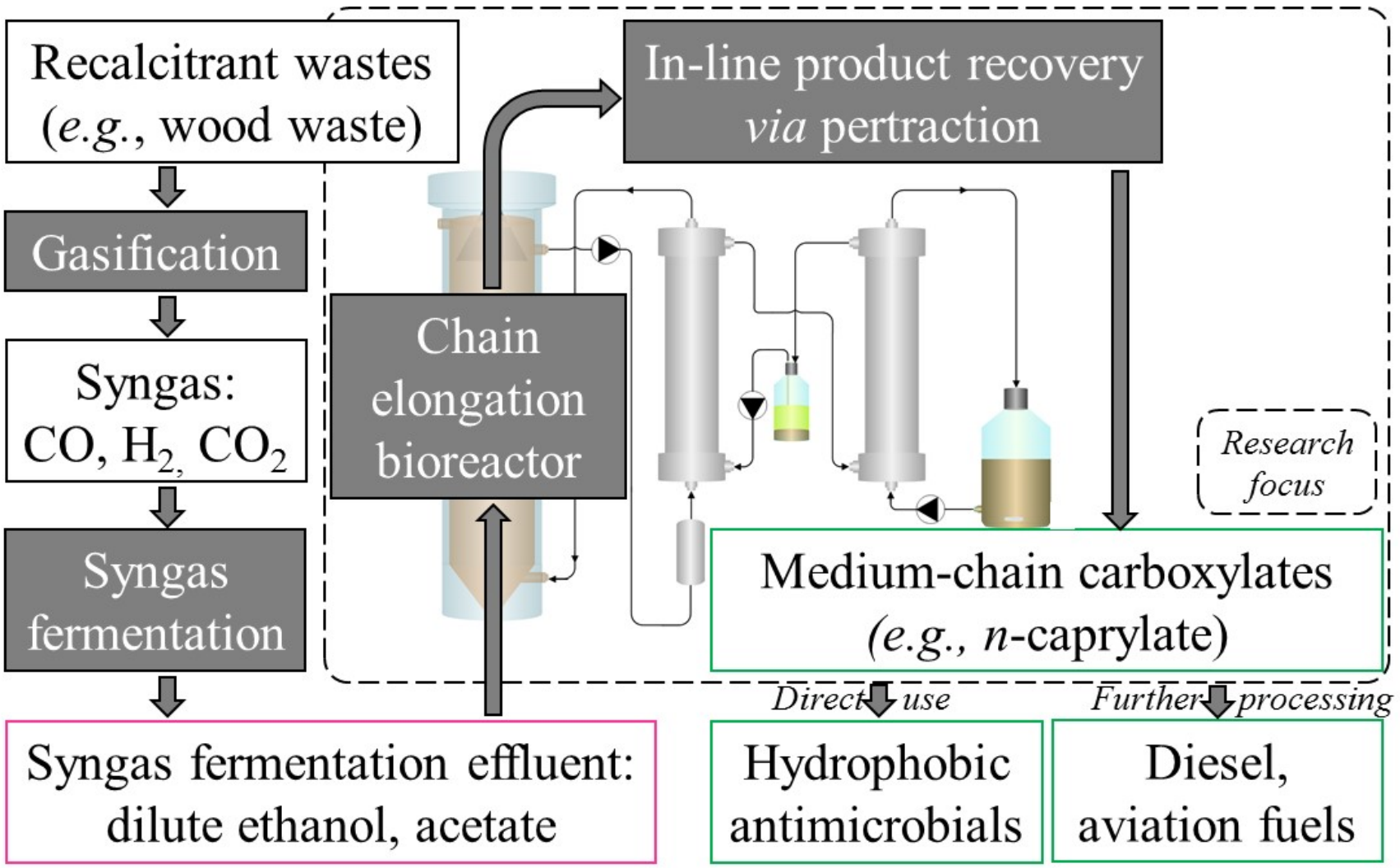

Figure 4.1: Integration of the carboxylate and syngas platforms. Through platform integration, sustainable energy-dense fuels and hydrophobic chemicals can be produced from recalcitrant lignocellulosic wastes.

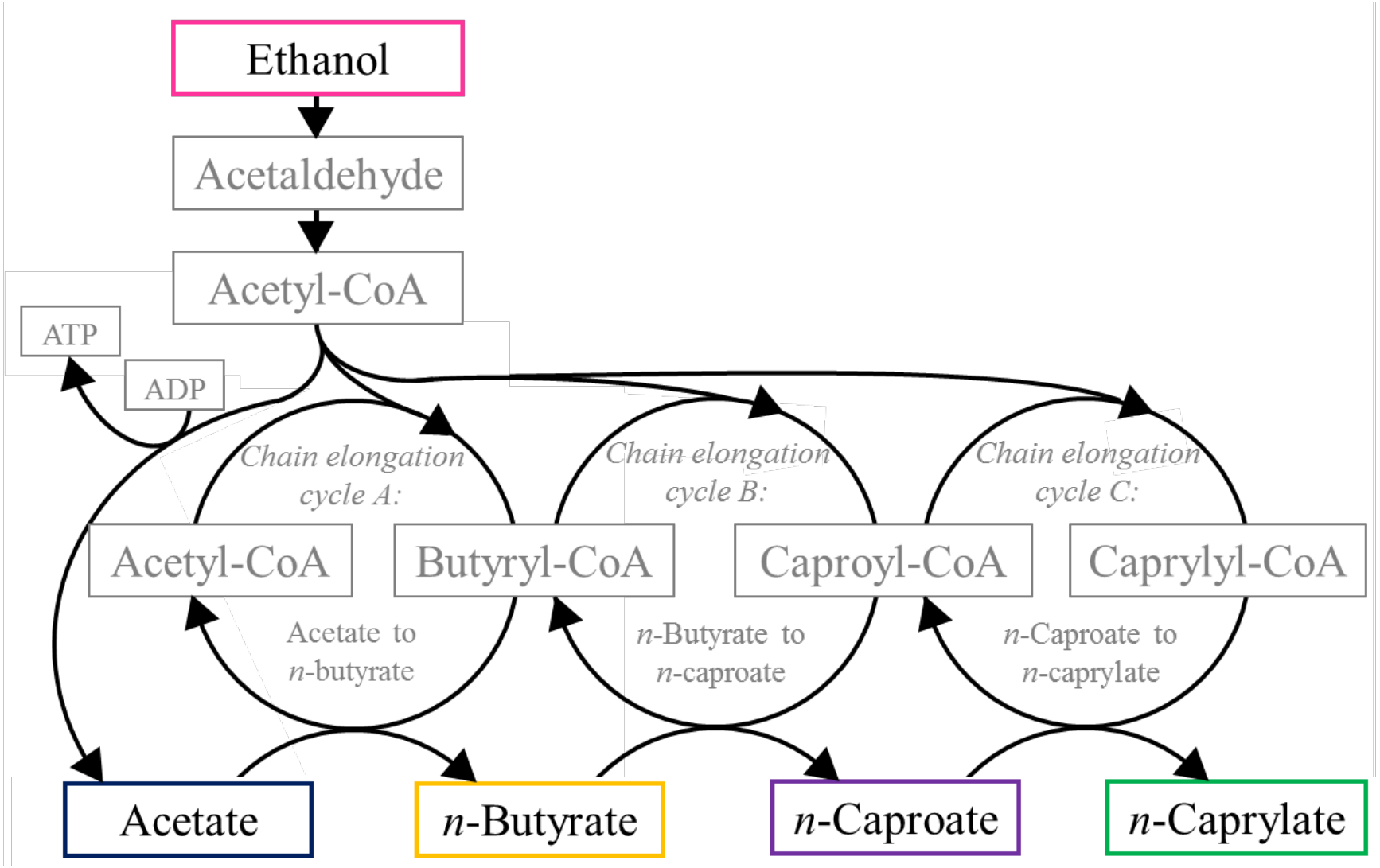

Figure 4.2: The reverse β-oxidation pathway. With the addition of ethanol, short-chain carboxylates (*e.g.,* acetate) can be chain elongated to medium-chain carboxylates (e.g., *n*-caprylate). Based on (Spirito et al., 2014).

n-Caproate and *n*-caprylate are two MCCs currently valued as specialty chemicals, and these chemicals have been considered for use in a variety of markets. Proposed applications include utilization as antimicrobial agents in agriculture (Desbois, 2012), as intermediates for fragrances and flavors (Kenealy et al., 1995), and as precursors for long-chain renewable diesel (Levy et al., 1981) and aviation fuels (Harvey and Meylemans, 2014). In all of these markets, a premium is available for longer-chain products (*e.g.*, *n*-caprylic acid) due to their increased hydrophobicity and energy density (Van Eerten-Jansen et al., 2013). Thus, while production of *n*-caproate has great potential, the prospects for *n*-caprylate production are even greater.

n-Caproate has been produced at productivities up to 123.1 g COD/L-d (Grootscholten et al., 2013d), but *n*-caprylate production has been limited (Figure 2.4). When *n*-caprylate production within reactor microbiomes was first reported, the maximum *n*-caprylate productivities observed were lower than 0.14 g COD/L-d (Steinbusch et al., 2011). Substantial improvements in *n*-caprylate productivity were reported by Grootscholten and his colleagues (Grootscholten et al., 2013b, Grootscholten et al., 2013d). In a continuously fed upflow anaerobic filter operated at short hydraulic retention times and at neutral pH, they observed *n*-caprylate productivities up to 4.4 g COD/L-d (Grootscholten et al., 2013d).

4.1.3 Product inhibition can limit bioreactor productivities of n-*caprylate and* n-*caproate*

Product inhibition is a central challenge for MCC production *via* fermentation systems because undissociated medium-chain carboxylic acids (MCCAs) can inhibit microbial activity (Desbois, 2012). Undissociated MCCAs (*e.g.*, *n*-caproic acid, *n*-caprylic acid) are hydrophobic, and hydrophobicity increases for MCCAs with longer carbon chains (Steinbusch et al., 2011). These MCCAs can therefore: penetrate the hydrophobic lipid membranes of microbial cells; dissociate into corresponding MCCs and protons; and exhaust cellular efforts of expelling excess

protons to maintain a neutral pH in the cytoplasm (Skrivanova et al., 2006). In MCC-producing bioreactor systems, accumulated MCCAs can therefore stall bioreactor productivity through product inhibition.

Two approaches have emerged to overcome product inhibition and increase MCC bioreactor productivity: 1) a neutral pH system with inhibition of methanogens *via* chemical addition (Steinbusch et al., 2011) or very short HRTs (Grootscholten et al., 2013d); and 2) a low pH system with in-line product recovery (Agler et al., 2012a). In the second approach, which was employed in the present study, the overall product recovery (transfer) rate for an individual MCC (*e.g.*, g *n*-caprylate-COD/d) is proportional to the concentration of an individual undissociated MCCA in the bioreactor broth (*e.g.*, g undissociated *n*-caprylic acid-COD/L). Therefore, increased residual MCCA concentrations in the bioreactor broth would lead to higher MCC product recovery and total production rates, unless the increased concentrations also lead to product inhibition.

4.1.4 Minimum inhibitory concentrations of n-*caproic acid and* n-*caprylic acid are unknown*

Little is currently known about the minimum inhibitory concentrations at which undissociated MCCAs will inhibit microbial activity. In lieu of minimum inhibitory concentration data, a literature review was conducted to determine the maximum reported concentrations of *n*-caproic acid and *n*-caprylic acid. For undissociated *n*-caproic acid (Figure 2.2), the highest accumulated concentrations from bioreactors that were fed carbohydrates (2.8 to 5.1 g COD/L, 12 to 20 mM) (Gómez et al., 2009, Zhao et al., 2008, Wang et al., 2007) or ethanol (2.7 g COD/L, 10.5 mM) (Ge et al., 2015) ranged from 11 to 22% of the solubility limit of undissociated *n*-caproic acid (23.8 g COD/L, 93 mM) (Xu et al., 2015). By comparison, the highest reported level of undissociated *n*-caprylic acid was less than 0.08 g COD/L (0.21 mM)

(Figure 2.5), and this value was achieved in a batch fixed-film system operated at pH 6.0 in which gaseous carbon dioxide and hydrogen were continuously fed (Zhang et al., 2013). The highest concentration of *n*-caprylic acid achieved within an ethanol-fed system was even lower (0.05 g COD/L, 0.14 mM) (Ge et al., 2015). These maximum *n*-caprylic acid concentrations range from 3 to 4% of the solubility limit of undissociated *n*-caprylic acid (1.7 g COD/L, 4.7 mM) (Xu et al., 2015). One study reported that *n*-caprylic acid is inhibitory (to *E. coli*) at 1.6 g COD/L (4.4 mM) (Skrivanova et al., 2006), but this concentration was nearly equal to the solubility limit, and was thus probably excessive. It is unclear to what concentration *n*-caprylic acid can be accumulated before it induces product inhibition or toxicity, and no product inhibition studies have been conducted to specifically relate MCC productivity to concentrations of undissociated MCCAs in the bioreactor broth.

4.1.5 Product ratios of n-*caprylate to* n-*caproate were consistently low*

In essence, *n*-caprylate has only been produced as a by-product of *n*-caproate production. The product ratio of *n*-caprylate to *n*-caproate production has remained low (Figure 2.6). The highest reported product ratio of *n*-caprylate to *n*-caproate was less than 1.5 (g COD/g COD) (Zhang et al., 2013). This ratio was observed in a fixed-film batch system operated at pH 6.0 with very low MCC productivity (0.07 g COD/L-d) in which carbon dioxide and hydrogen were continuously fed. For all ethanol-fed systems, *n*-caprylate to *n*-caproate product ratios were less than 0.6 (Agler et al., 2014), and systems that produced *n*-caprylate at rates higher than 1 g COD/L-d were marked by product ratios less than 0.06 (Grootscholten et al., 2013b). Ultimately, *n*-caprylate will remain a minor product unless rates and proportions of *n*-caprylate production increase to the same order of magnitude as high-rate *n*-caproate productivity (~10-100 g COD/L-d) (Grootscholten et al., 2013d, Grootscholten et al., 2013b).

4.1.6 Substrate ratios and levels affected the product ratios of n-*caproate to* n-*butyrate*

To explain what may affect *n*-caprylate to *n*-caproate product ratios, it is instructive to review early literature that documented increased product ratios of *n*-caproate to *n*-butyrate in the type strain *Clostridium kluyveri*. Batch studies of *C. kluyveri* demonstrated that increased substrate ratios of ethanol to acetate led to increased product ratios of *n*-caproate to *n*-butyrate (Bornstein and Barker, 1948, Weimer and Stevenson, 2012). This trend occurred even when the initial concentration of ethanol was fixed and the initial acetate concentration was increased (Figure 2.7, A-B). In addition, when the initial concentration of acetate was fixed and the initial concentration of ethanol was increased, the *n*-caproate to *n*-butyrate production ratio and the total *n*-caproate production increased until the initial ethanol concentration was 44 g COD/L and the initial ethanol to acetate substrate ratio was 6 (g COD/g COD) (Figure 2.7C) (Weimer and Stevenson, 2012). This finding suggested that substrate inhibition occurred near 44 g COD/L (460 mM) ethanol.

Continuously fed bioreactor studies of the type strain *C. kluyveri* provided additional evidence that increased ethanol to acetate substrate ratios led to increased *n*-caproate to *n*-butyrate product ratios. Ethanol and acetate were fed at either ethanol-limited or excess ethanol substrate ratios (Figure 2.7D), and the HRT was varied to evaluate the effect of different total organic loading rates (OLRs, 8 to 71 g COD/L-d) (Kenealy and Waselefsky, 1985). For several equivalent total organic loading rates, the ethanol-limited substrate ratio led to lower *n*-caproate to *n*-butyrate product ratios than the excess ethanol substrate ratios (~0.6 vs. ~0.8, respectively). Moreover, when the substrate ratios were fixed but the total organic loading rates were increased, the *n*-caproate productivity decreased at the highest loadings for each ratio, indicating substrate inhibition (overloading). Furthermore, when *n*-caproate productivity decreased because of

substrate inhibition at these high organic loading rates, *n*-butyrate productivity simultaneously increased. This led to decreased product ratios of *n*-caproate to *n*-butyrate, and batch studies with substrate inhibition yielded similar results (Figure 2.7, A-B). From these findings, it can be hypothesized that increased product ratios of *n*-caprylate to *n*-caproate could be achieved with increased substrate ratios of ethanol to acetate. However, these results also serve as a harbinger: excessive ethanol concentrations and loadings must be avoided to prevent substrate inhibition.

In the present study, ethanol and acetate were continuously fed at fixed substrate ratios to a reactor microbiome that was operated at a low pH and with in-line product recovery. Batch reactor microbiome experiments were also conducted in which the substrate ratios and concentrations were varied. I had several experimental objectives: 1) to achieve the maximum *n*-caprylate productivity with a high product ratio of *n*-caprylate to *n*-caproate; 2) to evaluate the relationship between residual concentrations of undissociated *n*-caprylic acid in the bioreactor broth and its effects on overall *n*-caprylate productivity; 3) to determine how substrate concentrations and ratios impact MCC production; and 4) to characterize microbial community changes within the reactor microbiome corresponding to periods of increased MCC productivity.

4.2 Materials and methods

4.2.1 Growth medium and inoculum

The modified basal medium was described previously, and it contained nutrients, yeast extract (1.25 g/L, 1.6 g COD/L), and sodium carbonate (0.032 g /L), but no gaseous carbon dioxide was added (Vasudevan et al., 2014). Ethanol and acetate were added to the basal medium at a fixed substrate ratio of 6 g COD/g COD (4 mol/mol) during start-up in Phase I, but this substrate ratio was increased to 15 g COD/g COD (10 mol/mol) for the remainder of the experiment beginning on Day 80 of Phase I, Period 5. For each operating period, the substrate

concentrations of ethanol and acetate were varied to achieve desired loading rates. The medium pH was adjusted with 5 M sodium hydroxide to the operating pH of the bioreactor. The inoculum was derived from a well-characterized reactor microbiome that was fed ethanol-rich yeast fermentation beer (Agler et al., 2012a). This reactor microbiome had been batch-fed semi-continuously (once every two days) throughout an operating period of more than three years at the time of inoculation (Ge et al., 2015). The inoculum was triple-washed in basal media, and approximately 100 mL of this inoculum was added to the continuously fed bioreactor.

4.2.2 Continuously fed bioreactor system

An upflow anaerobic filter was employed with constant bioreactor broth recycling through an in-line pertraction system (membrane-based liquid-liquid extraction) for product extraction, and this system was similar (but not identical) to the system that I described previously (Figure 3.1). The bioreactor was constructed as a vertically oriented cylinder, which was made of Plexiglas®, with an inner diameter of 6 cm. The total volume was 0.90 L, but Kaldnes K1 packing material (Evolution Aqua, Wigan, United Kingdom) was added, resulting in a working volume of 0.70 L. The bioreactor was wrapped with tubing in which hot water from a heating bath (VWR Scientific Model 1104, Radnor, PA, USA) was recirculated for temperature control, resulting in a constant temperature of 30±1°C inside the bioreactor. A pH probe (Mettler 405-DPAS SC K85, Columbus, OH, USA) was mounted at the top of the bioreactor. Automated pH control of the bioreactor broth was maintained with a controller (Eutech Instruments alpha-pH800, Vernon Hills, IL, USA) and a corresponding acid addition pump (Mityflex 913, Bradenton, FL, USA). Hydrochloric acid (0.5 M) was added to the well-mixed feed and recycle inlet at the base of the bioreactor. Fresh media containing ethanol and acetate was continuously fed from a refrigerated vessel (4°C) into the base of the bioreactor using a peristaltic feed pump

(Cole Parmer L/S Digital Economy Drive, Vernon Hills, IL, USA) at average rates of approximately 0.18 or 0.44 L/d (HRT = 3.9 or 1.6 d, respectively). The effluent continuously exited the bioreactor *via* an overflow line connected to the top of the bioreactor. The exit of the overflow line was submerged within a secondary effluent reservoir. An inverted funnel was used to collect the produced gas within the bioreactor and was connected to a flow meter (Ritter MGC-1, Bochum, Germany) (Figure 3.1). In addition, a gas-sample septum and a bubbler were placed in the gas collection system. A sampling port for biomass samples was placed halfway up the vertically oriented bioreactor.

4.2.3 Pertraction system

Product recovery was accomplished with a pertraction system (Figure 3.1) similar to those used in previous reports (Agler et al., 2012a, Ge et al., 2015). One forward and one backward membrane contactor (1.4 m^2 each, Membrana Liqui-Cel 2.5x8, X50 membrane, Charlotte, NC, USA) were used. The hydrophobic solvent was circulated continuously in the lumen of the hydrophobic hollow-fiber membrane modules; the solvent consisted of mineral oil with 30 g/L tri-*n*-octylphosphine oxide (TOPO) (Sigma Aldrich, St. Louis, MO, USA). The stirred alkaline extraction solution was initially buffered with 0.3 M sodium borate and was maintained at pH 9 with automated addition of 5 M sodium hydroxide using a controller (Eutech Instruments alpha-pH800, Vernon Hills, IL, USA) and a corresponding base pump (Mityflex 913, Bradenton, FL, USA). A constant bioreactor broth recycle flow of 130 L/d was maintained using a peristaltic pump (ColeParmer 7553-30, Vernon Hills, IL, USA). To prevent fouling or solids accumulation in the forward membrane contactor, bioreactor broth was drawn from the top of the anaerobic filter and was then pumped through a custom-built, 1.6-mm stainless-steel strainer (Danco 88886, Shorewood, IL, USA), a 65-µm filter (McMaster-Carr 44205K21,

Elmhurst, IL, USA), and a subsequent 5-µm filter (Pentek GS-6 SED/5, Upper Saddle River, NJ, USA). Peristaltic pumps (ColeParmer 7553-30, Vernon Hills, IL, USA) provided continuous recycle flows of 7 and 43 L/d for the mineral oil solvent and alkaline extraction solution, respectively.

4.2.4 Abiotic mass transfer experiments: n-*caproic acid recovery* via *pertraction*

For abiotic pertraction experiments, a similar system was used with the following modifications: the inoculum and basal medium were not used; an aqueous solution of procured synthetic *n*-caproate was adjusted to the pH of the bioreactor; this *n*-caproate solution was continuously fed to the abiotic upflow anaerobic filter; the flow rate of the bioreactor broth recycle was varied to determine the effects of flow rate on mass transfer (but all other flow rates were held constant, including the mineral oil solvent, the alkaline extraction solution, and the aqueous *n*-caproate feed solution) and larger forward and backward membrane contactors with identical hydrophobic hollow-fiber membranes were used (8.1 m^2 each, Membrana Liqui-Cel 4x13, X50 membrane, Charlotte, NC, USA).

4.2.5 Batch reactor microbiome experiments

Batch reactor microbiome experiments were conducted in 160 mL glass serum bottles to which 80 mL of basal medium was added. The initial concentrations and substrate ratios of ethanol and acetate in the basal medium were varied. MES buffer was also added to this media at concentrations that were equimolar to the initial ethanol concentrations, and the initial pH was adjusted to 5.4 with 5 M sodium hydroxide. Inoculum was prepared as described previously, and approximately 4 mL of well-mixed triple-washed inoculum was added to each 80 mL volume (5% inoculum, v/v). The batch reactor microbiomes were then: sparged with nitrogen gas; capped with butyl rubber stoppers; sealed and crimped with aluminum caps; inverted; and

incubated without shaking at 30°C. These serum bottles were then mixed well and sampled after 12 days, and liquid samples(pH 5.4±0.1) were collected in 2-mL Eppendorf tubes for determination of the concentrations of ethanol and carboxylates. Each treatment was conducted in triplicate batch bottles, and all data reported reflect the average values from these triplicates.

4.2.6 Operating strategy and calculations

This bioreactor experiment was divided into two phases: I) a start-up phase with continuous feeding (with the pertraction system off or on); and II) a high *n*-caprylate productivity phase (with continuous feeding and the pertraction system on). Each phase was then divided into several distinct operating periods. From period to period, several operating parameters were varied, including the: organic loading rate (OLR); HRT; bioreactor pH; and operation with or without pertraction. Each operating period was operated for at least five HRT periods, and average bioreactor loading rates and concentrations were reported.

Carboxylate productivities were also calculated as average values for each operating period. Herein, the average bioreactor effluent production rate (g COD/d) *plus* the average transfer rate *via* pertraction (g COD/d) were summed to yield the total production rate (g COD/d). Effluent production rates were calculated as the average bioreactor broth concentration divided by the average HRT for each period. Average transfer rates were calculated by first plotting the increasing amounts of individual carboxylates in the alkaline extraction solution against time. Least squares methods were then used to determine the slope and the sample standard deviation (LINEST function, Microsoft Excel). Production rates were divided by the working bioreactor volume to determine the total volumetric production rates (productivities) (g COD/L-d). All concentrations, rates, and yields were converted to a g COD basis. Feed flow rates were determined volumetrically; effluent rates were determined gravimetrically.

Uncertainty was represented by 95% confidence intervals: the standard error was first calculated as the quotient of the sample standard deviation divided by the square root of the number of samples; then, the standard error was multiplied by a t-value corresponding to the degrees of freedom (based on the number of samples). Uncertainty was propagated through calculations, and 95% confidence intervals were included with reported data (*e.g.*, productivities).

4.2.7 Liquid and gas analysis

Liquid samples (1.5 mL) were collected from the continuously fed bioreactor and the alkaline extraction solution every other day or daily. Bioreactor broth samples were collected from the broth recycle line between the 5-µm filter and the forward membrane contactor. Alkaline extraction solution samples were collected from the well-mixed reservoir (~3 L). Concentrations of carboxylates and ethanol were determined with separate gas chromatography (GC) systems (Usack and Angenent, 2015). The concentrations of methane, carbon dioxide, and hydrogen gases (>2000 ppm) were measured using a GC system (Usack and Angenent, 2015). Furthermore, the concentration of hydrogen gas (<2000 ppm) was determined using a reduction gas detector (RGD) (Trace Analytical RGD, Menlo Park, CA, USA). The RGD inlet was connected to a packed column (Restek, ShinCarbon ST 80/100, Bellefonte, PA, USA) for peak separation, which was installed in a GC system (Gow Mac 580, Bethlehem, PA, USA).

4.2.8 Biomass samples, DNA extraction, PCR, sequencing, and microbial community analysis

Biomass samples were from the bioreactor broth at 16 time points throughout the experiment, as well as one sample from the inoculum. The bioreactor broth was thoroughly mixed by quickly withdrawing and refilling a 60 mL syringe ten times. During this sampling, settled flocculent biomass was resuspended. The sample was collected in 2-mL Eppendorf tubes. These 2-mL samples were then centrifuged at 16,873 x *g* for 4 min and the supernatants were

discarded. Concentrations of wet solids in these pelleted biomass samples ranged from 23 to 76 mg/L. These pelleted biomass samples were stored at -80°C until further processing.

Genomic DNA was extracted using the PowerSoil DNA isolation kit (MO BIO Laboratories Inc., Carlsbad, CA). Modifications to the protocol include utilization of custom bead tubes containing a mixture of 300 mg of 0.1-mm diameter and 100 mg of 0.5-mm diameter silica/zirconia beads (Hospodsky et al., 2010), and physical cell lysis with bead-beating at 3450 oscillations/min for 45 s. The DNA amplification protocol was described previously (Regueiro et al., 2015) with the following exceptions: 1) Mag-Bind RxnPure Plus magnetic beads solution (Omega Biotek, Norcross, GA, USA) were used instead of Mag-Bind E-Z Pure; 2) only 20 ng DNA per sample were pooled instead of 100 ng. QIITA (qiita.microbio.me) was used for initial processing of the sequencing data. The sortmerna method was used to bin sequences into operational taxonomic units (OTUs) at 97% identity. Taxonomy was assigned for representative sequences selected for each OTU using the Greengenes v13.8 database from August 2013 (McDonald et al., 2012). The remaining analyses were performed in QIIME v1.9 (Caporaso et al., 2010). Singleton OTUs were removed from the dataset.

Community analysis, including beta diversity and unconstrained ordination, was performed as described previously (Regueiro et al., 2015) with the following exceptions: 1) the alpha diversity was calculated using the Shannon diversity index (Shannon, 1948) rather than Chao1; 2) the Pearson correlation coefficient was calculated for samples from Phase III with the functions cor and cor.test in the R stats package (Team, 2014). At a significance level of $p<0.05$ and $n = 11$, the relative abundance of an OTU would be positively correlated with *n*-caproate productivity if the Pearson r was greater than 0.602. Heatmaps were created to represent OTU relative abundances *via* the gplots package in R (Warnes et al., 2015).

4.3 Results and discussion

4.3.1 n-*Caprylate productivities and product ratios were the highest reported*

A maximum average medium-chain carboxylate (MCC) volumetric production rate (productivity) of 21.1 g COD/L-d (Figure 4.3) was achieved in an upflow anaerobic filter that was continuously fed ethanol and acetate. The corresponding *n*-caprylate productivity was 19.4 g COD/L-d, which is more than four times the highest *n*-caprylate productivity reported elsewhere (4.4 g COD/L-d, Figure 4.4) (Grootscholten et al., 2013d). The product ratio of *n*-caprylate to *n*-caproate was 11 (g COD/g COD) during this operating period (Phase II, Period 10, Days 163-174), and this product ratio was even higher (25) in an earlier operating period (Phase II, Period 8, Days 142-155). Both of these *n*-caprylate to *n*-caproate product ratios are much higher than the maximum product ratios that were observed previously (1.5 g COD/g COD, Figure 4.5) (Zhang et al., 2013).

Moreover, *n*-caprylate comprised 91% of the total carboxylate (MCC plus SCC) production from this operating period (on a COD basis). MCC pertraction efficiency was effective; 99% of the *n*-caprylate and 89% of the *n*-caproate produced during this period were recovered *via* in-line pertraction (membrane-based liquid-liquid extraction). This period of maximum *n*-caprylate productivity was sustained for 11 days (Table 4.1) at an HRT of 1.5 d (Table 4.2) (Phase II, Period 10, Days 163-174). The total organic loading rate (OLR) that supported this maximum period of *n*-caprylate productivity was 34.7 g COD/L-d (Figure 4.3). This OLR led to moderate average residual ethanol concentrations (9 g COD/L, 90 mM) (Figure 4.6A) and a deficit between the applied total OLR and the resulting total MCC productivity (Figure 4.6B). Finally, the substrate ratio of ethanol to acetate was 15 (g COD/g COD), and the substrate ratio of ethanol to non-ethanol organics (*i.e.*, acetate plus yeast extract COD) was 11.

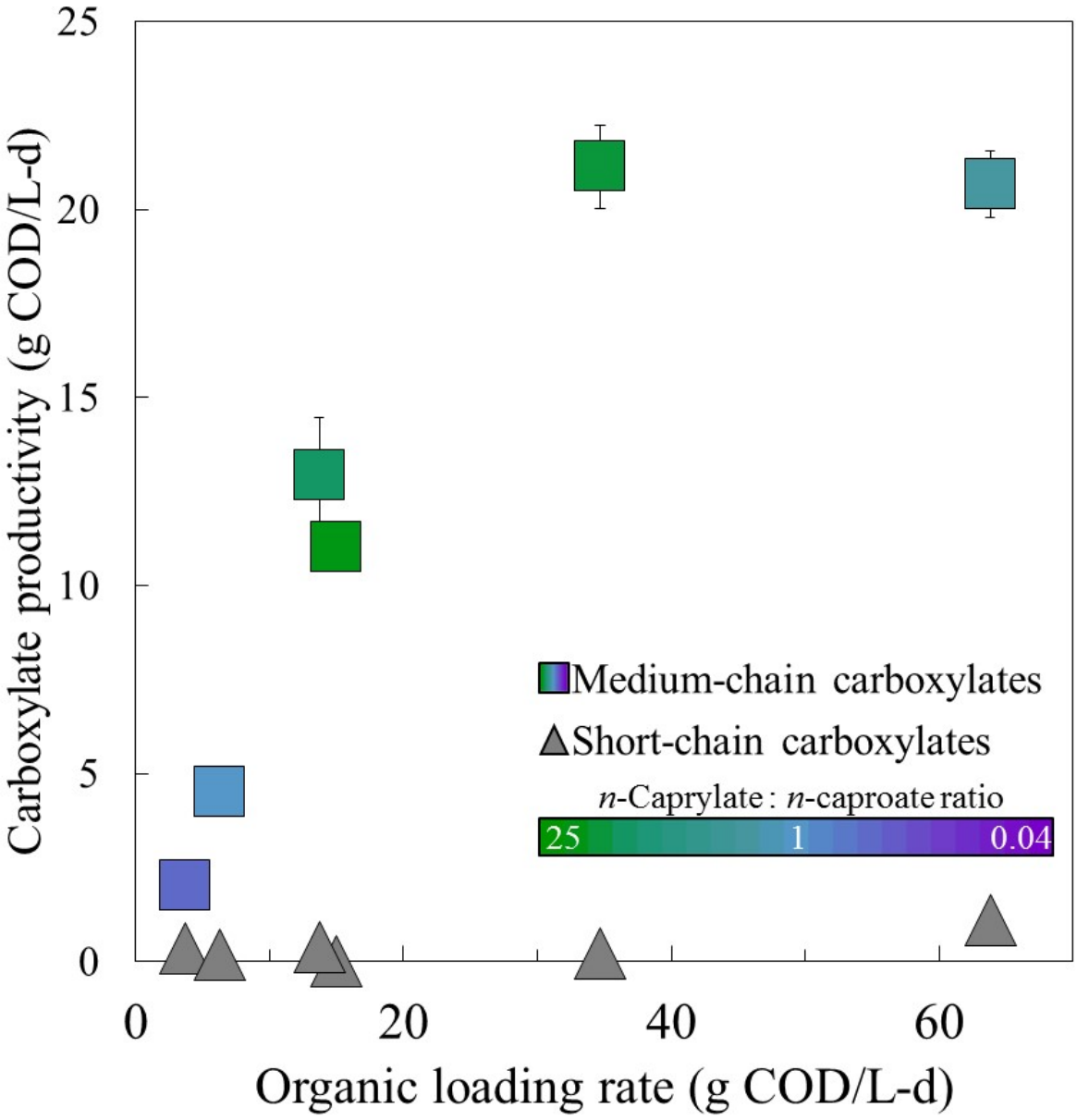

Figure 4.3: Carboxylate productivities and product ratios of *n*-caprylate : *n*-caproate. Medium-chain carboxylate (MCC) productivities improved to 21.1 g COD/L-d by increasing organic loading rates (OLRs) up to 34.7 g COD/L-d. *n*-Caprylate (green) was the predominant product, with a product ratio of *n*-caprylate to *n*-caproate of 25 (g COD/g COD) at an OLR of 15.0 g COD/L-d, and a product ratio of 11 (g COD/g COD) at an OLR of 34.7 g COD/L-d. Error bars represent 95% confidence intervals. Data shown are from Phase II only.

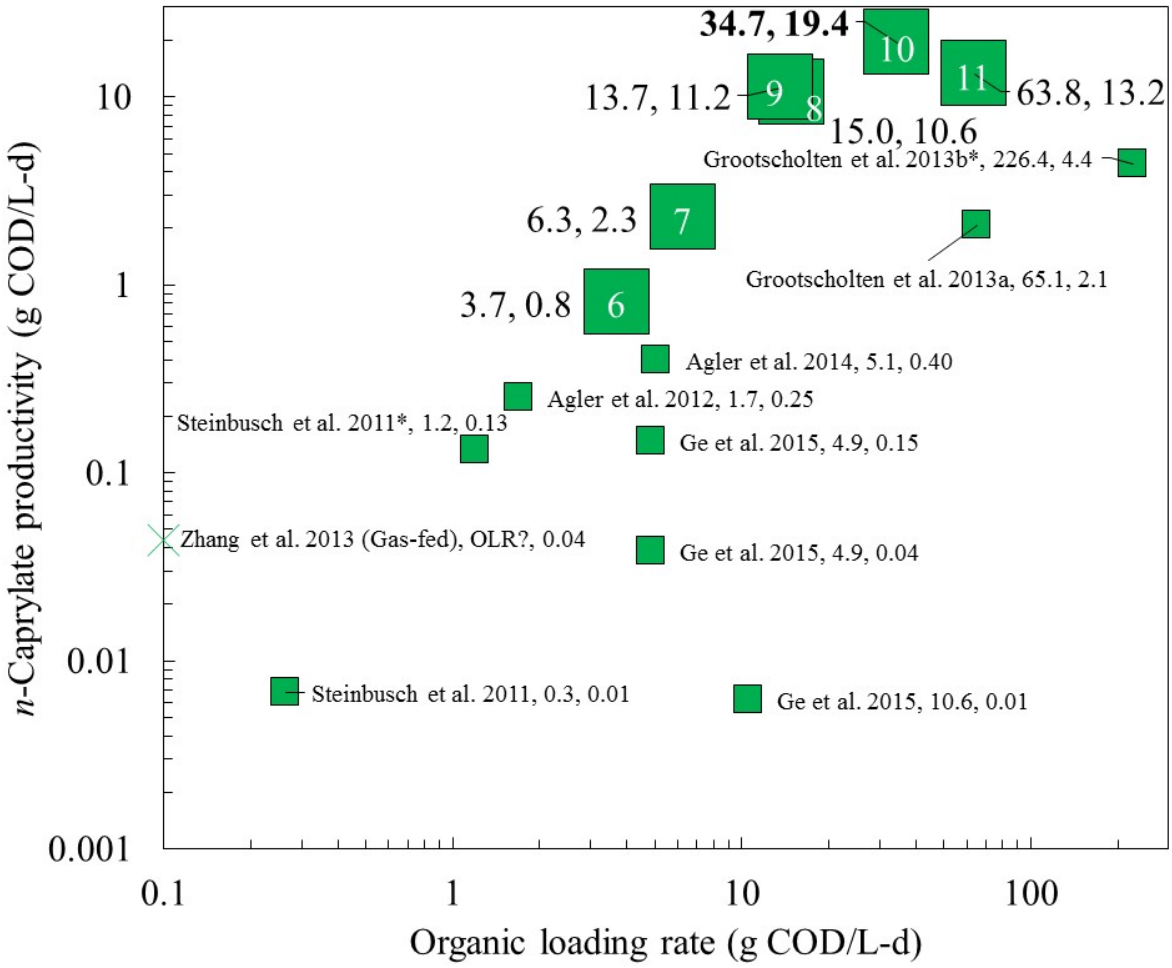

Figure 4.4: *n*-Caprylate productivities in ethanol-fed or gas-fed bioreactor studies, including Phase II of the present study. Results from eight studies in which *n*-caprylate production was reported are shown, including the present study (large squares). Operating periods from Phase II of the present study are labelled in white. Maximum instantaneous values reported are indicated (*). The referenced study, the organic loading rate, and the *n*-caprylate productivity are listed. Both *n*-caprylate productivities and organic loading rates are presented on logarithmic scales. One study (Zhang et al., 2013, X) produced *n*-caprylate in a bioreactor in which gas composed of carbon dioxide and hydrogen was fed; they did not present organic loading rates, so this marker was placed at an organic loading rate near the sum of the total carboxylate volumetric production rates. The present study achieved *n*-caprylate productivities up to 19.4 g COD/L-d (Period 10).

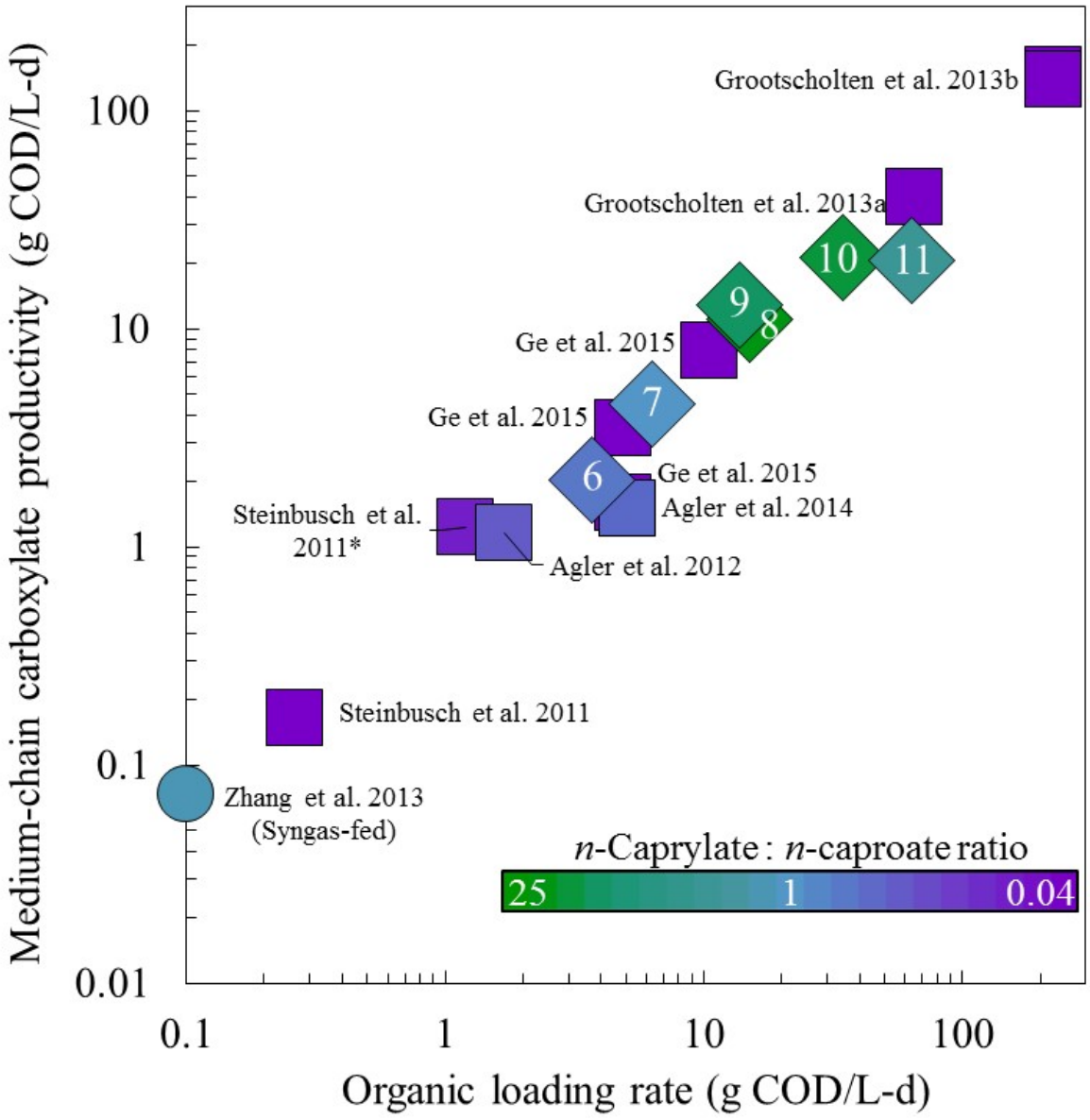

Figure 4.5: Medium-chain carboxylate productivities and product ratios of *n*-caprylate : *n*-caproate from ethanol-fed and gas-fed bioreactor studies, including Phase II of the present study. Results from eight studies in which *n*-caprylate production was reported are shown, including the present study (diamonds). Operating periods from Phase II of the present study are labelled in white. Indications include maximum instantaneous values reported (*). A color gradient was used to show the product ratio of *n*-caprylate (green) to *n*-caproate (purple). Blue represents a mixture of these two products. Both medium-chain carboxylate productivities and organic loading rates are presented on logarithmic scales. One study (Zhang et al. 2013, circle) produced *n*-caprylate from carbon dioxide- and hydrogen-gas; they did not present organic loading rates, so this marker was placed at an organic loading rate near the sum of the total carboxylate productivities. The present study achieved product ratios of *n*-caprylate to *n*-caproate as high as 25 (Period 8) and MCC productivities up to 21.1 g COD/L-d (Period 10).

Table 4.1: **Average bioreactor broth concentrations**. Average substrate and product concentrations in the bioreactor broth are reported for each operating period. Detection limits were approximately 0.05 g COD/L (0.5 mM) for ethanol and approximately 0.02 g COD/L (~0.1 mM) for other carboxylates. The following conversion factors (g COD/mol) were used to convert molar ethanol and carboxylate concentrations to a g COD-basis: ethanol, 96; acetate, 64; propionate, 112; *n*-butyrate, 160; *n*-valerate, 208; *n*-caproate, 256; *n*-heptanoate, 304; *n*-caprylate, 352. B.D.: below detection. Uncertainty is represented by 95% confidence intervals.

Operating conditions					**Average bioreactor broth concentrations**					
Phase #	Period #	Pertraction + / -	Start - End *d*	Bioreactor pH	[Ethanol]	[*n*-Caprylate]	[*n*-Caproate]	[*n*-Butyrate]	[Acetate]	[Other SCC]
					g COD/L					
I	1	+	0 - 15	5.8 ± *0.6*	1.01 ± *1.11*	*B.D.*	0.80 ± *0.50*	0.13 ± *0.08*	0.64 ± *0.12*	0.03 ± *0.03*
	2	+	15 - 54	5.6 ± *0.2*	0.10 ± *0.01*	*B.D.*	0.19 ± *0.07*	0.11 ± *0.05*	0.57 ± *0.09*	0.02 ± *0.01*
	3	+	54 - 64	5.4 ± *0.1*	0.10 ± *0.01*	0.05 ± *0.12*	0.03 ± *0.09*	0.01 ± *0.01*	0.39 ± *0.10*	0.01 ± *0.03*
	4	-	64 - 80	5.5 ± *0.1*	0.04 ± *0.04*	0.21 ± *0.14*	0.23 ± *0.12*	0.03 ± *0.03*	0.61 ± *0.08*	0.05 ± *0.03*
	5	-	80 - 98	5.3 ± *0.1*	0.25 ± *0.24*	0.76 ± *0.16*	1.03 ± *0.33*	0.60 ± *0.24*	0.75 ± *0.10*	0.15 ± *0.03*
II	6	+	98 - 128	5.2 ± *0.1*	0.03 ± *0.05*	0.03 ± *0.02*	0.07 ± *0.02*	0.08 ± *0.02*	0.22 ± *0.05*	0.01 ± *0.01*
	7	+	128 - 142	5.1 ± *0.1*	0.02 ± *0.05*	0.04 ± *0.02*	0.09 ± *0.02*	0.07 ± *0.02*	0.13 ± *0.06*	0.03 ± *0.02*
	8	+	142 - 155	5.0 ± *0.1*	0.99 ± *0.20*	0.09 ± *0.02*	0.06 ± *0.04*	0.00 ± *0.00*	0.01 ± *0.02*	0.06 ± *0.03*
	9	+	155 - 163	5.1 ± *0.1*	0.49 ± *0.24*	0.18 ± *0.03*	0.08 ± *0.03*	0.05 ± *0.05*	0.09 ± *0.04*	0.05 ± *0.03*
	10	+	163 - 174	5.1 ± *0.1*	8.67 ± *2.12*	0.34 ± *0.08*	0.28 ± *0.06*	0.11 ± *0.03*	0.13 ± *0.02*	0.09 ± *0.06*
	11	+	174 - 186	5.2 ± *0.1*	27.33 ± *3.01*	0.69 ± *0.10*	1.21 ± *0.11*	1.09 ± *0.38*	0.57 ± *0.12*	0.04 ± *0.02*

Table 4.2: **Average loading rates and carboxylate productivities.** Average productivities of medium-chain carboxylates (MCCs) (e.g., *n*-caprylate, *n*-caproate) and short-chain carboxylates (SCCs) are reported for each operating period. These total productivities were calculated as the sum of average bioreactor effluent production rates plus average transfer rates *via* pertraction for each operating period, normalized to the bioreactor working volume. Acetate was continuously fed to the bioreactor, so negative production rates indicate net consumption of acetate. Uncertainty is represented by 95% confidence intervals. Total organic loading rates (OLRs) include loading from ethanol, acetate, and yeast extract. For most of the experiment, to vary the ethanol and total organic loading rates, the concentrations of ethanol and acetate in the basal medium were changed (instead of the HRT). The substrate ratio of ethanol to acetate was approximately 6 g COD/g COD until it was increased to 15 g COD/g COD on Day 80 of Phase I, Period 5. For each operating period, the concentrations of ethanol and total organics (g COD/L) in the continuously fed basal medium can be calculated by multiplying the reported average ethanol and total organic loading rates (g COD/L-d) by the corresponding average HRT (d). The yeast extract concentration in the media was consistently 1.6 g COD/L (1.25 g/L), and the corresponding yeast extract loading rate was approximately 0.4±0.1 g COD/L-d throughout the first 8 operating periods (HRT = 3.9±0.1 d). In Period 9, the feed flow rate was increased, which decreased the HRT, and the yeast extract loading rate was consequently increased to 1.1±0.1 g COD/L-d (HRT = 1.5±0.1 d). No considerable changes were observed in the *n*-caprylate or the total MCC productivities between Period 8 and Period 9. Uncertainty is represented by 95% confidence intervals.

Operating conditions				**Loading rates**		**Average carboxylate productvities**				
Phase #	Period #	Pertraction + / -	HRT *d*	Total OLR *g COD/L-d*	Ethanol *g COD/L-d*	*n*-Caprylate *g COD/L-d*	*n*-Caproate *g COD/L-d*	*n*-Butyrate *g COD/L-d*	Net Acetate *g COD/L-d*	Other SCC *g COD/L-d*
I	1	+	4.2 ± *0.6*	2.1 ± *0.6*	1.4 ± *0.4*	0.0 ± *0.0*	0.5 ± *0.3*	0.0 ± *0.0*	-0.1 ± *0.1*	0.0 ± *0.0*
	2	+	4.8 ± *0.6*	1.8 ± *0.1*	1.2 ± *0.1*	0.0 ± *0.0*	0.3 ± *0.1*	0.3 ± *0.2*	-0.1 ± *0.0*	0.3 ± *0.1*
	3	+	3.8 ± *0.3*	1.7 ± *0.4*	1.2 ± *0.2*	0.0 ± *0.0*	0.6 ± *0.3*	0.0 ± *0.0*	-0.1 ± *0.0*	0.0 ± *0.0*
	4	-	4.5 ± *0.9*	1.8 ± *0.3*	1.2 ± *0.2*	0.0 ± *0.0*	0.1 ± *0.0*	0.0 ± *0.0*	-0.1 ± *0.0*	0.0 ± *0.0*
	5	-	4.4 ± *0.2*	3.8 ± *0.4*	3.2 ± *0.3*	0.2 ± *0.0*	0.2 ± *0.1*	0.1 ± *0.1*	0.0 ± *0.0*	0.0 ± *0.0*
II	6	+	3.7 ± *0.2*	3.7 ± *0.4*	3.1 ± *0.3*	0.8 ± *0.1*	1.2 ± *0.2*	0.3 ± *0.1*	-0.2 ± *0.0*	0.0 ± *0.0*
	7	+	3.8 ± *0.4*	6.3 ± *0.4*	5.6 ± *0.4*	2.3 ± *0.4*	2.2 ± *0.2*	0.0 ± *0.0*	-0.3 ± *0.0*	0.1 ± *0.1*
	8	+	3.3 ± *0.3*	15.0 ± *2.9*	13.7 ± *2.6*	10.6 ± *0.3*	0.4 ± *0.1*	0.0 ± *0.0*	-0.9 ± *0.2*	0.0 ± *0.0*
	9	+	1.6 ± *0.1*	13.7 ± *1.8*	12.2 ± *1.6*	11.2 ± *1.5*	1.7 ± *0.3*	0.0 ± *0.0*	-0.8 ± *0.1*	0.3 ± *0.2*
	10	+	1.5 ± *0.1*	34.7 ± *2.7*	31.8 ± *2.5*	19.4 ± *1.1*	1.7 ± *0.3*	0.1 ± *0.0*	-2.0 ± *0.2*	0.1 ± *0.0*
	11	+	1.5 ± *0.0*	63.8 ± *6.7*	59.1 ± *6.2*	13.2 ± *0.8*	7.5 ± *0.3*	0.7 ± *0.2*	-3.6 ± *0.4*	0.0 ± *0.0*

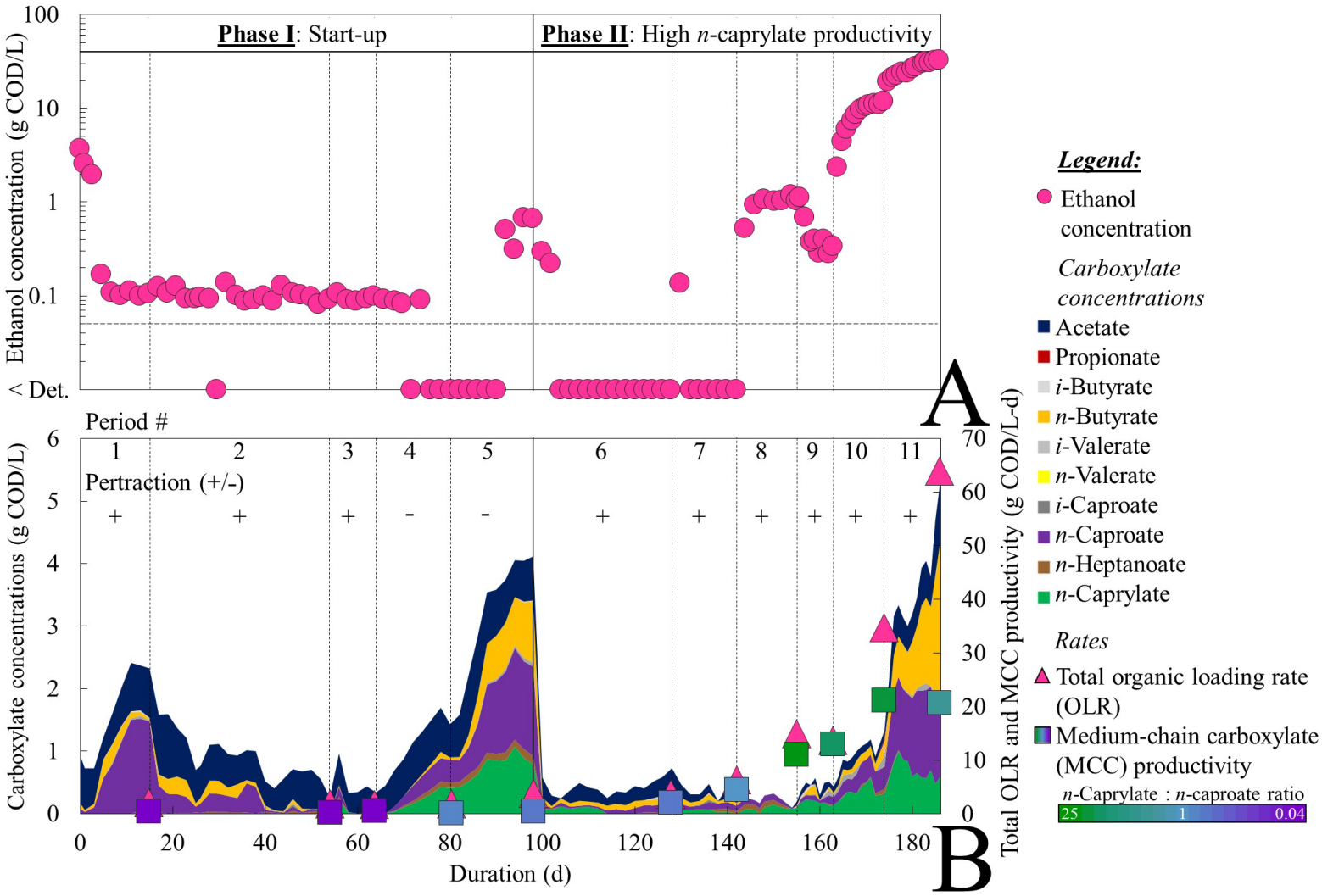

Figure 4.6: **Bioreactor broth concentrations, organic loading rates, and medium-chain carboxylate productivities.** Concentrations of ethanol (A) and carboxylates (B) in the bioreactor broth were determined from samples collected every other day or daily. Average medium-chain carboxylate (MCC) productivities (B) and total organic loading rates (OLRs) (B) for each operating period are also shown. Operating phases, operating periods, and presence (+) or absence (-) of product recovery *via* in-line pertraction are indicated. Detection limits were 0.05 g COD/L (0.5 mM) for ethanol and approximately 0.02 g COD/L (~0.1 mM) for carboxylates.

4.3.2 Start-up: continuous pertraction led to low production of n-*caproate and no* n-*caprylate*

Before achieving the maximum *n*-caprylate productivity and product ratios in Phase II (Period 10), the bioreactor was operated through a sequence of distinct operating periods during a start-up phase. In Phase I, inoculum was added to the upflow anaerobic filter and continuous media addition was immediately initiated (Phase I, Period 1, Days 0-15). The substrate ratio of ethanol to acetate was 6 (g COD/g COD). Upon start-up, the residual concentration of ethanol decreased to approximately 0.1 g COD/L (1 mM) (Figure 4.6A), and the concentration of carboxylates, especially *n*-caproate, increased in the bioreactor (Figure 4.6B), even though the pertraction system was on. The pH of the bioreactor was not well-controlled and drifted from pH 5.0 to 7.6, which decreased the: 1) concentration of the hydrophobic undissociated *n*-caproic acid; 2) product recovery efficiency *via* pertraction; and 3) overall n-caproate productivity. Therefore, the pH controller was repaired and the bioreactor was re-inoculated with fresh basal medium on Day 15 of Period 2. No improvement was observed in the 39 days of Period 2 (Days 15-54), so the bioreactor was again re-inoculated on Day 54 from the same semi-continuously fed and well-characterized reactor microbiome. This time, the inoculum was not triple-washed in basal medium, resulting in a spike of MCCs. The MCC productivity did not continue, however, so the pertraction system was turned off to start Period 4.

4.3.3 n-*Caprylate was produced without pertraction, but concentrations rose to inhibitory levels*

On Day 64, pertraction was turned off. This action was taken to deliberately encourage the standing concentration of hydrophobic, inhibitory, and undissociated medium-chain carboxylic acids (MCCAs, *e.g.*, undissociated *n*-caprylic acid and *n*-caproic acid) to increase in the bioreactor broth. The rationale used was based in ecology: MCC-producing members of the microbiome are likely to have lower susceptibility to inhibition and toxicity from their own

MCCA products, which should provide them a competitive advantage over other microbes. This strategy worked: *n*-caprylate and *n*-caproate accumulated in the bioreactor broth, and although the productivities of *n*-caproate and *n*-caprylate did not increase immediately, the production of *n*-caprylate was observed for the first time in this study (Table 4.1). The product ratio of *n*-caprylate to *n*-caproate also increased, which can be seen from the color of the squares in Figure 4.6B as they began to shift from purple to blue. It is important to note that this observed increased in the product ratio of ethanol to acetate did not require an increase in the substrate ratio of ethanol to acetate. Moreover, loading rates, the HRT, and the bioreactor pH were each maintained at similar levels as in Periods 1-3 of Phase I, which confirms that turning the pertraction system off was the operational change that led to improved *n*-caprylate production.

In Period 5, the substrate addition was changed in two ways. First, the organic loading rate was increased from 1.8 to 3.8 g COD/L-d (Table 4.2). Second, the substrate ratio of ethanol to acetate was increased from 6 to 15 g COD/g COD. The rationale for increasing the substrate ratio was based on previous research. For example, in one reactor microbiome study, *n*-caprylate to *n*-caproate product ratios of 0.5 g COD/g COD and *n*-caprylate productivities of 0.3 g COD/L-d were observed when the substrate ratio of ethanol to other organics (*e.g.*, dilute-acid pretreated corn fiber COD) was 11 g COD/g COD (Agler et al., 2012a). When they subsequently transitioned to using real yeast fermentation beer, which contained a substrate ratio of ethanol to other organics of 2.4 g COD/g COD, *n*-caprylate production ceased.

In Period 5, increasing the organic loading rate and substrate ratio of ethanol to acetate led to increases in the: productivities of *n*-caprylate and *n*-caproate; *n*-caprylate to *n*-caproate product ratio; and the bioreactor broth concentrations of residual ethanol (Figure 4.6A) as well as several carboxylates (Figure 4.6B). Of these carboxylates, the residual concentrations of

n-caprylate, then *n*-caproate, and finally *n*-butyrate each increased and stagnated in a sequence. Corresponding concentrations of undissociated *n*-caprylic acid (0.21 g COD/L, 0.6 mM) and *n*-caproic acid (0.27 g COD/L, 1.1 mM) each increased (Phase I, Period 5, Days 80-98). This average concentration of undissociated *n*-caprylic acid is higher than those observed in previous studies (Figure 4.7). Moreover, two observations suggest that this concentration led to product inhibition: 1) the production of reverse β-oxidation products, including *n*-caprylate, *n*-caproate, and *n*-butyrate, each increased at the beginning of Period 5 before stagnating near Day 94; and 2) the residual ethanol concentration spiked from below detection to approximately 0.5 g COD/L (5 mM) on Day 92, indicating that ethanol consumption rates had decreased. This pattern of product inhibition leading to increased substrate concentrations was observed again in Period 11. To relieve this product inhibition, I turned on the pertraction system on Day 98 to start Period 6 and Phase II.

4.3.4 Pertraction and increased loading led to high n-*caprylate productivities and product ratios*

In Phase II, the use of pertraction improved the *n*-caprylate production. The residual concentrations of carboxylates and corresponding undissociated carboxylic acids all decreased beginning on Day 98 (Phase II, Period 6). At equivalent organic loading rates, the average *n*-caprylate productivity increased from 0.2 to 0.8 COD/L-d from Period 5 to Period 6, (Table 4.2). The organic loading rate was then increased in a sequence of five operating periods from 3.7 to 34.7 g COD/L-d (Figure 4.6B), which increased the *n*-caprylate productivity from 0.8 to a maximum of 19.4 g COD/L-d in Phase II, Period 10 (Figure 4.6B). The product ratio of *n*-caprylate to *n*-caproate was also improved from 0.7 g COD/g COD in Period 6 to 11 g COD/g COD in Period 10.

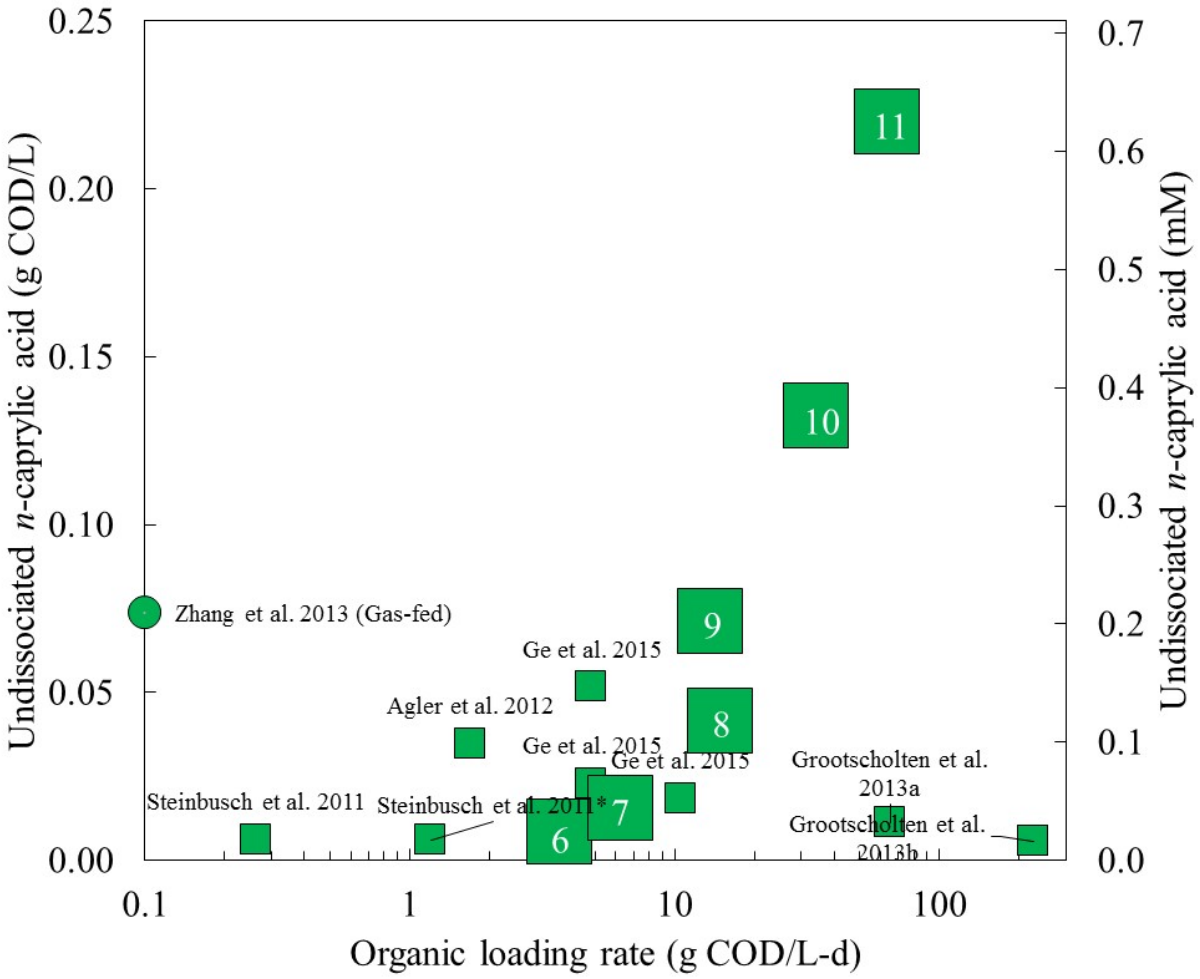

Figure 4.7: Undissociated *n*-caprylic acid concentrations in ethanol-fed or gas-fed bioreactors studies, including Phase II of the present study. Results from seven studies in which *n*-caprylate production was reported are shown, including the present study (large squares). Operating periods from Phase II of the present study are labelled in white. Maximum instantaneous values reported are indicated (*). Organic loading rates are presented on logarithmic scales. One study (Zhang et al. 2013, circle) produced *n*-caprylate in a bioreactor in which gas composed of carbon dioxide and hydrogen was fed; they did not present organic loading rates, so this marker was placed at an organic loading rate near the sum of the total carboxylate volumetric production rates. Undissociated *n*-caprylic acid concentration data was not available for Agler et al. 2014. The present study reached undissociated *n*-caprylic acid concentrations in the bioreactor broth up to 0.22 g COD/L (0.6 mM) at a pH of 5.2 (Period 11), which is 13% of the solubility limit of undissociated *n*-caprylic acid (1.7 g COD/L, 5 mM). This high concentration led to product inhibition.

It was also confirmed that the organic loading rate, and not hydraulic retention time, was the key driver for increased MCC productivity. Specifically, at comparable OLRs near 14 g COD/L-d, the total MCC productivities were relatively unchanged when the hydraulic time was reduced from 3.3 to 1.6 days (Table 4.2, Periods 8-9). The yeast extract and carbonate loading rates were also implicitly increased when the HRT was reduced. Other reports suggested that these factors would be critical in improving MCC productivity (Grootscholten et al., 2013d), but no evidence was apparent from the present study to confirm this claim.

4.3.5 Overload: stagnated MCC productivity; increased methane and hydrogen gas production; decreased ethanol consumption; and inhibitory concentrations of undissociated n-*caprylic acid*

When the organic loading rate was increased to its maximum level (63.8 g COD/L-d), the *n*-caprylate productivity decreased (Figure 4.4), the *n*-caprylate to *n*-caproate product ratio decreased (Figure 4.3), and the MCC productivity stagnated (Figure 4.3) (Phase II, Period 11, Days 174-186). The concentrations of hydrogen gas and methane also increased for the first time in this study to levels above 3,000 and 30,000 ppm, respectively (Figure 4.8). The production of methane at pH 5.2 was almost certainly caused by hydrogenotrophic methanogens, and the corresponding carbon dioxide consumption that was observed also supports this explanation.

This overloading event also resulted in the maximum observed concentration of undissociated *n*-caprylic acid in the bioreactor broth (Figure 4.7). The average concentration of undissociated *n*-caprylic acid increased up to 0.22 g COD/L (0.6 mM) in the bioreactor broth, which is approximately 13% of the solubility limit (1.7 g COD/L, 4.7 mM). In Phase I, Period 5, this same concentration led to product inhibition before the pertraction system was turned on to start Phase II. Based on a thorough literature review, this residual concentration of undissociated *n*-caprylic acid is the highest that has been accumulated in a bioreactor broth (Figure 4.7).

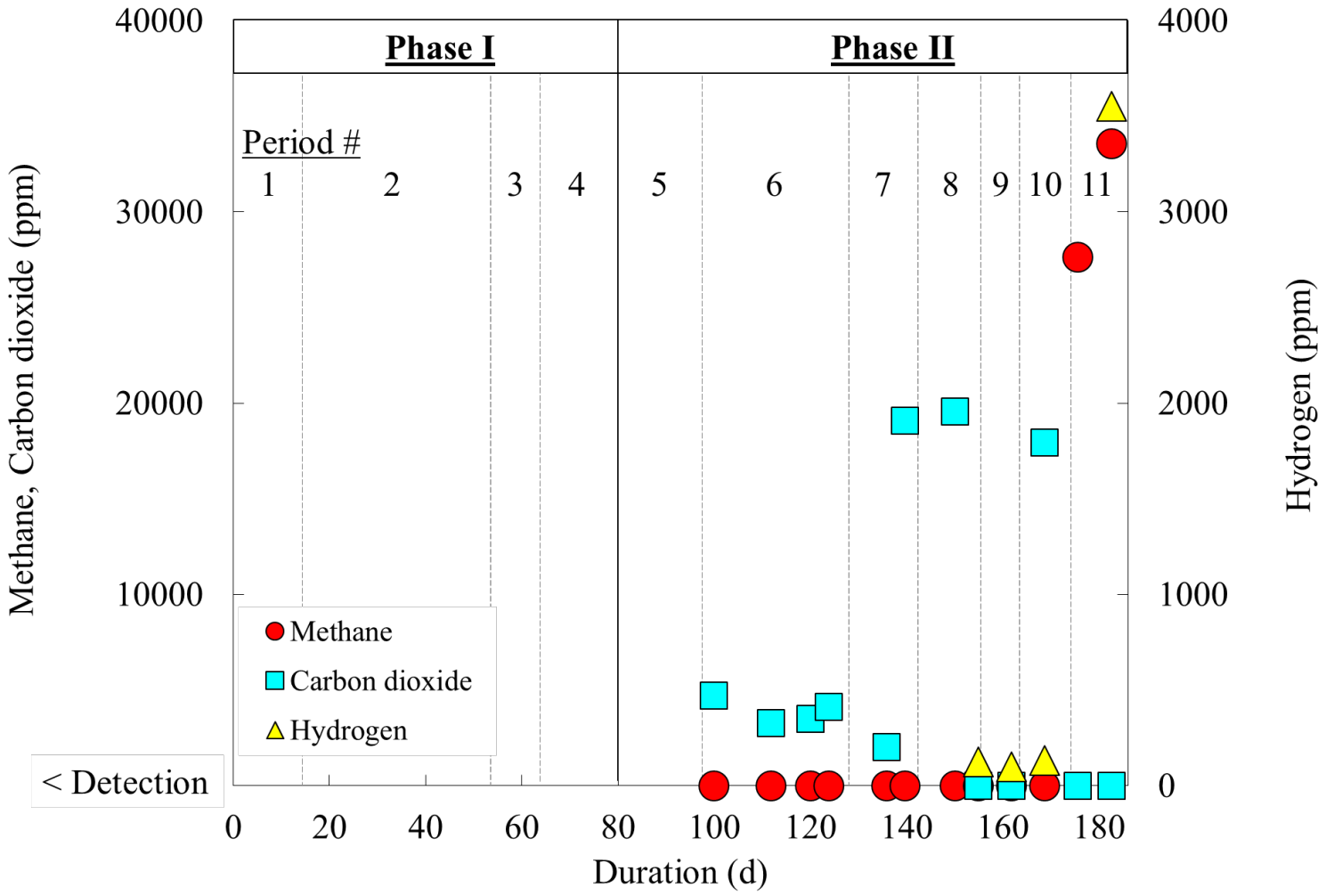

Figure 4.8: Gas composition during phase of high *n*-caprylate productivity (Phase II). Gas concentrations were determined in the second phase of bioreactor operation. Hydrogen was quantified using the reduced gas detector at concentrations beneath 2000 ppm; it was quantified with a gas chromatograph at higher concentrations. Methane concentrations were undetectable until Phase II Period 11, and this increase corresponded with increasing hydrogen concentrations and undetectable carbon dioxide concentrations.

Concomitant with increased residual concentrations of undissociated *n*-caprylic acid, the residual concentrations of ethanol also rose (Figure 4.6A). In earlier periods, the average residual ethanol levels remained below 1 g COD/L (10 mM) (Table 4.1). Periods 10 and 11 were marked by average ethanol concentrations of 9 and 27 g COD/L (90 and 285 mM), respectively. The highest residual ethanol concentration (33 g COD/L, 347 mM) was observed on the final day of operation (Phase II, Period 11, Day 186). These concentrations were below the concentration (44 g COD/L, 460 mM) previously observed to be inhibitory in pure culture studies of the type strain *Clostridium kluyveri* (Weimer and Stevenson, 2012) and enzymatic studies of yeast (Chen and Jin, 2006), but it is unlikely that identical inhibitory levels are applicable for this reactor microbiome.

Inhibited ethanol consumption had already been observed before the residual ethanol concentrations spiked during Periods 10 and 11. The percentage of ethanol consumed declined from greater than 98% in earlier periods to 82% and 70% in Periods 10 and 11, respectively. Product inhibition is the most likely explanation: the undissociated *n*-caprylic acid concentrations in Periods 10 and 11 grew with increasing organic loading rates to levels that were much higher than those seen in other studies (Figure 4.7), and increases in these concentrations were correlated with decreases in the percentage of ethanol consumed. Although no clear studies have been conducted to determine minimum inhibitory levels of undissociated *n*-caprylic acid, results from this study suggest that inhibition occurred between concentrations of 0.1 to 0.2 g COD/L (0.3 to 0.6 mM) undissociated *n*-caprylic acid.

4.3.6 Increased pertraction transfer rates could have relieved the product inhibition

Throughout operation, the pertraction system was consistently effective in MCC recovery. On average, 99% of the *n*-caprylate and 95% of the *n*-caproate produced were

recovered *via* the pertraction system. These MCC recovery rates were comparable to rates achieved in our lab following optimization of an analogous pertraction system (Ge et al., 2015). In the period of maximum MCC production, pertraction recovered 98% of the MCCs produced. The lowest MCC recovery rate was 94%, and this occurred during the overloaded period when the increased residual concentrations in the bioreactor broth led to greater product losses through the effluent.

If I would have increased the broth recycle flow rate during the final overloaded period, this would have reduced the concentration of residual undissociated *n*-caprylic acid. This assertion is based on an abiotic mass transfer study of *n*-caproic acid that I had completed previously (Figure 4.9). Using an analogous pertraction system, I determined that the flow rate of the abiotic reactor broth recycle (and not the mineral oil solvent nor the alkaline extraction solution) was directly proportional to the overall mass transfer coefficient. To achieve a higher MCC mass transfer rate (g COD/d) with a constant membrane surface area (m^2), a bioreactor system would be required to either 1) sustain a higher residual MCCA concentration (g COD/L) or 2) increase the overall mass transfer coefficient, which could be accomplished by increasing the bioreactor broth recycle flow rate. In essence, if I would have increased the bioreactor broth recycle flow rate near the end of Phase II, the same n-caprylate productivity could have been achieved with a lower residual concentration of *n*-caprylic acid. Furthermore, if I had increased the bioreactor broth recycle flow rate before the overloading event, it is expected that a higher pertraction efficiency would have reduced the inhibitory *n*-caprylic acid concentrations, and an even higher *n*-caprylate productivity could have been achieved.

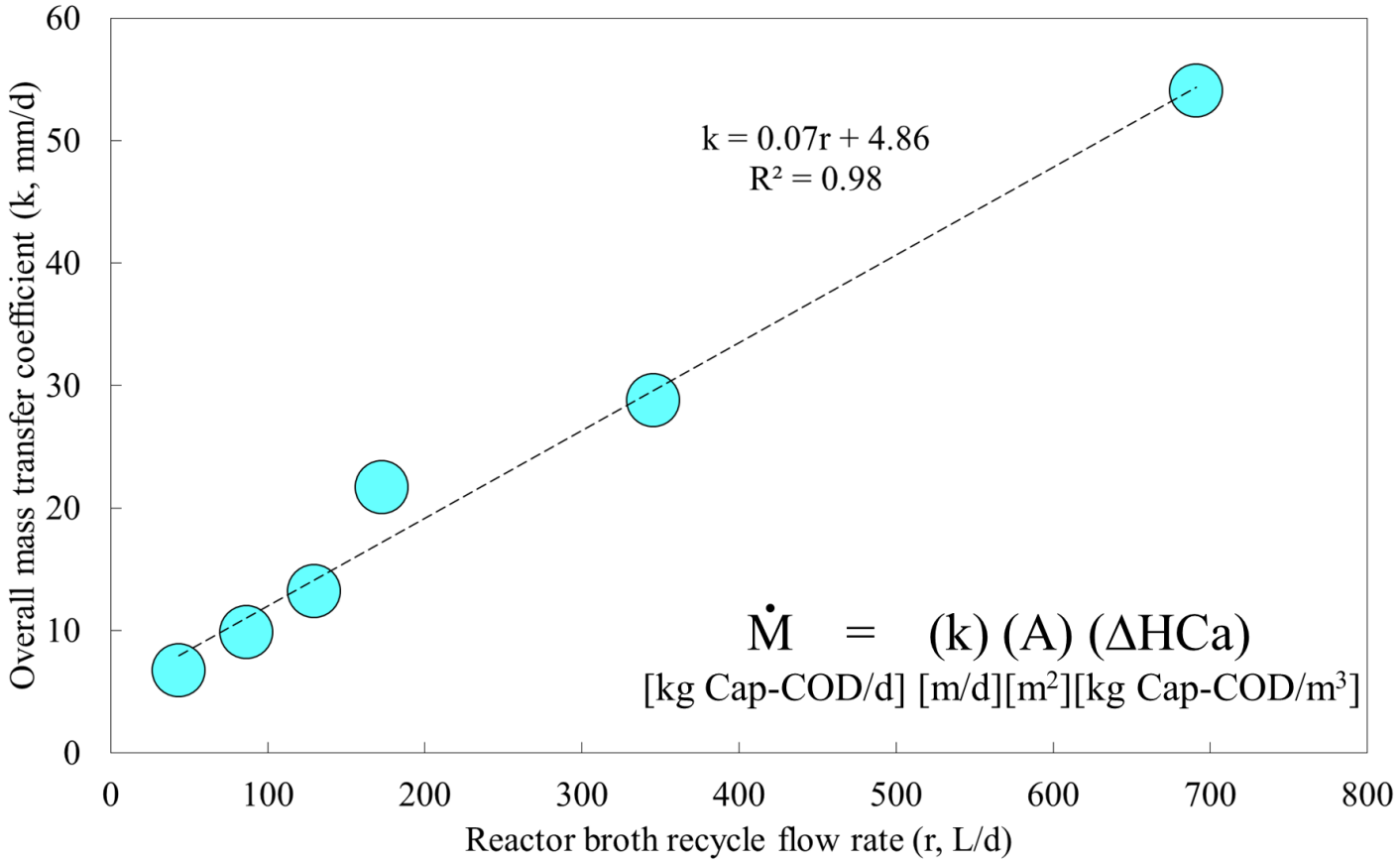

Figure 4.9: The overall mass transfer coefficient was directly proportional to the abiotic reactor broth recycle flow rate. In an abiotic *n*-caproate transfer experiment that used a similar pertraction system, we determined that the overall mass transfer coefficient (k) was directly proportional to the reactor broth recycle flow rate (r). Increasing the recycle flow rates of mineral oil solvent or the alkaline extraction solution did not affect mass transfer rates, indicating that mass transfer-limitations were at the interface of the reactor broth and the hydrophobic membrane contactor. The overall mass transfer coefficient was linearly correlated to the reactor broth recycle flow rate through the highest flow rates that the pumps could provide (690 L/d). In the continuously fed bioreactor experiment, however, we maintained a constant recycle flow rate (r), mass transfer coefficient (k), and membrane surface area (A). With these values fixed, improvements in MCC transfer and production rates could only be achieved by increasing the concentrations of undissociated medium-chain carboxylic acids (MCCAs) in the bioreactor broth.

4.3.7 Substrate ratios and levels affected n-*caprylate product ratios and production*

In another experiment, high substrate ratios and low substrate concentrations were observed to improve *n*-caprylate product ratios and concentrations in batch reactor microbiomes (Figure 4.10). With the initial concentration of ethanol held constant, the initial concentration of acetate was increased, which decreased the substrate ratio of ethanol to acetate. Treatments with higher substrate ratios of ethanol to acetate generally led to higher product ratios of *n*-caprylate to *n*-caproate (Figure 4.10A), regardless of the initial substrate concentration (Figure 4.11). This result was analogous to results from studies showing that increased substrate ratios of ethanol to acetate led to increased product ratios of *n*-caproate and *n*-butyrate in the type strain *Clostridium kluyveri* (Bornstein and Barker, 1948, Weimer and Stevenson, 2012, Kenealy and Waselefsky, 1985). This finding was also consistent with the observation that higher product ratios of *n*-caprylate to *n*-caproate resulted when the substrate ratio of ethanol to pretreated corn fiber COD was 11 g COD/g COD, instead of a substrate ratio of 2.4 g COD/g COD once yeast fermentation beer was used (Agler et al., 2012a).

In a batch reactor microbiome experiment in which the initial substrate ratio of ethanol to acetate was fixed (13.5 g COD/g COD), lower substrate concentrations led to increased product ratios of *n*-caprylate to *n*-caproate, as well as higher concentrations of n-caprylate (Figure 4.10B). This trend can also be clearly seen in Figure 4.11. Substrate inhibition was apparent at initial ethanol concentrations of 28.8 g COD/L (300 mM) ethanol, and it was confirmed that the ethanol (and not acetate) was the cause of this inhibition (Figure 4.10C). Because these batch reactor microbiomes were derived from the same inoculum as was used in the continuously fed bioreactor, this suggests that the Period 11 average residual ethanol concentration of 27.3 g COD/L (284 mM) would have caused substrate inhibition (Phase II, Period 11, Days 174-186).

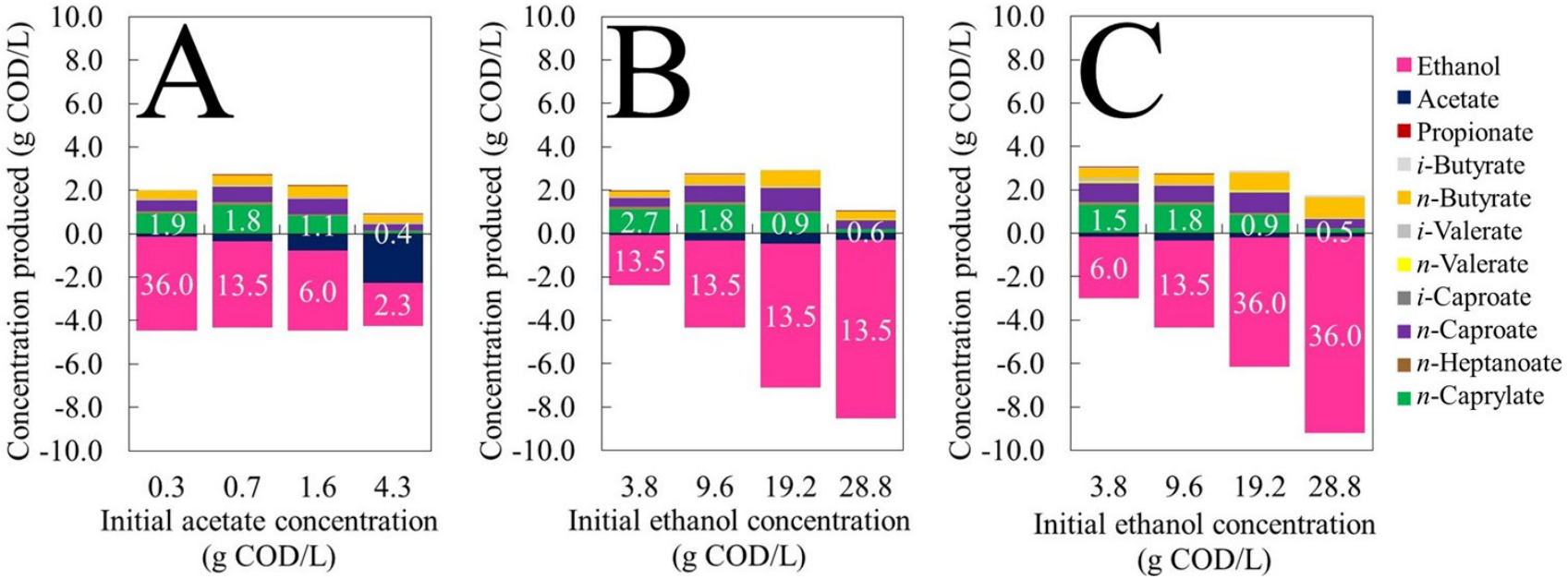

Figure 4.10: Substrate ratios and concentrations affected medium-chain carboxylate product ratios and concentrations in batch reactor microbiomes. The concentrations of ethanol and carboxylates that were either produced (positive values) or consumed (negative values) are shown for three batch experiments of reactor microbiomes. In all experiments, ethanol and acetate were fed, and each concentration represents the average of triplicate biological batch bottles. The temperature of the bioreactors was controlled at 30°C, the pH was maintained at approximately 5.4, and the duration was 12 d. The initial substrate ratio (ethanol to acetate) for each treatment is displayed (in white) upon the concentration of the ethanol consumed, and the product ratio (*n*-caprylate to *n*-caproate) for each treatment is displayed (in white) upon the concentration of the *n*-caprylate produced.

(A) The initial concentration of ethanol was fixed (9.6 g COD/L, 100 mM) and the initial concentration of acetate was varied. When the initial concentration of acetate was increased (which consequently decreased the initial substrate ratio of ethanol to acetate), the product ratio of *n*-caprylate to *n*-caproate decreased. Increased substrate ratios of ethanol to acetate led to increased *n*-caprylate product ratios.

(B) The initial substrate ratio of ethanol to acetate was fixed (13.5 g COD/g COD) and the substrate levels were varied. At this fixed substrate ratio, the lower substrate concentrations resulted in the higher product ratios of *n*-caprylate to *n*-caproate, as well as the higher concentrations of *n*-caprylate. At initial ethanol concentrations of 28.8 g COD/L (300 mM), considerable substrate inhibition of medium-chain carboxylate production was observed.

(C) The initial acetate concentration was fixed (~0.7 g COD/L, ~10 mM) and the initial concentrations of ethanol were varied. An initial concentration of ethanol of 28.8 g COD/L (300 mM) led to substrate inhibition of chain elongation, even with fixed acetate concentrations.

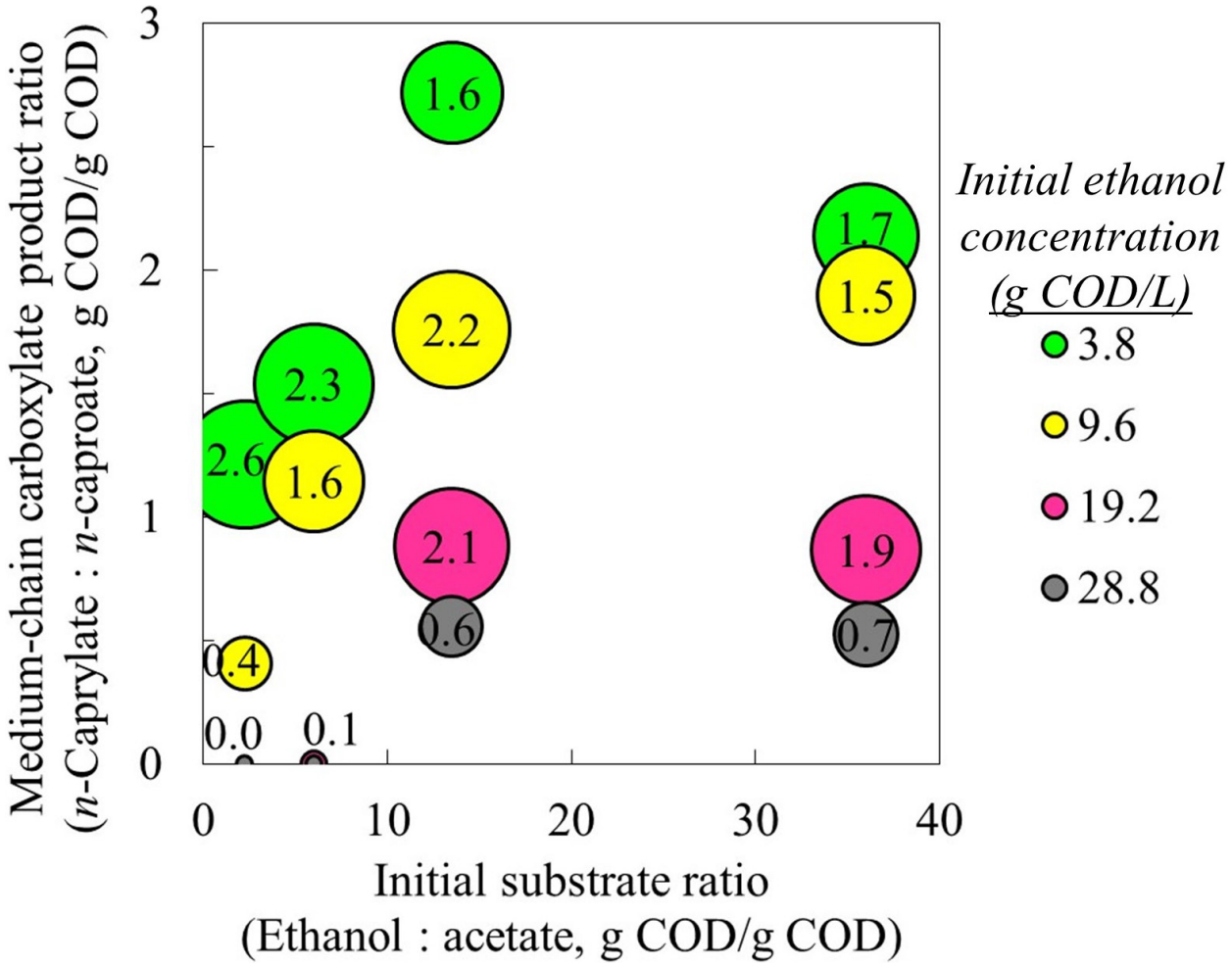

Figure 4.11: Increased substrate ratios and decreased substrate concentrations led to increased product ratios in batch reactor microbiomes. Using the same data set as presented in Figure 4.10, it is clearly shown that increased substrate ratios led to increased product ratios of *n*-caprylate to *n*-caproate. The total accumulated concentration of *n*-caprylate (pH 5.4±0.1, 12 days incubation) is indicated by the size of the dot, as well as by the corresponding black text (value listed is g *n*-caprylate COD/L). Four initial concentrations of ethanol were evaluated, and substrate inhibition was apparent at 28.8 g COD/L (300 mM) ethanol for all substrate ratios.

4.3.8 Microbial community analysis showed the abundant OTUs Rhodocyclaceae K82 *spp. and* Acinetobacter *spp., but a surprising absence of* Clostridium kluyveri

Changes in the reactor microbiome were also investigated. Over the course of the entire experiment, 1634 operational taxonomic units (OTUs) were detected from high-quality sequence reads. 48 OTUs each comprised at least one percent of the relative OTU abundance for one or more microbial community samples (Figure 4.12). Moreover, these 48 OTUs accounted for between 88.1 and 96.0% of the total high-quality sequence reads for each sample. The highest observed relative abundance of a single OTU was 70.8% for a Rhodocyclaceae *K82* spp. (Phase II, Period 9, Day 163). While the type strain *Clostridium kluyveri* is known to convert ethanol into MCCs, the highest relative abundance observed for an OTU from the genus *Clostridium* was less than two percent (Phase I, Period 2, Day 30).

During the phase of high *n*-caprylate productivity (Phase II), 36 OTUs comprised at least one percent of the relative abundance for one or more microbial community samples (Figure 4.13). An *Acinetobacter* spp. and a Rhodocyclaceae *K82* spp. were the predominant OTUs during this phase. Beginning on Day 150 (Phase II, Period 8), the relative abundance of an *Acinetobacter* spp. receded while the relative abundance of a Rhodocyclaceae *K82* spp. increased. Moreover, when the bioreactor was overloaded (Phase II, Period 11, Day 174), the relative abundance of a Rhodocyclaceae *K82* spp. decreased. Finally, of these 36 OTUs, five were linearly correlated ($p<0.05$) to *n*-caprylate productivities, including: 1) *Desulfosporosinus meridiei* ($p = 0.01$)*, 2)* an *Oscillospira* species ($p = 0.02$), 3) a species of *Burkholderia* ($p = 0.02$), and 4-5) two OTUs classified as unknown Ruminococcaceae ($p = 0.002$; $p = 0.04$).

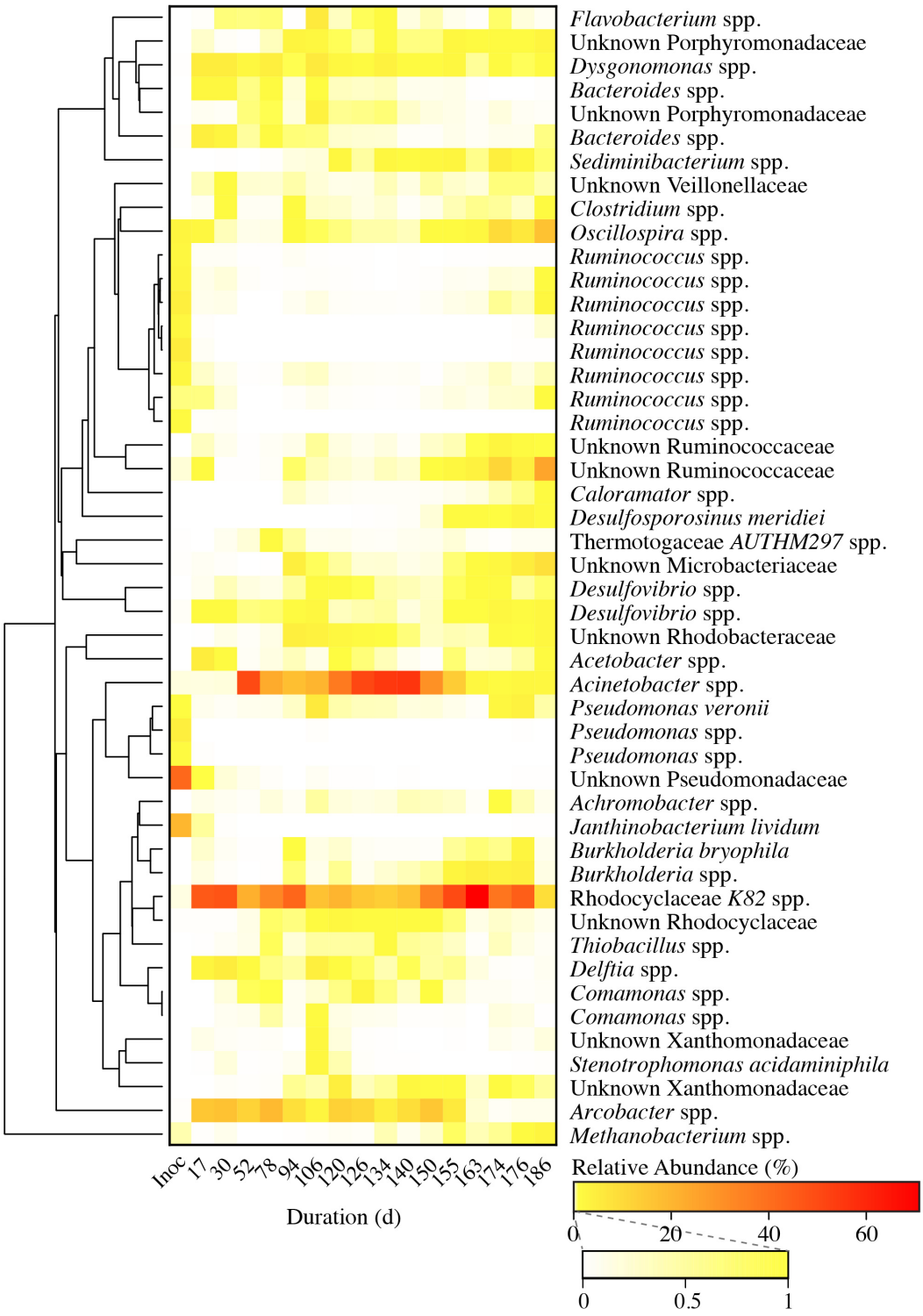

Figure 4.12: OTU relative abundances throughout bioreactor operation. Relative abundances of operational taxonomic units (OTUs) varied throughout bioreactor operation. Each of the 48 OTUs listed comprised at least one percent of the relative abundance for one or more of the samples collected during bioreactor operation, as well as the inoculum. Dominant OTUs included a Rhodocyclaceae *K82* spp. and an *Acinetobacter* spp., which comprised up to 70.8 and 55.5% of the relative abundance, respectively. Phylogenetic similarity is indicated.

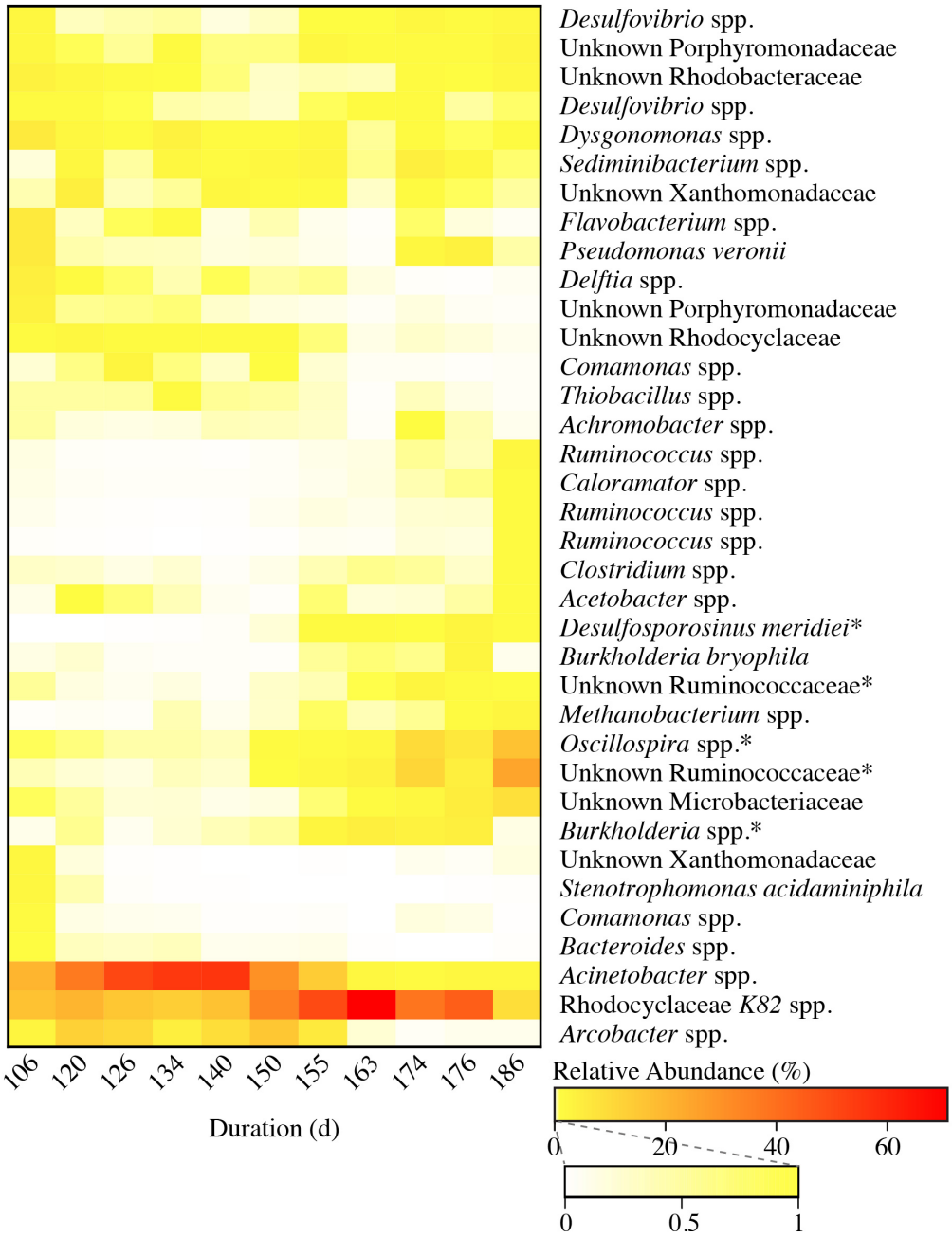

Figure 4.13: **OTU relative abundances during the phase of high *n*-caprylate productivity (Phase II).** During Phase II, each of the 36 operational taxonomic units (OTUs) listed comprised at least one percent of the relative abundance for one or more of the samples collected from this phase. OTUs were clustered hierarchically (average linkage) based on the Bray-Curtis dissimilarity index. OTUs were grouped together based on both the average relative abundance and abundance profile throughout the duration of Phase II. This resulted in the localization of OTUs with lower abundances in the top half, and OTUs with higher abundances in the bottom half. In Phase II, an *Acinetobacter* spp. grew in dominance up to 55.5% of the relative abundance. Subsequently, a Rhodocyclaceae *K82* spp. became dominant, comprising up to 70.8% of the relative. Relative abundances of five OTUs (asterisks) were correlated ($p<0.05$) with *n*-caprylate productivities rates. Data shown are from Phase II only.

4.3.9 Constrained ordination showed that substrate inhibition led to a microbial community shift

Metrics of overall community diversity and correlation to bioreactor function were also determined. No clear trends in alpha diversity (community richness and evenness) were apparent from the Shannon diversity index metric (Figure 4.14). This meant that although the presence of individual OTUs may have burgeoned or diminished, the number of OTUs within the community and their relative proportions were unchanged throughout bioreactor operation. The beta diversity, or dissimilarity of OTU composition between samples, was determined for the entire experiment (Figure 4.15) as well as for the phase of high *n*-caprylate productivity (Figure 4.16A). There was a clear trend in sample dissimilarity from earlier samples (lighter circles) to later samples (darker circles). The final sample from the overloaded period (darkest circle, Phase II, Period 11, Day 186) was the most dissimilar sample from the cluster of earlier bioreactor samples (lighter circles). This indicated that the OTUs and their relative composition in this final sample comprised a considerably different reactor microbiome than before it was overloaded.

Constrained ordination was used to evaluate if beta diversity in Phase II was correlated to specific changes in operating conditions, environmental parameters, or functional performance. Two parameters explained 88% of the variation seen in the beta diversity: 1) residual ethanol concentrations in the bioreactor broth; and 2) hydraulic retention time (Figure 4.16B). Moreover, the sample day number was not a significant ($p>0.1$) predictor of community dissimilarity when considered in the model along with average hydraulic retention time and average residual ethanol concentrations. The results from constrained ordination confirmed conclusions from bach experiments (Figures 4.10 and 4.11): residual ethanol concentrations near 28 g COD/L (~300 mM) led to substrate inhibition. Substrate inhibition, rather than the preceding product inhibition, was ultimately responsible for the microbial community shift.

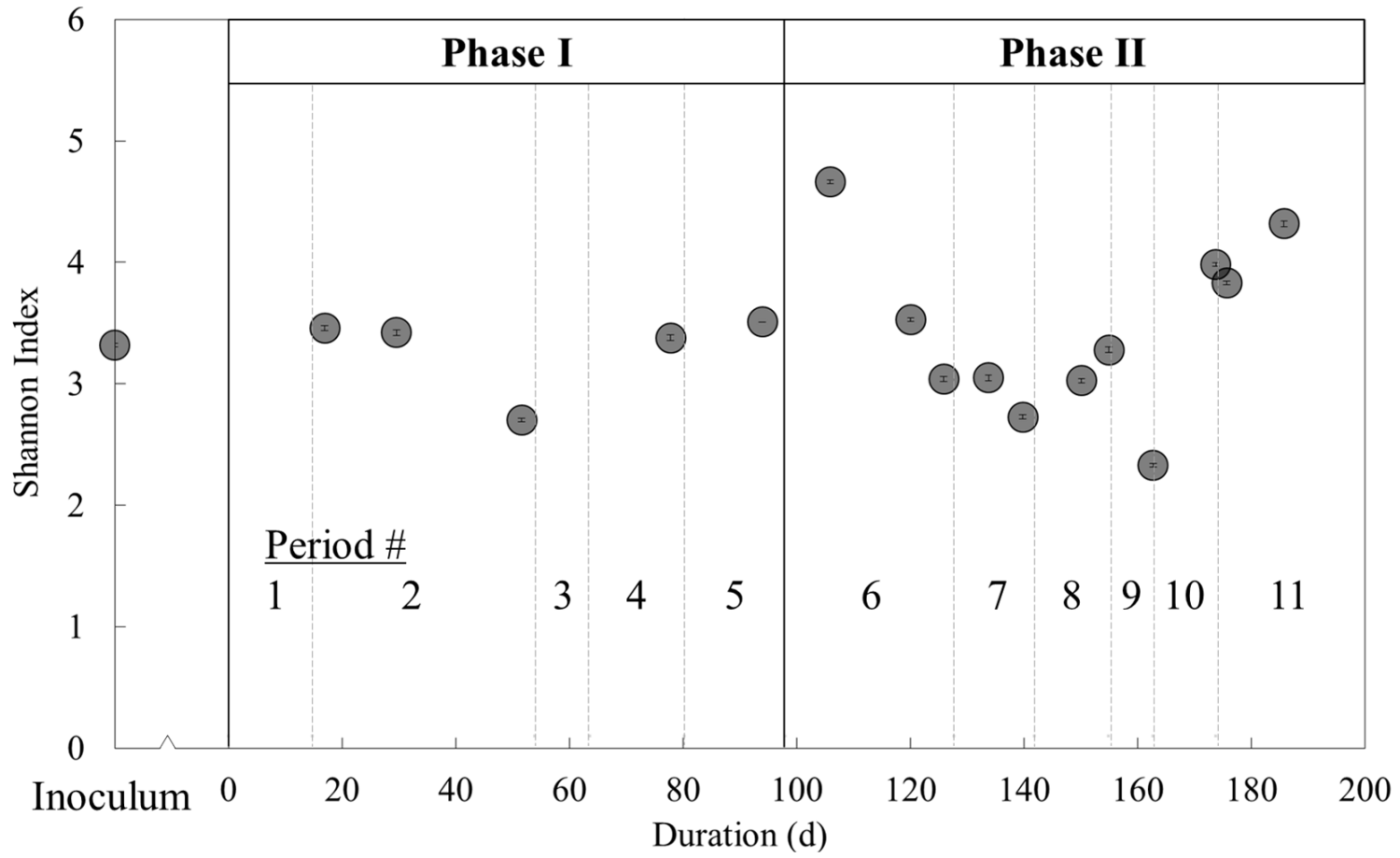

Figure 4.14: Alpha diversity of the reactor microbiome throughout operation. The Shannon index was used to determine the evenness and richness for the 16 samples collected throughout the duration of bioreactor operation, as well as the inoculum sample. Uncertainty is represented by 95% confidence intervals based on ten independent rarefactions.

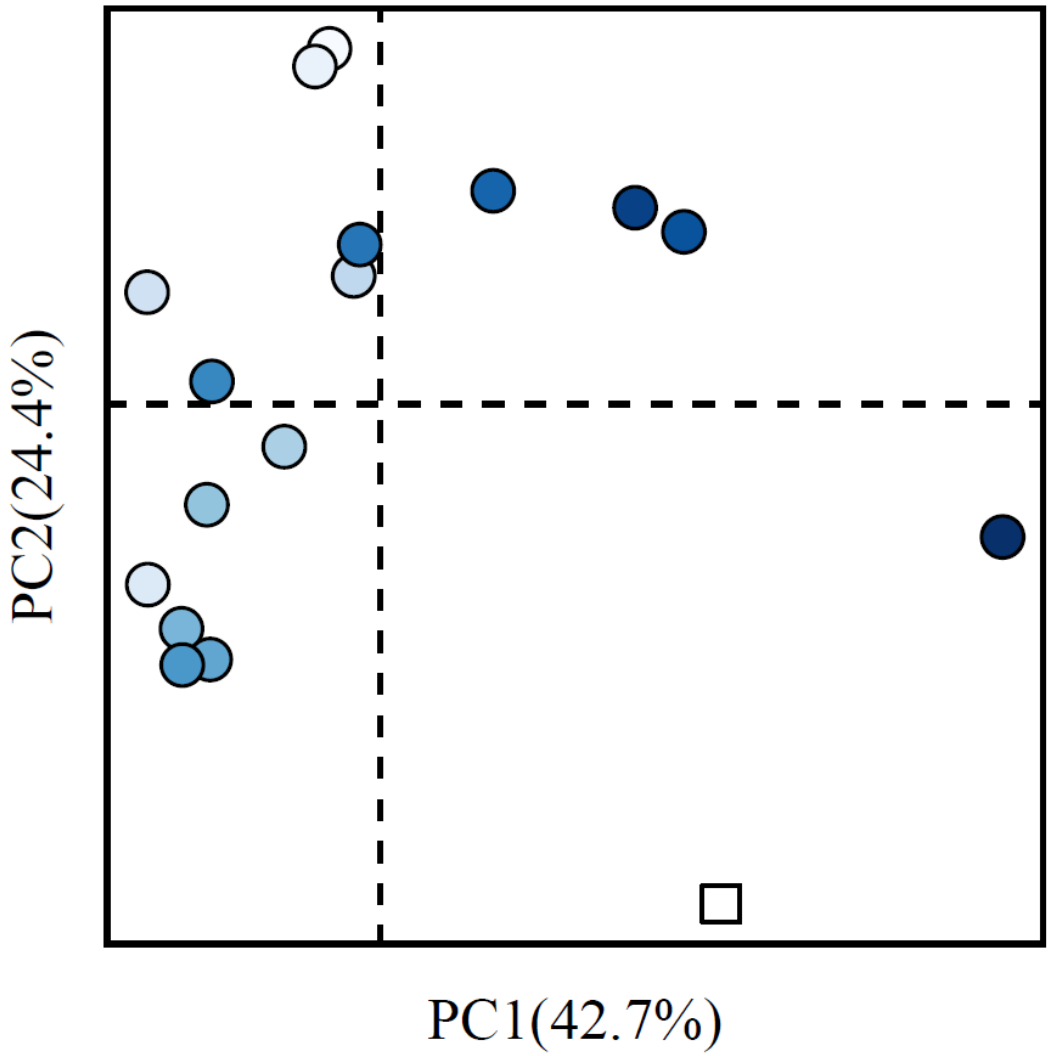

Figure 4.15: Beta diversity of the reactor microbiome throughout operation. Principal coordinates analysis (PCoA) was used to determine the dissimilarity between community samples taken throughout bioreactor operation based on the weighted UniFrac metric. The first two principal coordinate (PC) axes are shown. PC1 explains 43% of the overall phylogenetic variation, while PC2 explains 24%. Darker circles represent samples taken later in bioreactor operation; lighter circles represent earlier samples. The white square represents the inoculum.

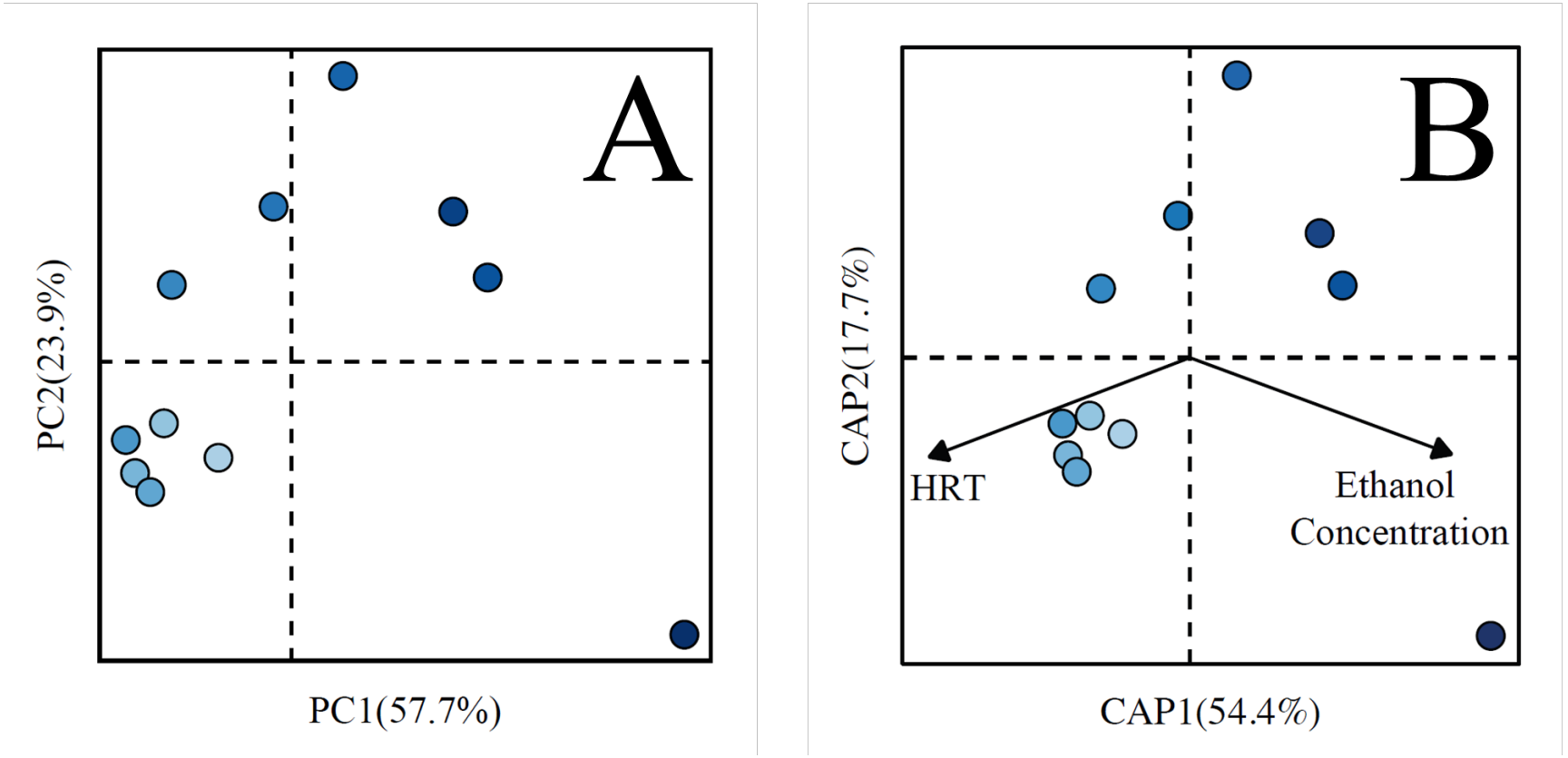

Figure 4.16: **Beta diversity and constrained ordination during the phase of high *n*-caprylate productivity (Phase II).** Principal coordinates analysis (PCoA) (A) and capscale analysis (dbRDA) (B) were performed for Phase II. The five lighter blue circles (lower left quadrants) represent samples from early in Phase II (Periods 6 and 7), while the three darkest circles (rightmost) represent samples from the end of Phase II (Period 11). Average residual ethanol concentrations in the bioreactor broth and average hydraulic retention times (HRTs) were not collinear (VIF<5), but they were significant variables ($p<0.05$) that explained 88% of the variation seen in the PCoA. Data shown are from Phase II only.

4.3.10 Product inhibition was responsible for overloading and stalled n-*caprylate production*

Although substrate inhibition was responsible for the microbial community shift in Period 11 of Phase II, product inhibition remained ultimately responsible for the overloading event. Importantly, the organic loading rate (63.8 g COD/L-d) applied in Phase 11 would not have caused substrate inhibition if the ethanol consumption rates had not already been inhibited by high concentrations of undissociated *n*-caprylic acid (product inhibition). Organic loading rates and ethanol loading rates much higher than 64 g COD/L-d have been fed and consumed by similar reactor microbiomes in upflow anaerobic filters. In one example, ethanol, acetate, and yeast extract were loaded at a total OLR of 226.4 g COD/L-d and an ethanol loading rate of 172.8 g COD/L-d (the substrate ratio of ethanol to acetate was 3.2 g COD/g COD) (Grootscholten et al., 2013d). The maximum productivities of *n*-caprylate and *n*-caproate were 4.4 and 123.1 g COD/L-d, respectively (the product ratio of *n*-caprylate to *n*-caproate was 0.04 g COD/g COD). The total organic and ethanol consumption rates were 154.1 and 115.2 g COD/L-d, respectively. The key difference between this example and Period 11 of Phase II is that the operating pH was 5.2 in the present study, and was near neutral in the study led by Grootscholten (2013d). Therefore, the residual concentrations of undissociated MCCAs, especially *n*-caprylic acid, created an inhibitory environment and ultimately led to the functional demise of this reactor microbiome.

4.3.11 n-*Caprylate production strategy and areas for further research*

To further improve the *n*-caprylate productivity and product ratio, four items deserve focus. First, high substrate ratios of ethanol to acetate and appropriate substrate levels (*e.g.,* concentrations, loading rates) are critical. Optimizing these parameters requires a range of

substrate treatments, but large steps (2x) between loading rates or initial concentrations provided sufficient resolution in the present study. Substrates beyond ethanol also deserve investigation.

Second, product concentrations of undissociated n-caprylic acid should be kept low, but not too low. For example, in Period 4, I turned off the pertraction system to allow the *n*-caprylate-producing microbes to outcompete other members of the community, and this resulted in a sustained production of *n*-caprylate for 122 days (Days 64-186). Additional studies should focus on carefully determining the minimum inhibitory concentrations of undissociated *n*-caprylic acid on chain-elongating microbes. If possible, these studies could be conducted in continuously fed reactor microbiomes with pH control. One strategy would be to add *n*-caprylate to the feed at varied concentrations, and net productivities of *n*-caprylate (under constant ethanol and acetate loading rates) could be calculated. Pertraction would not necessarily be required for such a study, but to maintain non-inhibitory concentrations of undissociated *n*-caprylic acid, a high rate of product removal is essential for highly productive systems. Product removal can only be satisfied in two ways: either through product loss into the effluent (*e.g.*, dilution) or product recovery (*e.g.*, *via* pertraction).

Third, the reactor microbiome in the present study suggests that new species (*i.e.,* not *Clostridium kluyveri*) can produce *n*-caprylate. Deeper investigations should focus on understanding the capacities and activities of the abundant and correlated species that were reported herein. Moreover, these communities should be closely examined to study resilience following overloading events, and subsequent studies should continue to use the tools from constrained ordination and others to link relative abundance and metabolic activity to bioreactor performance.

Finally, to ensure commercial implementation, selection of substrates, operating parameters, and product recovery strategies should be based on life-cycle and techno-economic analyses. For example, economic and environmental prices should be linked to operating parameters (*e.g.,* pumping rates), annualized investments (*e.g.,* membrane size), and product types (*e.g.,* current and prospective market values for *n*-caproate *vs. n*-caprylate). Because this study is the first to show high *n*-caprylate productivities and product ratios, it is hypothesized that *n*-caprylate cannot be produced at such a high rate without pertraction. Thus, an economic model could determine whether the premium available for *n*-caprylate can justify the added capital and operating costs associated with membrane contactors and fast pumping rates, respectively.

4.4 Conclusions

- *n*-Caprylate production was sustained for 122 days in a continuously fed reactor microbiome. The maximum *n*-caprylate productivity achieved was 19.4 g COD/L-d.
- The corresponding product ratio of *n*-caprylate to *n*-caproate was 11 g COD/g COD, and the maximum observed product ratio was 25 g COD/g COD.
- In the final operating period, the concentration of residual undissociated *n*-caprylic acid accumulated to an inhibitory level of 0.22 g COD/L (0.6 mM).
- The use of pertraction was critical in achieving such a high *n*-caprylate productivity.
- If the bioreactor broth recycle flow rate would have been increased, the pertraction system would have reduced the inhibitory concentration of residual undissociated *n*-caprylic acid, which would have probably resulted in even higher *n*-caprylate productivities.
- The *n*-caprylate productivity, product ratio, and accumulated undissociated concentration of *n*-caprylic acid that we reported were higher than any previously reported values.
- Substrate ratios and substrate levels affected MCC product ratios and production in both continuously fed and batch reactor microbiomes.

- The reactor microbiome analysis indicated that species of *Acinetobacter* and Rhodocyclaceae *K82*, were dominant, and that five OTUs (but not *Clostridium kluyveri*) were abundant and correlated with n-caprylate productivity.

- Constrained ordination showed that the residual ethanol concentration in the bioreactor broth and average hydraulic retention time explained 88% of the variation seen in the PCoA.

- This study promotes the integration of the carboxylate and syngas platforms to convert diverse and recalcitrant waste carbon into valuable hydrophobic and energy-dense liquid products.

4.5 Acknowledgements

16S rRNA sequence data and metadata are available on QIITA (http://qiita.microbio.me; study ID 10294) and the EBI database (www.ebi.ack.uk, accession number: in submission). This work was supported by the NSF SusChEM Program (Award # 1336186), as well as by the U.S. Army Research Laboratory and the U.S. Army Research Office (Contract/Grant number W911NF-12-1-0555), which were awarded to L.T.A. L.A.K. was supported by the National Science Foundation (NSF) through the Graduate Research Fellowship Program (GRFP), and by Cornell University's graduate school. C.M.S. was supported by the STAR Fellowship Assistance Agreement number FP-91763801-0, which was awarded by the United States Environmental Protection Agency. The authors wish to thank Prof. Jim Gossett (Cornell University) for his careful review of the manuscript. Gratitude is also expressed for the contributions of: Dylan Kahlstorf; Juan Guzman; Mytien Nguyen; Lauren Harroff; and Dr. Jiajie Xu.

CHAPTER 5

SUMMARY AND RECOMMENDATIONS FOR FUTURE WORK

In this chapter, research conclusions and suggestions for future work are proposed. From the results presented, new options are now available for the production of liquid fuels and chemicals from waste carbon. First, the types of substrates that can be converted to medium-chain carboxylates have been expanded. Specifically, our demonstration of *n*-caproate production from lactate in a continuously fed bioreactor was the first of its kind. Residual lactate concentrations, bioreactor pH, and use of pertraction were all key parameters for effective operation. Moreover, the successful use of a reactor microbiome in which *Megasphaera elsdenii* was nearly absent implies that other microbes must be able to complete this conversion. Finally, this work promotes consideration of other waste streams for use in the carboxylate platform, including those rich in lactate or lactate-precursors (*e.g.*, carbohydrates).

Second, *n*-caprylate productivities and product ratios of *n*-caprylate to *n*-caproate were greatly improved in a reactor microbiome that was continuously fed ethanol and acetate. The *n*-caprylate productivities achieved were over four times greater than previously reported, and the corresponding product ratio of *n*-caprylate to *n*-caproate was over seven time greater than previous reports. Moreover, undissociated *n*-caprylic acid concentrations reached inhibitory levels that have never been achieved before, and increased pertraction rates would have likely further increased the *n*-caprylate productivity. Therefore, further improvements of the *n*-caprylate productivity are likely and should be pursued. Again, the reactor microbiome analysis indicated that expected chain-elongating species (*e.g., Clostridium kluyveri*) were not abundant, suggesting that other species are responsible for *n*-caprylate production.

For future work, emphasis should first be placed on carefully determining the impacts of pH and concentrations of undissociated medium-chain carboxylic acids on chain-elongating bacteria. Specifically, minimum inhibitory concentrations of undissociated *n*-caproic acid, and especially *n*-caprylic acid, should be determined. If possible, these studies should be conducted in continuously fed reactor microbiomes at controlled and varied pH values. By adding these products to the feed at varied concentrations, net volumetric production rates (productivities) of medium-chain carboxylates (under constant substrate loading rates) could be calculated (with attention paid to propagating uncertainty). These net productivities should then be plotted as functions of undissociated concentrations of *n*-caproic acid and *n*-caprylic acid in the reactor broth. Product inhibition should take place; therefore, it is suggested that these experiments could take place without product recovery (*e.g.,* pertraction). Moreover, each reactor microbiome will have its own inhibition limits, as was observed in Chapter 4. Therefore, evaluation of diverse inocula, substrates, and environmental conditions should be pursued.

Second, our characterization of the reactor microbiomes suggest that unanticipated species (*i.e.,* neither *Megasphaera elsdenii* nor *Clostridium kluyveri*) are responsible for *n*-caproate and *n*-caprylate production. Therefore, deeper investigation should focus on both the abundant and correlated species that were observed in these studies. In addition, biomass samples from the bottom of the anaerobic filter should be collected and analyzed, especially fixed-film samples, if possible. Moreover, these communities should be closely examined in subsequent studies to continue to attempt to link relative abundance to metabolic activity and ultimately, to bioreactor performance.

Finally, to ensure commercial implementation, selection of substrates, operating parameters, and product recovery strategies should be based on life-cycle and techno-economic analyses. At the bench and in pilot-plant facilities, each of these decisions will ultimately limit the applicability of the results. For example, if we seek to convert wastes from dairy processing facilities into medium-chain carboxylates, we should first understand substrate costs (or values), logistics, and chemical composition (*e.g.,* lactose vs. lactate). Moreover, superior scientific questions and optimal processes will be developed if we link economic and environmental prices to operating parameters (*e.g.,* pumping rates), annualized investments (*e.g.,* membrane size), and product types (*e.g.,* current and prospective market values for *n*-caproate *vs.* *n*-caprylate).

Chain elongation of waste carbon can produce medium-chain carboxylate products, which can be produced as higher-value alternatives to gaseous products. Targeted scientific questions, smart experimental design, clear thinking, and grounded conclusions will continue to expand and improve this platform. By addressing economic, social, and ecological challenges, chain elongation of waste carbon is poised to produce sustainable liquid fuels and chemicals. Adoption of these types of resource recovery processes can support healthy and productive global communities and ecosystems for generations to come.

APPENDIX

APPENDIX 1

PROTOCOLS

Protocol 1: Basal medium

The basal medium contained (per liter) the following:

#	Component	Amount (g/l)
1	Yeast extract	1.25
2	NaCl	1.17
3	$(NH_4)SO_4$	1.17
4	$CaCl_2 \cdot 2H_2O$	0.065
5	$MgSO_4 \cdot 7H_2O$	0.065
6	$MnSO_4 \cdot H_2O$	0.026
7	$FeSO_4 \cdot 7H_2O$	0.026
8	$ZnSO_4 \cdot 2H_2O$	0.026
9	$CoCl_2 \cdot 2H_2O$	0.0026

10) KH_2PO_4 (0.40 mL of 22.5 g/L

11) Na_2CO_3 (0.40 mL of 80 g/L)

12) 5 ml/L of 2X vitamin solution

2X vitamin solution for basal medium:

Component	Chem Formula	Amount (per liter)
pyridoxine	$C_8H_{11}NO_3$	10 mg
thiamine	$C_{12}H_{17}N_4OS$	5 mg
riboflavin	$C_{17}H_{20}N_4O_6$	5 mg
calcium pantothenate	$C_{18}H_{32}CaN_2O_{1(}$	5 mg
thiotic acid	$C_8H_{14}O_2S_2$	5 mg
paraamino benzoic acid	$C_7H_7NO_2$	5 mg
nicotinic acid	C6H5NO2	5 mg
vitamin B12	$C_{63}H_{88}CoN_{14}O$	5 mg
d-biotin	$C_{10}H_{16}N_2O_3S$	2 mg
folic acid	$C_{19}H_{19}N_7O_6$	2 mg
2-mercaptoethanesulfonic a	C2H6O3S2	2 mg

Preparing viatmins:
prepare in hood, start with less than 1 L DI water
add ones from 25C first (except 2-mercaptoethanesulfonic)
then add ones from 4C

Protocol 2: HPLC

Angenent Lab HPLC Protocol- Aminex HPX-87H Column

You need to be a registered user of the BRL with a valid BRL user login for computers to work with the HPLC. This protocol does not substitute for initial personal training on the HPLC. For now, Michaela, Miriam (mr625) and Hanno (HR95) are allowed to train you. For questions, you can also contact Jose Moran-Mirabal (jmm248) from the Walker-lab.
You need to sign up to use the HPLC at: http://www.my.calendars.net/brl_hplc
NOTE: You should always check the method files you are using to be sure that they have all the steps you need!! If you are not sure what should be in the method file please ask Miriam or Michaela!

Preparation and start-up

1) Preparing the solvent. 0.005 M sulfuric acid (H_2SO_4).
    a) In a clean glass bottle add 0.278 mL HPLC-grade sulfuric acid (18M, 99.999% pure)per one liter MILLI-Q water. Mix well.

!! This is very dilute acid, but it is still hazardous! So obey all safety measures for handling acids. Put your name and date in the log-book

2) Change solvent bottle (for most other applications water is used as the solvent, if anything else than water is used, rinse the liquid "suckers" before placing into the new solvent) and waste container (plastic container large enough to hold all solvent for the day).

3) Turn on all units to be used in your protocol (one or two detectors, and fraction collector chiller if needed).

4) Start the computer, login with BRL user account, start LCSolutions software, choose instrument 1 in the Operation tab.

5) When system configuration window opens, make sure, that all detectors you want to use are added. After adding all components with the blue arrow pointing to the right, Click AUTO CONFIGURATION, click OK.

6) Purge the pumps.
    a) open pump drains by turning the valve 180^o counter-clockwise.
    b) turn the pumps off ("pump" button).
    c) push the "purge" button. Purging will automatically stop after 3 minutes.
    d) close the drains, turn pumps on ("pump" button).

Open method file "SystemPrep" (from the "Angenent Lab" folder under c:\LabSolutions\data\AngenentLab\SystemPrep) in the LC Realtime Analysis window. This method will purge all lines in the instrument (especially the autosampler [3x] and the RI detector) and allow you to install the guard and analytical columns (Micro-Guard Cation H guard column and Aminex HPX-87H analytical column [the latter labeled with "Angenent Lab"] are stored in the refrigerator in the HPLC lab).

7) Start the method. Wait until the initial high flow ramped down to 0.2 mL/min as programmed in the "System Prep" file (after about 60 minutes).

8) Add the guard column, making sure that the flow is going in the proper direction. First connect the inlet, wait for drops to flow out (1-2 minutes), then connect the outlet. Be careful with the screw connections, the plastic threads can get stripped easily.

9) Add the analytical column, making sure that the flow is going in the proper direction. First connect the inlet, wait for drops to flow out (1-2 minutes), then connect the outlet. Be careful with the screw connections, the plastic threads can get stripped easily.

10) Since we are using a temperature of 65 C celsius, open and run the method "RampTemp25to65C&flow. This takes 40 min. 65 C temperature is recommended for our specific column and it helps avoiding bacterial/fungal growth and reduces the resistance to flow, but might give less resolution if you have a complicated sample mix. We had bad experience with running the column at room temperature (pressure became too high, pump shut down). This method also slowly increases the flow rate from 0.2 mL/min to the operating flow rate of 0.6 mL/min to protect the analytical column from fast pressure changes. You can also choose to run this method as the first thing in your batch table with injection of a plain water sample. This way you save yourself 40 min waiting before starting your batch run.

11) Open your batch table (see below on constructing a batch table). Click start batch (green triangle) to start running your samples.

Running samples
Making a batch table:
1) On the LCSolution entrance window, select offline editor.
2) Select "batch processing" in the left panel.
3) Select "wizard" in the left panel.
4) Do not set checkmarks in the first window at startup…shutdown etc. In the next window select standard and unknown. In the next window do not set any checkmarks (at create filenames, clear all calibrations,…). Select new folder, file name, (both labeled with the date). Specify your standard, sample, and tray information as prompted by the wizard. In the batch table, specify sample type "initialize calibration curve" for first std., and control for the following standards, if you do a one-point calibration. Specify the method file "Analysis_HColumn 65C_30min" (30 min proved to be a good run-time, if you need a shorter time, change the method file and save it as a new one), 40 microliter injection vol, tray number is 0 for standards and 1 for the samples.

Note: If possible create one standard solution that contains all the components to be analyzed in your samples. Prepare 3-6 concentration levels of your standard. If you have many samples, repeat individual standards throughout your analysis to check for consistent analysis, e.g. every 10^{th} sample measure a standard.
5) Modify the table as necessary.

6) Add one row at the end of the table, set the vial to "-1", and select the method file "Shutdown Flow and Temp_HColumn". This method will cool down the column and keep the instrument at a constant, low flow rate once your batch table has finished.
Save this batch table and call it up in the LCSolutions realtime analysis window to start your analysis

Loading samples:
1) Load vials into the sample tray in EXACTLY the order shown in your batch table (standards go into the small tray (name "0") on the right, samples into the big tray (name "1"). Make sure the sample tray "clicks in" when you replace it.

Shut down
1) If not already done in the batch table, run the method "Shutdown Flow and Temp_Hcolumn. It takes 30 min for the column to cool down. While pumping at a low flow rate, remove the analytical column, screw in the end caps and place it in its box in the refrigerator.
2) Remove the guard column, screw in end caps and place in the refrigerator.
3) Change the solvent back to Milli-Q water. Make sure to wash of the tubing and filters that go into the solvent so you do not contaminate the water with sulfuric acid.
4) Switch the effluent tubes back into the big water effluent collection barrel (ensure that the barrel is not full). Neutralize your collected sulfuric acid effluent with sodium bicarbonate (1 mol H_2SO_4 requires 2 mol bicarbonate), the neutralized solution can be flushed down the sink.
5) Select the method file "SystemWash at End" and run it. This basically does the same thing as the start up program (purging autosampler and RI detector cell), but in reverse.
6) When the method is finished, purge the pumps as in step 6 of set-up.
7) Leave the pumps flowing at 0.05 mL/min, close LC solutions and log out.

➔ make sure that you leave the workspace clean and in order.

NOTE: You should always check the method files you are using to be sure that they have all the steps you need!! If you are not sure what should be in the method file please ask Miriam, Michaela or Hanno !

Data analysis:

1) Go to the LCSolutions "Postrun analysis" window.

2) To prepare calibration curves from your standards: Follow the steps outlined in the LCSolutions manual (page 28). Or do the following:

- Check that the baseline is set properly and that the peaks are integrated properly: open each data file and if necessary adjust the baseline manually. Save the file.
- click the "postrun" in the LCsolution launcher
- click the (LC Data Analysis) icon in the (postrun) assistant bar. The (LC data analysis window appears). Pull down the chromatogram view window (it is hidden above the (Compound Table View).
- Select [open data file] in the [file] menu and select a pre-measured data file (the standard with the highest level). The data file opens

- Click the (wizard) icon in the assistant bar. The [compound table wizard] appears.
- Make sure that appropriate peak integration parameters are set
    - detector A
    - Ch1 for RID detector (if only RID detector was used, if both detectors were used, RID might be detector B)
    - width 5 sec
    - slope 20 uV/min
    - drift 0 uV/min
    - T.DBL 15 min
    - Min Area/Height 100 count
    - Calculated by Area
- Register the retention time of the peaks to be identified and click [next]. Here are some examples for the RID detector, derived in April 22nd, 2010 at 65 C Celsius:

RETENTION TIMES HPLC RUN T= 65 °C, 04/08/2010		
COMPOUND	*RT DETECTOR A (UV)*	*RT DETECTOR B (RID)*
OXALIC ACID	7.0	7.3
GLUCOSE	_	8.9
FRUCTOSE	9.4	9.6
SUCCINATE	10.7	10.9
FUMARATE	11.4	11.7
LACTATE	11.8	12.1
FORMATE	12.9	13.1
FORMALDEHYDE	_	13.4
ACETATE	14.2	14.4
ACETOIN	16.7	16.9
ACETALDEHYDE Interferes with butanediol	17.9	18.1
BUTANEDIOL	_	17.8 / 18.5
METHANOL Interferes with butanediol	–	19.0
BUTYRATE	19.6	19.7
ACETONE	_	20.7
ETHANOL	_	21.5

- specify the quantitative calculation method and the calibration curve type and click [next]. Settings should be
    - external standard
    - calculated by Area
    - # of calibration levels = 1 (5, if you do a calibration curve for the first time, and have to verify linearity. Thereafter you only need one standard concentration, or one level).
    - Curve fit type: linear
    - Zero: do not force through
    - Weighting method: none
    - X-axis: Area/hight
    - Units: mM
    - Decimals: 2
    - Group type: not used
- set how you want to identify peaks and click [next]. Settings should be:
    - Window/Band: Window
    - Window: 5 %
    - Peak selection: closest peak
    - Retention time update: none
- the [Compound Table Wizard 5/5] screen appears. Provide detailed settings for the compound table and click [finish]
- provide detailed settings (compound names, type: target, channel, concentration. The [compound table wizard] is completed. Click finish
- click lc data analysis icon in the bar to the very left, you might have to go one level up.
- Click the (apply to method) icon
- Name the method file (e.g. “calibration curve HColumn 65C Hanno). Save. The [select method parameters] screen appears. Don’t make any changes, just click OK.

3) Run a batch table to create the calibration curve:

- Make sure that the HPLC is done with the analysis, you should close the real time analysis window, it’s even best to log out and restart the postrun application. If you don’t do it, the batch table for your calibration curve might not run, you might get the error message “file read closed” .
- In the postrun application click “batch processing” in the assistant bar
- Select “new batch file” in the file menu
- Drag and drop the data files which are set as the calibration levels from the data explorer to the batch table
- Specify the method file that you just created in the method file field for all lines of the batch table, make sure both are shown in the analysis type screen
- Set the [sample type] cells, set the first line to “standard-initialize calibration curve”; set the following lines to “standard-add calibration level”; set the level for each line
- Save the batch table under new name, e.g. “batch table calibration curve”. RUN the file.
- Viewing the calibration curve: open the most recently processed standard sample data file (the last file in your calibration curve batch table). When you open a previous one, an incomplete

calibration curve is displayed. Make sure that the baseline is set properly, the integration is not messed up.
- Note: if you are using both detectors (RI and UV-Vis), you will have to prepare a calibration curve for each detector – choose between detectors in main menu bar.

4) Analyzing your data:
- check all data files that the peaks have been integrated well, if necessary, adjust the baseline manually and save the data file.
- Create a new batch table in the "Postrun analysis" window from the menu list on the left. Drag all sample results files from the Explorer Window into your batch file. Choose your calibration file as the method file for all your samples. Save this analysis batch file. "Run" the batch file by pushing on the start button. Note: if you are using both detectors (RI and UV-Vis), you will have to run the analysis with the calibration files for each detector. Make sure, again, that the integration is OK.

5) For retrieving the data:
- close the postrun window and open the browser window from the LCsolution start window
- Choose "LC quant browser" from the menu on the left
- drag your sample data files into the batch table window, make sure that correct detector is selected.
- make sure you chose the right detector in the bar on top of the page.
- you can see your results for each data file and compound by highlighting the line of the data file in the batch table and highlighting the compound in the compound table. The concentration for the highlighted compound appears in the batch table. Verify that integration/baseline are OK.

6) For export of summary data tables with all analytical data (no chromatograms), open your analysis batch file in the Browser Window and export the data into a .txt file which can be opened in Excel on your own computers. Make sure you chose detector B (RI detector) in the bar on top of the window. Note: if you are using both detectors (RI and UV-Vis), you will have to export the results files for both detectors (switch between detectors in main menu bar).

7) Lastly, move your exported data files from the LCSolutions data folder on the HPLC computer to your own "Enterprise" account folders!!! Data files will be deleted automatically from the HPLC computer to prevent data overflow – methods files will remain stored! No external storage devises are allowed with the HPLC computer. You can retrieve your data from Enterprise via external devise or email on any of the laptop computers in the BRL office area.

Protocol 3: Procedure for GC evaluation of individual Volatile Fatty Acids (VFAs)

Updated June 15, 2015 by Lauren Harroff

Sample Preparation and Storage:

1. Centrifuge samples and filter (0.2 μm) to remove any suspended solids.
2. Undiluted samples (no formic acid added) may be stored in 4° C refrigerator or freezer for subsequent analysis. Depending on the sample, it may need to be centrifuged and/or filtered again after thawing. If there is any possibility of suspended solids, make sure to refilter or centrifuge.
3. Each sample vial will contain: 3 mM 2-ethylbutytric acid (internal standard), sample (diluted to <7 mM for individual VFA of interest), and 2% formic acid (to raise total volume to 1 mL or 500μL)
    a. Add appropriate volume of sample to obtain <7 mM of the specific VFA of interest. If measuring multiple VFAs, multiple dilutions may be needed.
    b. Add stock internal standard. There should be a stock of 30 mM 2-ethylbutryic acid diluted in 2% formic acid. If using 1 mL total volume in the vial, add 100 μL of this stock solution. If using 500 μL total volume, add 50 μL stock solution.
    c. Add 2% formic acid to bring total volume to either 500 μL or 1 mL.
    d. Close vial immediately after adding formic acid.

    *** Note: Final pH of sample must be approximately 2 in order to volatilize the fatty acids in the sample. Depending on the alkalinity of the sample, this will restrict options for choosing dilutions. If sample contains very low concentrations of VFAs, a more concentrated formic acid solution can be used for dilutions to allow lower pH at higher sample concentration.

Standard Preparation:

The stock solution of volatile fatty acids (stored in the refrigerator in B68) contains 10 mM each of: formic, acetic, propionic, isobutyric, butyric, isovaleric, valeric, isocaproic, caproic, and heptanoic acids.

Make at least 5 standards of varying dilutions to create a standard curve. Typically a curve is created with 1, 2, 3, 5, and 7 mM. Choose appropriate concentrations based on expected concentrations in samples. If sample concentrations are low, the GC can detect accurately down to about 0.1 mM, but the standard curve needs to include points in this range. Standards cannot be created above 7 mM because the pH will not be sufficiently low to volatilize the fatty acids.

Make additional "check standards" of known concentration to mix in the run with samples. This provides quality control because the measured concentrations can be compared to the known concentrations. (See below in "Loading Samples" for more details.)

Make several blank vials of only 2% formic acid. These will be run as the first vial, after the set of standards, after every 5 samples, and as the final vial.

Start-up: (GC 1, closest to fume hoods)

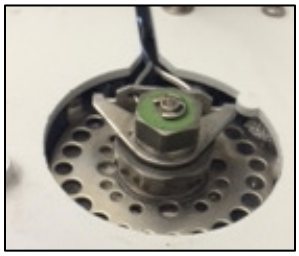
Step 4b

1. **FIRST** turn on the compressed air, helium, and hydrogen cylinders by opening the main cylinder valves.
2. Locate the ball valves that open the gas lines to the individual GCs. Valves for most gases can be found on manifolds at the center of the lab bench where the GCs are located. Valves for hydrogen are located next to the hydrogen gas cabinet. Open the appropriate ball valves for each gas (air, helium, and hydrogen) labeled as GC 1.
3. Add name, date, and planned number of samples to the logbook.
4. If the septum has not been changed for over 50 injections (recorded in logbook), change it now.
    a. Remove the injector tower by lifting straight up off of the support rod. Place injector tower on the top of GC 2 or on shelf.
    b. Remove the nut (green in photo) at injection site.
    c. Remove green septum and discard. Septum may be lodged inside the nut.
    d. Place in new septum and replace nut. Only finger tighten the nut. It does not need to be overly tight.
    e. Replace injector tower by aligning metal support rod with appropriate port on the bottom of the tower.
5. If the glass injector sleeve has not been replaced for over 150 injections (recorded in log book), replace now. If acetate measurements are important, check the glass injector sleeve for contamination even if it has been recently replaced.


Step 5c

    a. Remove injector tower.
    b. Open top door of the GC.
    c. Use wide wrench located on bench next to the GCs to loosen the larger nut underneath septum nut.
    d. Squeeze pointed forceps together and insert into injection port.
    e. Allow forceps to expand and pull straight up to remove glass injector sleeve.
    f. If contamination is visible, place used injector sleeve in glass Nalgene bottle labeled 25% H_2SO_4 and containing other glass sleeves. Use forceps to remove clean sleeve from bottle.
    g. Rinse new sleeve with ethanol followed by DI water.
    h. Dry with compressed air from the lab bench.
    i. Use forceps to drop new, clean sleeve into injection port with flared end at the top.
    j. Tighten nut with wrench. Again, does not need to be overly tight but this one is a bit harder than the septum nut.
    k. Replace injector tower.
6. Turn the switch on the bottom left corner of the front face of the machine on.
7. Turn on the communication module (box located to the left of the GC).

8. On the Windows 98 computer, open "Instrument 1 (online)" from the desktop. If "Instrument 1 (offline)" is already open, close that before opening the online program.
9. After Chemstation loads on the GC, check that the oven, front injector, and front detector are all on and temperatures are set to 70, 200, and 275° C, respectively.
10. Empty waste vials and methanol (Solvent A) from the injection tower into the GC waste bottle (stored under the right-hand fume hood when back is to the windows).
11. Refill Solvent A with fresh methanol (found under the right-hand fume hood in B68A).
12. Empty and refill Solvent B vial with DI water.

***Both Solvent A and Solvent B should be filled completely! The needle only lowers down to about the 2 mL mark, so if the vials contain less than 2 mL of liquid, the needle will not be cleaned.

13. Remove and clean needle.
    a. Open door on the injection tower.
    b. Swing open the tab located about halfway up the syringe barrel that is holding the needle in place.
    c. Unscrew the nut holding the plunger and slide nut up.
    d. Pull needle forward from point D on the photo and then lift up to remove. (Otherwise the needle tip will get caught on the bottom stand.)
    e. Remove plunger and clean the plunger and syringe barrel using ethanol, soap, and DI water. Check that the plunger moves smoothly through the barrel.
    f. Fill a small beaker with DI water and check that the needle takes up and dispels water properly.
    g. Replace needle properly. Hold needle at an angle and align needle tip with position on gray stand. Then slide into position at point D. Rescrew the nut a point C and replace the tab at point B.

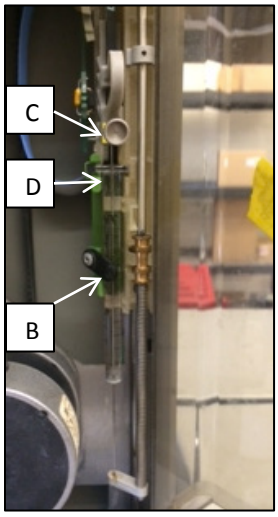

Step 13

Start-up: (GC 3, closest to windows)

1. **FIRST** turn on the compressed air, helium, and hydrogen cylinders by opening the main cylinder valves.
2. Locate the ball valves that open the gas lines to the individual GCs. Valves for most gases can be found on manifolds at the center of the lab bench where the GCs are located. Valves for hydrogen are located next to the hydrogen gas cabinet. Open the appropriate ball valves for each gas (air, helium, and hydrogen) labeled as GC 3.
3. Turn on gases at the GC. Turn needle valves on Detector A panel (top left) for air, hydrogen, and aux gas (helium) to the left to turn on. Valves should be turned all the way open, but do not force them. They can get stuck.
4. Add name, date, and planned number of samples to the logbook.
5. If the septum has not been changed for over 50 injections (recorded in logbook), change it now.
    a. Remove the injector tower by lifting straight up off of the support rod. Place injector tower on the top of GC 2 or on shelf.
    b. Remove the nut (black in photo) at injection site.
    c. Remove green septum and discard. Septum may be lodged inside the nut.
    d. Place in new septum and replace nut. Only finger tighten the nut. It

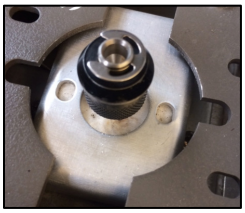
Step 5b

does not need to be overly tight.

e. Replace injector tower by aligning metal support rod with appropriate port on the bottom of the tower.

6. If the glass injector sleeve has not been replaced for over 150 injections (recorded in log book), also replace this now. If acetate measurements are important, check the glass injector sleeve for contamination even if it has been recently replaced.
    a. Remove the injector tower by lifting straight up off of the support rod. Place injector tower on the top of GC 2 or on shelf.
    b. Unscrew black septum cover at injection site.
    c. Remove green septum and discard. Septum may be lodged inside the cover.
    d. Squeeze pointed forceps together and insert into injection port.
    e. Allow forceps to expand and pull straight up to remove glass injector sleeve.
    f. If contamination is visible, place used injector sleeve in glass Nalgene bottle labeled 25% H_2SO_4 and containing other glass sleeves. Use forceps to remove clean sleeve from bottle.
    g. Rinse new sleeve with ethanol followed by DI water.
    h. Dry with compressed air from the lab bench.
    i. Use forceps to drop new, clean sleeve into injection port with flared end at the top.
    j. Place in new septum and replace cover. Finger tighten.
    k. Replace injector tower by aligning metal support rod with appropriate port on the bottom of the tower.
7. Turn the switch on the bottom right corner of the right face of the machine on.
8. Turn on the communication module (box located to the left of the GC).
9. On the Windows 98 computer, open "Instrument 3 (online)" from the desktop. If "Instrument 3 (offline)" is already open, close it before opening the online program.
10. After Chemstation loads on the GC, check that the oven, front injector, and front detector are all on and temperatures are set to 70, 200, and 275° C, respectively.
11. Empty waste vials and methanol (Solvent A) from the injection tower into the GC waste bottle (stored under the right-hand fume hood when back is to the windows).
12. Refill Solvent A with fresh methanol (found under the right-hand fume hood in B61A).
13. Empty and refill Solvent B vial with DI water.

***Both Solvent A and Solvent B should be filled completely! The needle only lowers down to about the 2 mL mark, so if the vials contain less than 2 mL of liquid, the needle will not be cleaned.

14. Remove and clean needle.
    a. Open door on the injection tower.
    b. Swing open the tab located about halfway up the syringe barrel that is holding the needle in place.
    c. Unscrew the nut holding the plunger and slide nut up.
    d. Pull needle forward from point D on the photo and then lift up to remove. (Otherwise the needle tip will get caught on the bottom stand.)
    e. Remove plunger and clean the plunger and syringe barrel using ethanol, soap, and DI water. Check that the plunger moves smoothly through the barrel.
    f. Fill a small beaker with DI water and check that the needle takes up and dispels water properly.
    g. Replace needle properly. Hold needle at an angle and align needle tip with position on gray stand. Then slide into position at point D. Rescrew the nut a point C and replace the tab at point B.

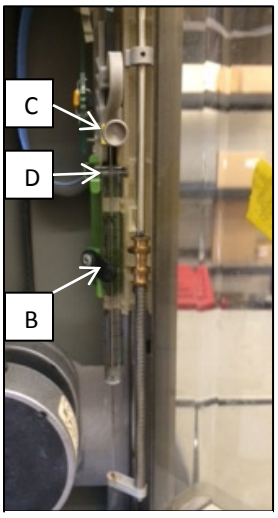

Step 14

15. Once the GC reaches operating temperatures (~15 minutes), light the detector.
    a. Press “SIG 1” button on the front face of the GC twice to display the signal output from Detector A.
    b. Open the top door of the GC.
    c. Push the “FID Ignite” button on the Detector A panel on the top left of the front face of the GC. Simultaneously hold a lit match or lighter over the detector.
    d. Release the “FID Ignite” button. If the signal output maintains a reading of 12-15, then the detector is lit. If the signal drops back to 0-0.5, try to ignite again.
16. Allow 15 minutes to equilibrate. The signal output should maintain a steady reading (~25) before starting a run.

Loading Samples (this can be performed while waiting for the GC to warm up)

1. Load your samples into the autosampler trays. Ensure that the “Vial 1” position on the tray is aligned with the “1” position on the autosampler.
2. Include a blank vial containing only 2% formic acid as the first vial, after the set of standards, after every 5 samples, and as the final vial.
3. Approximately every 10 vials add one of the “check standards” created during “**Standard Preparation**”.
4. As best as can be predicted, try to load the samples in order from most dilute to most concentrated.
5. For quality control, recommended run length is a maximum of 50 vials including blanks and standards. After a long period of time, the GC measurements tend to fluctuate.

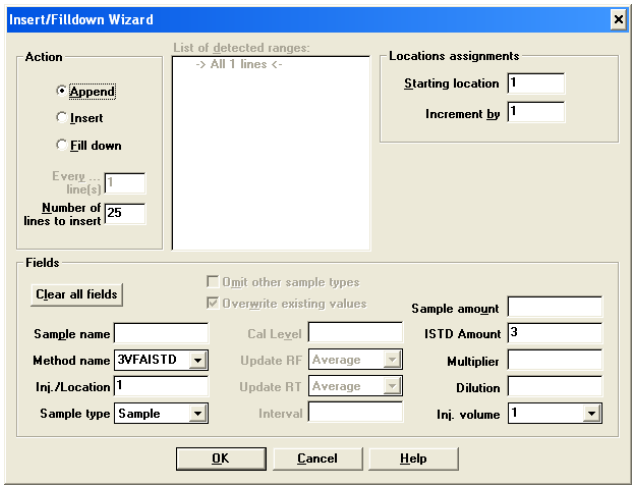

Steps 3- 10

Loading Sequence on the Computer

1. From the “Online” computer program (Instrument 1 or 3 depending on which machine is being used), click “New Sequence” from the “Sequence” menu.
2. Open “Sequence Table” from the “Sequence” menu.

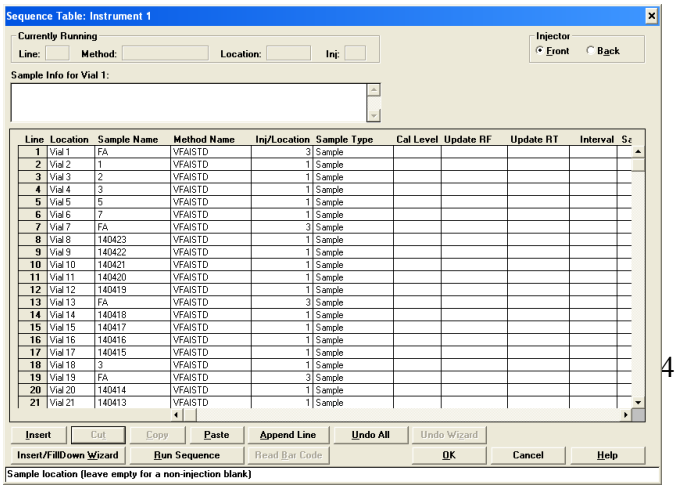

3. Open “Insert/FillDown Wizard”.
4. For “Starting location” enter “1” to indicate the location of your first vial.
5. For “Number of lines to insert” enter the total number of vials you are running (standards + blanks + samples)
6. For “Method name” enter “VFAISTD” for GC 1 or “3VFAISTD” for GC 3. *Steps 11- 14*
7. For “Inj./Location” enter “1” to indicate the number of times each vial will be sampled.
8. Scroll to the right, and enter “3” For “ISTD Amount” to indicate that each vial contains 3 mM of the internal standard.
9. For “Inj. volume” enter “1”.
10. Leave other fields blank and press “OK”.
11. “Cut” the first line if it was left blank.
12. Under “Sample Name” enter the individual sample name for each vial.
13. For every formic acid blank, change “Inj/Location” to “3” and change “ISTD Amount” to blank (Do not enter “0” or you will receive an error.)
14. Click “OK”.
15. Open “Sequence Parameters” from the “Sequence” menu.
16. Enter your initials for “Operator Name”.
17. Enter the folder name where you will find your data for “Subdirectory”. We typically use initials followed by the date. (Ex: LH140428 for a run on April 28, 2014).
18. Click “OK”.
19. A message will be displayed asking permission to create the subdirectory you have named. Click “OK”.
20. If you will use the same or similar sequence in the future, save your sequence under “Save Sequence as” from the “Sequence” menu.

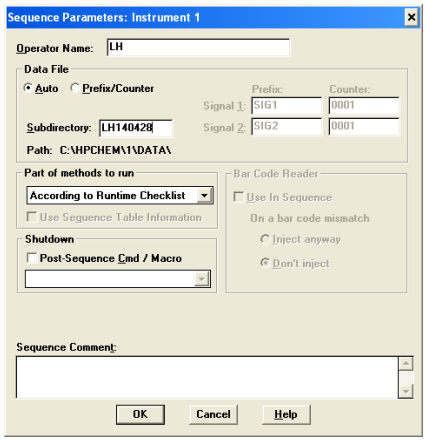

Steps 15-18

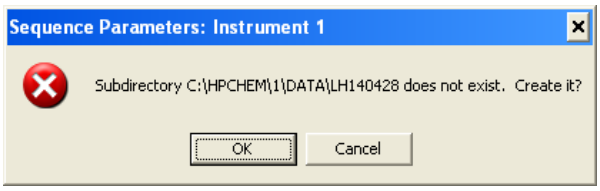

Step 19

Starting Injections

1. Check that the method displayed on the main screen of the online program reads “VFAISTD.M” for GC 1 or “3VFAISTD.M” for GC 3.
2. Check that the box above “Start” and “Stop” buttons is green and reads “Ready”.
3. Once it is ready, press “Start”.
4. Wait for the GC to run through the syringe and needle cleaning process and inject the first blank before walking away. Most problems occur during this first injection.

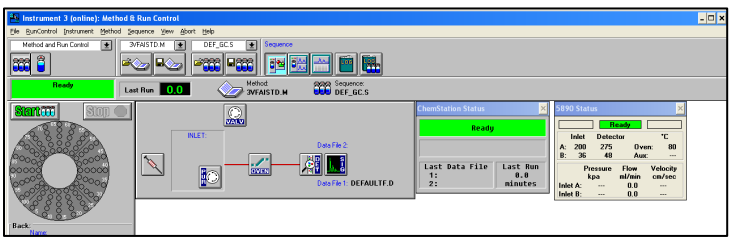

5. If the computer displays a plunger error or injector error message, check that the plunger of the syringe moves freely and takes up and dispels water appropriately. Clean the needle and syringe again if necessary and restart the sequence.
6. If possible, create a standard curve and check for a linear relationship as soon as the standards have finished running. (See **"Data Analysis"** for instructions.) This step allows potential errors to be identified before all samples have been run.

Steps 1-3

Shutting Down: (GC 1, closest to fume hoods)

1. Close the "Instrument 1 (Online)" program on the computer, and turn off the communication module.
2. On the front of the GC, push the "Oven" button and turn the temperature off. Do the same for "Front Inlet" and "Front Det".
3. Once each component has cooled to at least 100° C, turn off the GC.
4. Turn off the helium, hydrogen, and compressed air cylinders ONLY if none of the other GCs are running.

Shutting Down: (GC 3, closest to windows)

1. Close the "Instrument 3 (Online)" program on the computer, and turn off the communication module.
2. Turn off the hydrogen valve at the GC to extinguish the detector flame.
3. On the front of the GC, push the "OVEN TEMP" button and turn the temperature off. Do the same for "INJ A TEMP" and "DET A TEMP".
4. Once each component has cooled to at least 100° C, turn off the GC.
5. Turn off the helium, hydrogen, and compressed air cylinders ONLY if none of the other GCs are running.

Data Analysis

1. Open "Instrument 1 (offline)" for GC 1 or "Instrument 3 (offline)" for GC 3
2. Open "Load Signal" from the "File" menu.
3. Under the folders "HPCHEM", "1" (or "3" for GC 3), and "DATA", find the folder with the subdirectory name that you created previously from "Sequence Parameters".

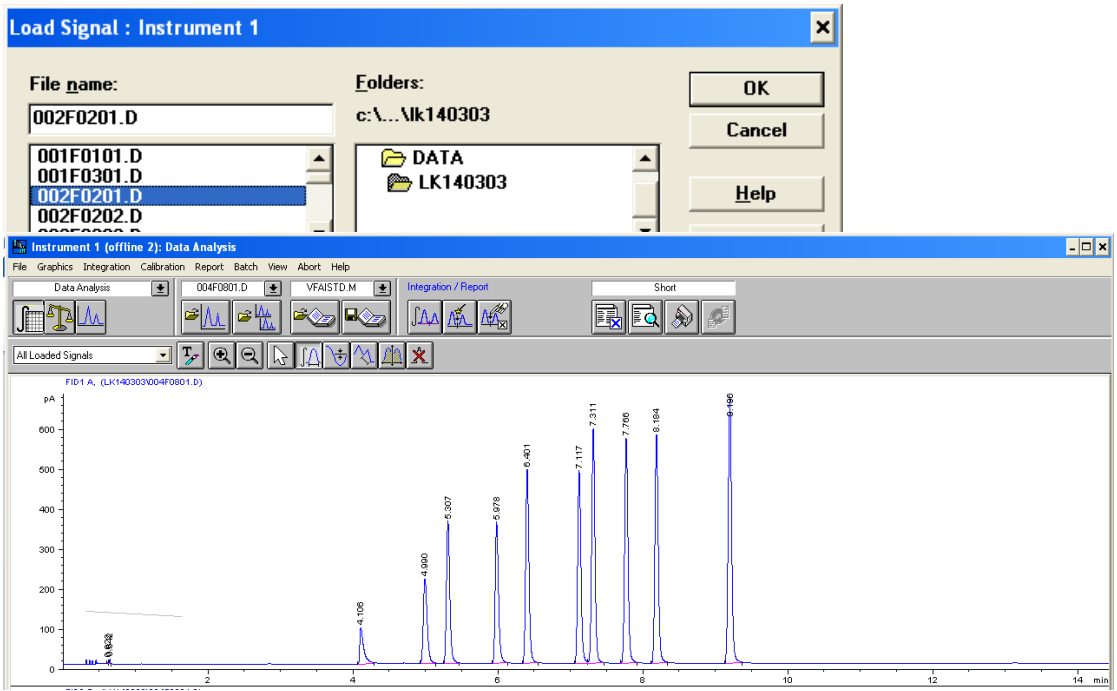

4. Select the first standard vial. Usually the file name will read “002F0201.D” because the first vial was a blank. The first number (“002”) indicates the location number of the vial. Click “OK”.
5. Check that the method displayed on the main screen is “VFAISTD.M” or “3VFAISTD.M”.
6. Click the integration button. If an error or warning message is displayed, click “OK”. Those errors will be fixed later.
7. Click the manual integration button.
8. Remove and unwanted peaks by dragging the mouse above the peak.
9. Select “New Calibration Table” from the “Calibration” menu.
10. For “Default Amount” enter the mM concentration of the first standard, usually “1”. Click “OK”. If asked to overwrite the existing calibration table, select “Yes”.

Steps 2-4

11. On the table, name the compound for each peak. There should be 10 peaks that come out in the following order:

Step 10

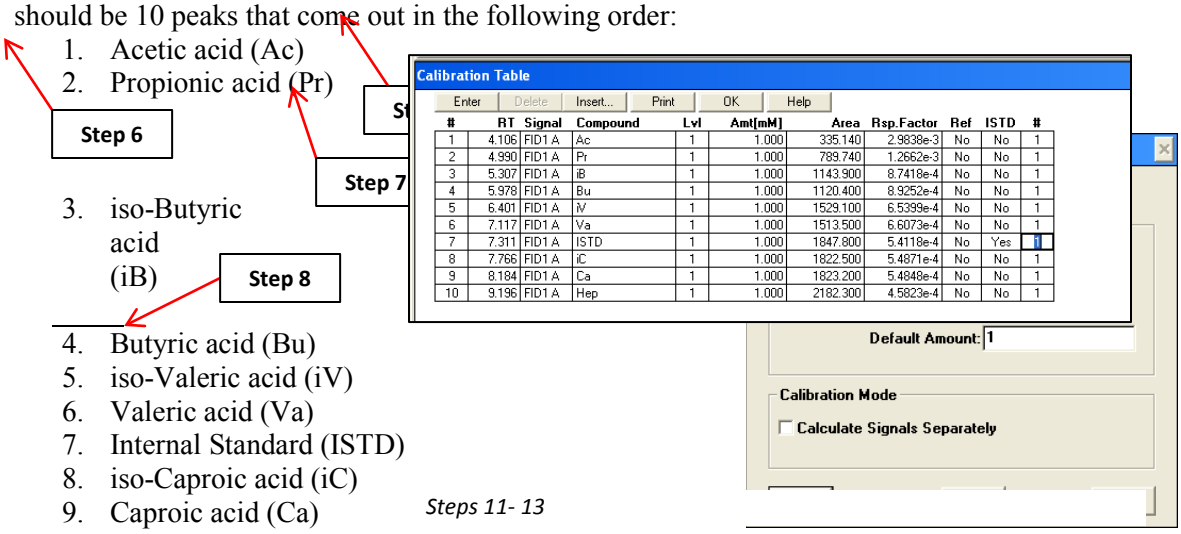

1. Acetic acid (Ac)
2. Propionic acid (Pr)
3. iso-Butyric acid (iB)
4. Butyric acid (Bu)
5. iso-Valeric acid (iV)
6. Valeric acid (Va)
7. Internal Standard (ISTD)
8. iso-Caproic acid (iC)
9. Caproic acid (Ca)
10. Heptanoic acid (Hep)

Steps 11- 13

12. For peak #7 (“ISTD”), on the column named “ISTD” change the drop-down back from “No” to “Yes”.
13. Click the blank box immediately to the right from the “#” column and enter “3” for “ISTD Amount”. Click “OK”. The remaining rows for the “#” column should fill in with “1” to indicate the ISTD that you have just named.

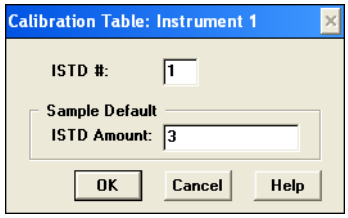

Step 13

14. Load the next standard vial by selecting “Load Signal” from the “File” menu. The computer will automatically recognize the correct peaks identified in the calibration table, so steps 6 and 7 do not need to be repeated for the remaining vials.
15. Select “Add Level” from the “Calibration” menu.
16. Enter the concentration of the standard for “Default Amount” and click “OK”.
17. Repeat steps 14 and 15 to load all standards.
18. At this point, the curves will look approximately like a straight vertical line because the ISTD concentrations are incorrect. On the calibration table, change the “Amt[mM]” values to “3” for all levels of the internal standard.
19. The computer will create a standard curve for each individual VFA. Check that all curves have a strong linear correlation (~ 0.995 or higher) by clicking on each compound name on the table.
20. Save the standard curve as a method. From the “File” menu, select “Save As” and then “Method”. Change the method name to something you will recognize. We typically use the same name as the

subdirectory (Ex: LH140428). Click "OK", leave "Comment for method history" blank, and click "OK" again.

21. From the "Batch" menu, select "Load Batch". In the right-hand box, select the subdirectory name you used for "Sequence Parameters". Open the folder "hpchem", "1" for GC 1 or "3" for GC 3, "data", and then double click the subdirectory name. In the box on the left click the batch name. There should only be one listed. It will either be called "DEF_GC.B" or another name that you gave it when creating the sequence. Click "OK".
22. Under "Method to Process Batch Data", click "Other Method", and select the method name that you just saved in step 20. Under "Select Runs for Batch Processing" click "Select All". Click "OK".
23. Wait for the batch to load. Click the "Start" button with a green arrow located towards the bottom of the screen.
24. Wait for the program to analyze each data file. Depending on the number of samples this may take 5-15 minutes. When the "Start" button is highlighted again, then the batch is finished.
25. From the "Batch" menu select "Output Batch Report" to export the data report to Excel.
26. The Excel report can be found under My Computer/Local Disk (C:)/ HPCHEM/ 1 or 3 (depending on GC used)/ DATA/ your subdirectory name (LH1404228). In that folder you will find a folder with data for each sample that was analyzed. At the end of those folders is an Excel file called "REPORT01.xls" that contains all of the analyzed results.
27. Open the Excel file. Select the "Labels" worksheet. Select cells E3:E25 and copy them. Select the "Data" worksheet. Select cell C1, "Paste Special", and "Transpose" to insert the correct column names. The first column for each VFA shows the retention time of the peak measured. The second column gives the concentration in mM calculated based on the created standard curves.

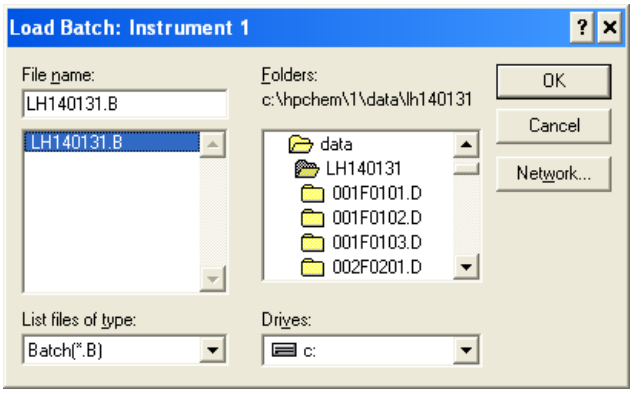

Step 21

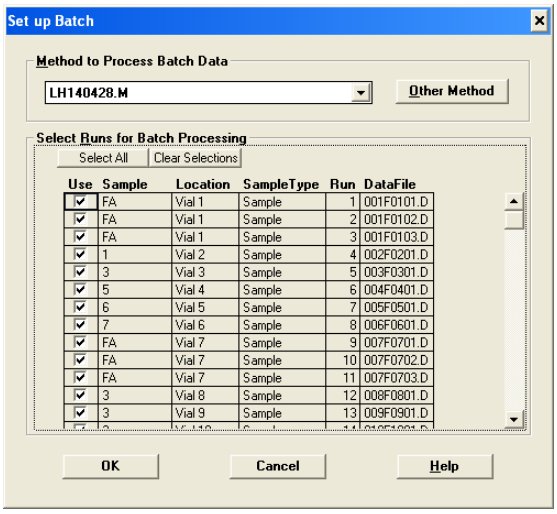

Step 22

Protocol 4: Procedure for GC evaluation of solvents

Updated June 15, 2014 by Lauren Harroff

Sample Preparation and Storage:

4. Centrifuge samples and filter (0.2 μm) to remove any suspended solids.
5. Dilute samples to < 1.5 g/L of the solvent of interest with DI water.
6. Samples may be stored in 4° C refrigerator or freezer for subsequent analysis. Depending on the sample, it may need to be centrifuged and/or filtered again after thawing. If there is any possibility of suspended solids, make sure to refilter or centrifuge.

Standard Preparation:

The stock solution of solvents (stored in the refrigerator in B68) contains 10 g/L each of: acetone, butanol, and ethanol. If you want to measure methanol or propanol you will need to make your own standards.

The GC can detect concentration between about 25 mg/L (0.025 g/L) and 1.5 g/L.

Make at least 5 standards of varying dilutions to create a standard curve. Typically a curve is created with standards at 0.25, 0.5, 1.0, 1.25, and 1.5 g/L. If expected sample concentrations are low, create a curve to include points in that range. (i.e. 25- 150 mg/L).

Make additional "check standards" of known concentration to mix in the run with samples. This provides quality control because the measured concentrations can be compared to the known concentrations. (See below in "Loading Samples" for more details.)

Make several blank vials of only DI water. These will be run as the first vial, after the set of standards, after every 5 samples, and as the final vial.

Start-up:

17. The solvent GC is labeled GC 2 and is located in Morrison Hall, B68A.
18. **FIRST** turn on the compressed air, helium, and hydrogen cylinders by opening the main cylinder valves.

19. Locate the ball valves that open the gas lines to the individual GCs. Valves for most gases can be found on manifolds at the center of the lab bench where the GCs are located. Valves for hydrogen are located next to the hydrogen gas cabinet. Open the appropriate ball valves for each gas (air, helium, and hydrogen) labeled as GC 2.
20. Turn on gases at the GC. Turn needle valves on Detector A panel (top left) for air, hydrogen, and aux gas (helium) to the left to turn on. Valves should be turned all the way open, but do not force them. They can get stuck.
21. Add name, date, and planned number of samples to the logbook.
22. If the septum has not been changed for over 50 injections (recorded in logbook), change it now. Note that there is no glass pre-column sleeve for the solvent GC, as there is for GCs 1 and 3.
    a. Remove the injector tower by lifting straight up off of the support rod.
    b. Unscrew black septum cover at injection site.
    c. Remove green septum and discard. Septum may be lodged inside the cover.
    d. Place in new septum and replace cover. Finger tighten.
    e. Replace injector tower by aligning metal support rod with appropriate port on the bottom of the tower.

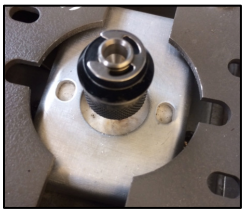
Step 6b

23. Turn the GC on using the power switch on the bottom right corner of the right face of the GC.
24. Turn on the communication module (box located to the left of the GC).
25. On the Windows 98 computer, open "Instrument 2 online" from the desktop. If "Instrument 2 offline" is already open, close it before opening the online program.
26. After Chemstation loads on the GC, check that the oven, front injector, and front detector are all on and temperatures are set to 100, 220, and 240° C, respectively.
27. Empty waste vials from the injection tower. These can be emptied into the sink.
28. Empty and refill Solvent A and Solvent B vials with DI water. Note that this is different than for GCs 1 and 3. No methanol is used for needle cleaning on the solvent GC.

***Both Solvent A and Solvent B vials should be filled completely with DI water! The needle only lowers down to about the 2 mL mark, so if the vials contain less than 2 mL of water, the needle will not be cleaned in between samples.

29. Remove and clean needle.
    a. Open door on the injection tower.
    b. Swing open the tab located about halfway up the syringe barrel that is holding the needle in place.
    c. Unscrew the nut holding the plunger and slide nut up.
    d. Pull needle forward from point D on the photo and then lift up to remove. (Otherwise the needle tip will get caught on the bottom stand.)
    e. Remove plunger and clean the plunger and syringe barrel using ethanol, soap, and DI water. Check that the plunger moves smoothly through the syringe barrel.
    f. Fill a small beaker with DI water and check that the needle takes up and dispels water properly.
    g. Replace needle properly. Hold needle at an angle and align needle tip with position on gray stand. Then slide into position at point D. Rescrew the nut a point C and replace the tab at point B.

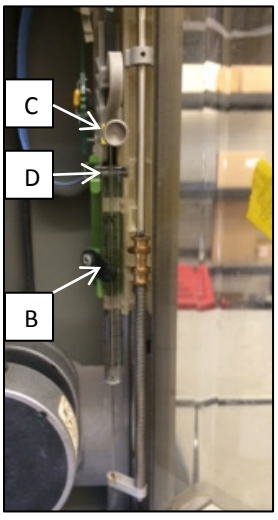

Step 13

30. Once the GC reaches operating temperatures (~15 minutes), light the

detector.

a. Press “SIG 1” button on the front face of the GC twice to display the signal output from Detector A.
b. Open the top door of the GC.
c. Push the “FID Ignite” button on the Detector A panel on the top left of the front face of the GC. Simultaneously hold a lit match or lighter over the detector.
d. Release the “FID Ignite” button. If the signal output maintains a reading above 12-15, then the detector is lit. If the signal drops back to 0-0.5, try to ignite again.

31. Allow 15 minutes to equilibrate. The signal output should maintain a steady reading around 60 before starting a run.

Loading Samples (this can be performed while waiting for the GC to warm up)

6. Load your samples into the autosampler trays. Ensure that the “Vial 1” position on the tray is aligned with the “1” position on the autosampler.
7. Include a blank vial containing only DI water as the first vial, after the set of standards, after every 5 samples, and as the final vial.
8. After approximately every 10 vials, add one of the vials of the “check standards” created during “**Standard Preparation**”.
9. As best as can be predicted, try to load the samples in order from most dilute to most concentrated.
10. For quality control, recommended run length is a maximum of 50 vials including blanks and standards. After a long period of time, the GC measurements tend to fluctuate.

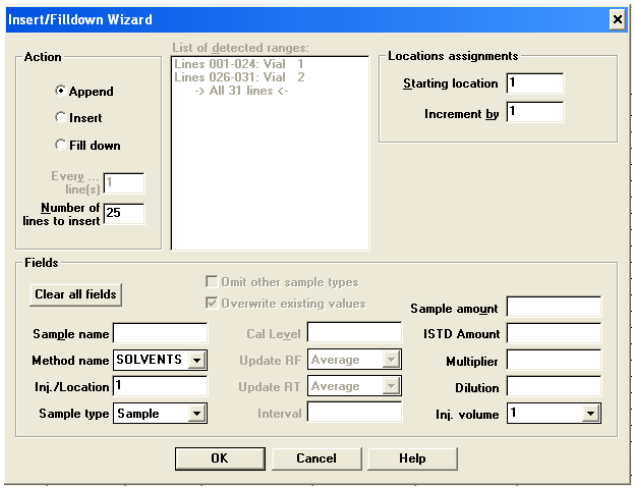

Steps 3- 10 (Loading Sequences)

Loading Sequence on the Computer

21. From the “Instrument 2 Online” computer program click “New Sequence” from the “Sequence” menu.
22. Open “Sequence Table” from the “Sequence” menu.
23. Open “Insert/FillDown Wizard”.
24. For “Starting location” enter “1” to indicate the location of your first vial.
25. For “Number of lines to insert” enter the total number of vials you are running (standards + blanks + samples)
26. For “Method name” enter “SOLVENTS”

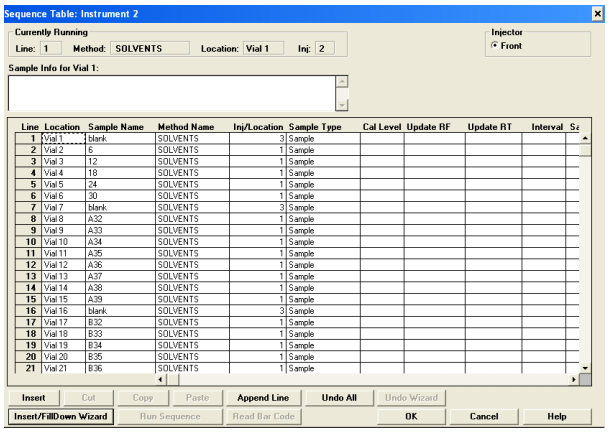

Steps 11- 13 (Loading Sequences)

***Note, that for the "SOLVENTS" method, the oven temperature is 100°C. In this case, methanol and ethanol peaks will overlap. Decreasing the oven temperature (e.g., to 80°C) will allow the peaks to separate better. You may have to play with the temperature to get this to work well. Additionally, if you decrease the initial temperature, make that it increases in the temperature cycle to at least 180°C to evaporate and elute all injected material. ***

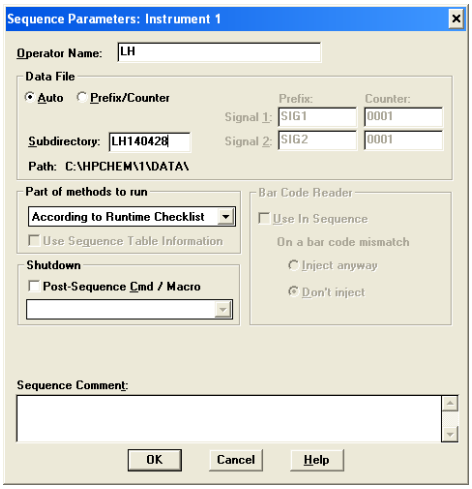

Steps 15-16

27. For "Inj./Location" enter "1" to indicate the number of times each vial will be sampled.
28. For "Inj. volume" enter "1".
29. Leave other fields blank and press "OK".
30. "Cut" the first line if it was left blank.
31. Under "Sample Name" enter the individual sample name for each vial.
32. For every water blank, change "Inj/Location" to "3".
33. Click "OK".
34. Open "Sequence Parameters" from the "Sequence" menu.
35. Enter your initials for "Operator Name".
36. Enter the folder name where you will find your data for "Subdirectory". We typically use initials followed by the date. (Ex: LH150615 for a run on June 15, 2015).
37. Click "OK".
38. A message will be displayed asking permission to create the subdirectory you have named. Click "OK".

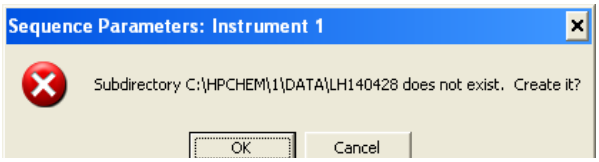

Step 18

39. If you will use the same or similar sequence in the future, save your sequence under "Save Sequence as" from the "Sequence" menu.

Starting Injections

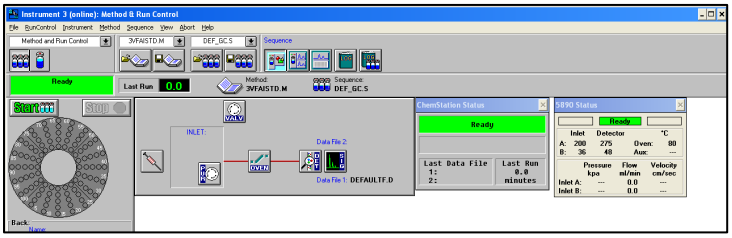

Steps 1-3

7. Check that the method displayed on the main screen of the online program reads "SOLVENTS".
8. Check that the box above "Start" and "Stop" buttons is green and reads "Ready".
9. Once it is ready, press "Start".
10. Wait for the GC to run through the syringe and needle cleaning process and inject the first blank before walking away. Most problems occur during this first injection.
11. If the computer displays a plunger error or injector error message, check that the plunger of the syringe moves freely and takes up and dispels water appropriately. Clean the needle and syringe again if necessary and restart the sequence.

12. If possible, create a standard curve and check for a linear relationship as soon as the standards have finished running. (See **"Data Analysis"** for instructions.) This step allows potential errors to be identified before all samples have been run.

Shutting Down:

6. Close the "Instrument 2 Online" program on the computer, and turn off the communication module.
7. Turn off the hydrogen valve at the GC to extinguish the detector flame.
8. If GC 1 is not being used, turn off the ball valve for hydrogen located on the manifold at the hydrogen gas cabinet that corresponds to GC 2. If none of the other GCs are running, turn off the hydrogen at the cylinder as well.
9. On the front of the GC, push the "OVEN TEMP" button and turn the temperature off. Do the same for "INJ A TEMP" and "DET A TEMP".
10. Once each component has cooled to at least 100° C, turn off the GC.
11. Turn off the valves for air and aux gas (helium) at the GC. Again, do not force the valves past their natural stopping point.
12. Turn off the ball valves for air and helium at the manifolds located in the center of the lab bench. For the air, only turn off the valve if GC 3 is not running.
13. Turn off the helium and compressed air at the cylinders ONLY if none of the other GCs are running.

Data Analysis

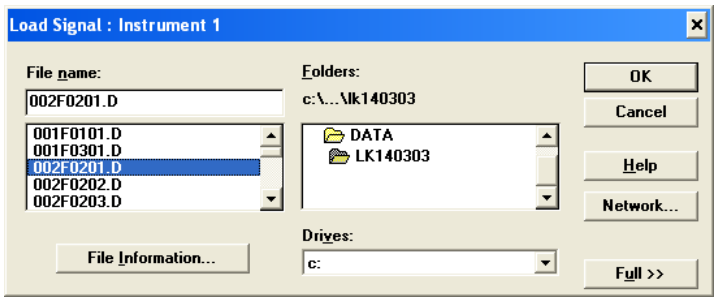

28. Open "Instrument 2 (offline)"
29. Open "Load Signal" from the "File" menu.
30. Under the folders "HPCHEM", "2" and "DATA", find the folder with the subdirectory name that you created previously from "Sequence Parameters".

Steps 2-4

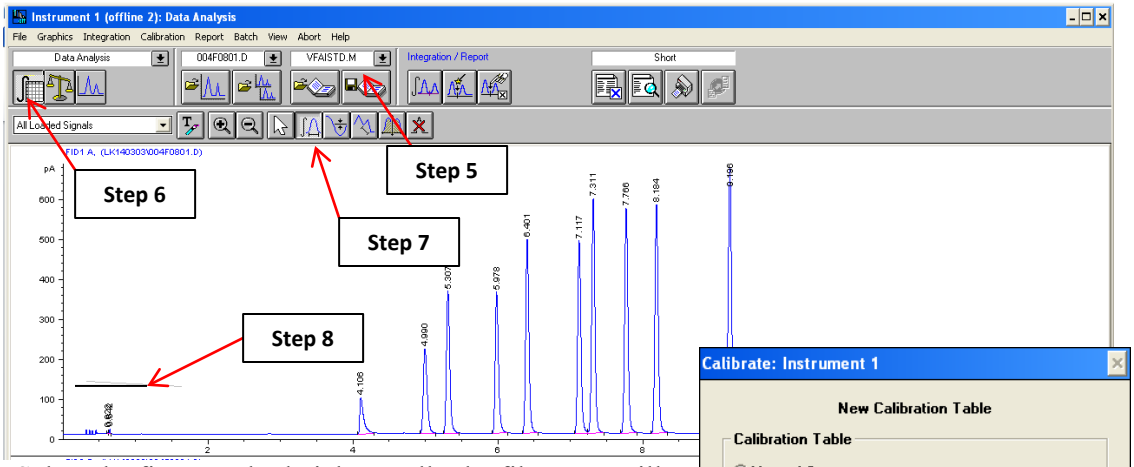

31. Select the first standard vial. Usually the file name will read "002F0201.D" because the first vial was a blank.

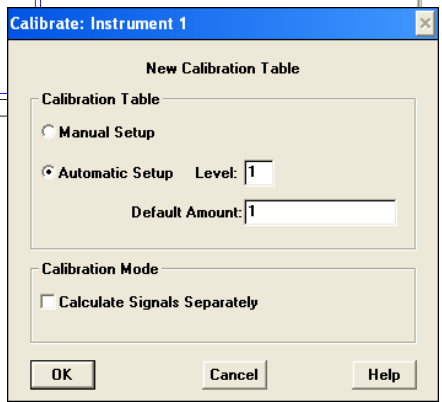

The first number (“002”) indicates the location number of the vial. Click “OK”.

32. Click the integration button.
33. Click the manual integration button.
34. Remove and unwanted peaks by dragging the mouse above the peak.
35. Select “New Calibration Table” from the “Calibration” menu.
36. For “Default Amount” enter the g/L concentration of the first standard. Click “OK”. If asked to overwrite the existing calibration table, select “Yes”.
37. On the table, name the compound for each peak. If using the premade standard, there should be 3 peaks that come out in the following order:
    1. Acetone (Retention Time= 1.66)
    2. Ethanol (Retention Time= 2.26)
    3. Butanol (Retention Time= 3.91)

Step 9

38. Load the next standard vial by selecting “Load Signal” from the “File” menu. The computer will automatically recognize the correct peaks identified in the calibration table, so steps 5-7 do not need to be repeated for the remaining vials.
39. Select “Add Level” from the “Calibration” menu.

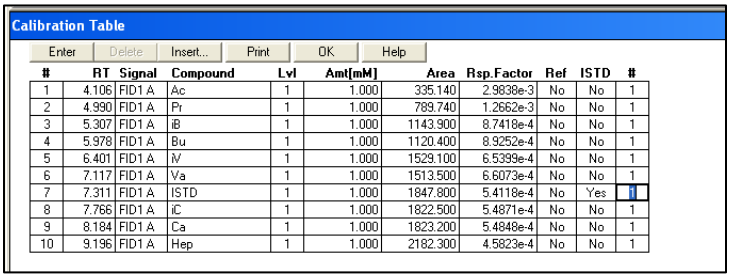

#	RT	Signal	Compound	Lvl	Amt[mM]	Area	Rsp.Factor	Ref	ISTD	#
1	4.106	FID1 A	Ac	1	1.000	335.140	2.9838e-3	No	No	1
2	4.990	FID1 A	Pr	1	1.000	789.740	1.2662e-3	No	No	1
3	5.307	FID1 A	iB	1	1.000	1143.900	8.7418e-4	No	No	1
4	5.978	FID1 A	Bu	1	1.000	1120.400	8.9252e-4	No	No	1
5	6.401	FID1 A	iV	1	1.000	1529.100	6.5399e-4	No	No	1
6	7.117	FID1 A	Va	1	1.000	1513.500	6.6073e-4	No	No	1
7	7.311	FID1 A	ISTD	1	1.000	1847.800	5.4118e-4	No	Yes	1
8	7.766	FID1 A	iC	1	1.000	1822.500	5.4871e-4	No	No	1
9	8.184	FID1 A	Ca	1	1.000	1823.200	5.4848e-4	No	No	1
10	9.196	FID1 A	Hep	1	1.000	2182.300	4.5823e-4	No	No	1

Step 10

40. Enter the concentration of the standard for “Default Amount” and click “OK”.
41. Repeat steps 11-13 to load all standards.
42. The computer will create a standard curve for each individual solvent. Check that all curves have a strong linear correlation (~ 0.995 or higher) by clicking on each compound name on the table.
43. Save the standard curve as a method. From the “File” menu, select “Save As” and then “Method”. Change the method name to something you will recognize. We typically use the same name as the subdirectory (Ex: LH150615). Click “OK”, leave “Comment for method history” blank, and click “OK” again.
44. From the “Batch” menu, select “Load Batch”. In the right-hand box, select the subdirectory name you used for “Sequence Parameters”. Open the folder “hpchem”, “2” ,“data”, and then double click the subdirectory name. In the box on the left click the batch name. There should only be one listed. It will either be called “DEF_GC.B” or another name that you gave it when creating the sequence. Click “OK”.
45. Under “Method to Process Batch Data”, click “Other Method”, and select the method name that you just saved in step 16. Under “Select Runs for Batch Processing” click “Select All”. Click “OK”.
46. Wait for the batch to load. Click the “Start” button with a green arrow located towards the bottom of the screen.
47. Wait for the program to analyze each data file. Depending on the number of samples this may take 5-15 minutes. When the “Start” button is highlighted again, then the batch is finished.

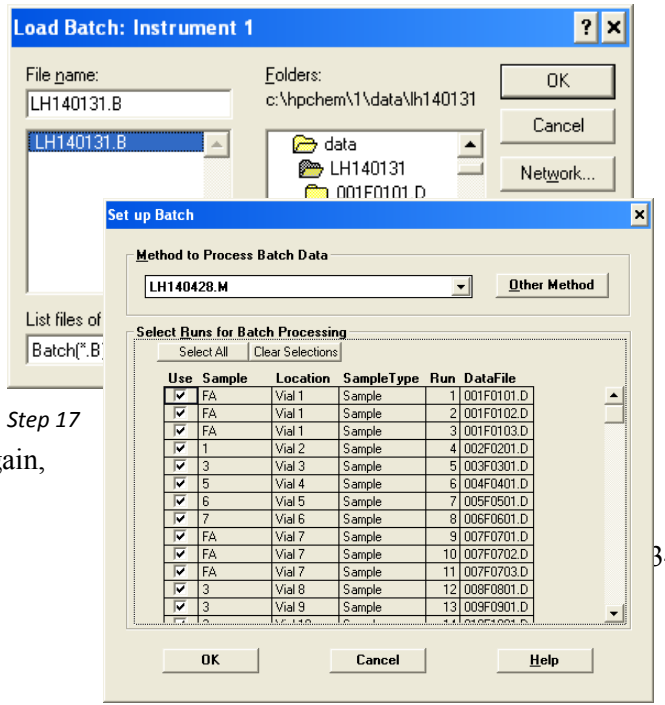

Use	Sample	Location	SampleType	Run	DataFile
☑	FA	Vial 1	Sample	1	001F0101.D
☑	FA	Vial 1	Sample	2	001F0102.D
☑	FA	Vial 1	Sample	3	001F0103.D
☑	1	Vial 2	Sample	4	002F0201.D
☑	3	Vial 3	Sample	5	003F0301.D
☑	5	Vial 4	Sample	6	004F0401.D
☑	6	Vial 5	Sample	7	005F0501.D
☑	7	Vial 6	Sample	8	006F0601.D
☑	FA	Vial 7	Sample	9	007F0701.D
☑	FA	Vial 7	Sample	10	007F0702.D
☑	FA	Vial 7	Sample	11	007F0703.D
☑	3	Vial 8	Sample	12	008F0801.D
☑	3	Vial 9	Sample	13	009F0901.D

Step 17

48. From the “Batch” menu select “Output Batch Report” to export the data report to Excel.
49. The Excel report can be found under My Computer/Local Disk (C:)/ HPCHEM/2/ DATA/ your subdirectory name (LH150615). In that folder you will find a folder with data for each sample that was analyzed. At the end of those folders is an Excel file called “REPORT01.xls” that contains all of the analyzed results.
50. Open the Excel file. Select the “Labels” worksheet. Select cells E3:E25 and copy them. Select the “Data” worksheet. Select cell C1, “Paste Special”, and “Transpose” to insert the correct column names. The first column for each compound shows the retention time of the peak measured. The second column gives the concentration in g/L calculated based on the created standard curves.

Step 18

Protocol 5: Procedure for Gas GC Evaluation of N_2, CH_4, and CO_2

1 Limit of detection

Limit of detection 250 ppm（0.025%）**Note**: This limit of detection is from the company specifications. So if your samples are not detected, you should measure the real limit of detection.

2 Sample preparation and storage

There are three ways of sample preparation for gas GC:

a. Take the bottles which you want to measure to gas GC table.
b. Transfer gas sample to gas bags.
c. If your reactor is stationary in the Morrison lab, sample directly from the reactor via a sampling port. Bring water vial to reactor and submerge the needle in the water after the sample is withdrawn.

3 Procedure

3.1 Start-up

a. **First** turn on the compressed air, helium and hydrogen.

b. Add name, data, and planned number of samples to the logbook (C:\Documents and Settings\User\Desktop\Gas GC\logbook_N2 _CH4_CO2).

c. If the septum has not been changed for over 100 injections (recorded in logbook), change it now.

I. Remove the nut at injection site.

II. Remove blue septum and discard. Septum should be lodged inside the nut.

III. Place in new septum and replace nut.

IV. Check for connection leaks using Liquid Leak Detector.

Step c

d. Turn the switch on the top left corner of the front face of the machine to “ON”.

e. Turn the TCD filament current control switch to high.

f. On the Windows 98 computer, open “Peak 393-32bit CO2 N2” from desktop.

g. Open control file (e.g., “JJ2 TCD_N2_CH4_CO2.CON”)

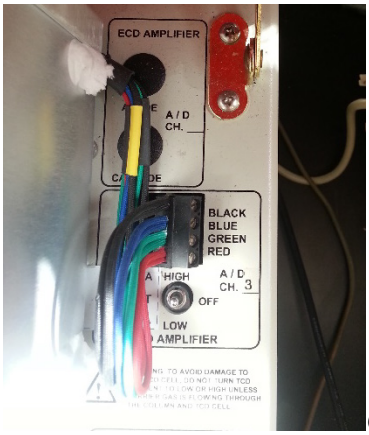

h. After ChemStation loads on the Gas GC, check that the oven and detectors temperatures are set 40 and 100℃, and the gas flow rates of Carrier 1, H2 1 and Air 2 are set 13, 31, 20, 2 and 3 psi, respectively. After 2-3min, the "Ready run" will change green, check that both the actual temperatures and gas flow rates are the same as the set.

Step e

3.2 Starting Injections

a. Clean needle and make sure no water is inside.

b. Inject syringe to prepare sample container and wash 3 times using sample gas. Take more than 500 µl, then submerse needle into water vial to prevent gas leaking. Then adjust the sample volume to 500 µl.

c. Click "Zero channel" button to make baseline zero.

d. Inject sample quickly, then immediately press Spacebar on the keyboard.

4 Calibration

a. Turn on the pure compressed gas(Methane is in digestion room (Rm B61A); CO_2 and N_2 are in carboxylate room (Rm B68A))

b. Remove syringe plunger and inject needle into regulator for 2 second to flush the syringe. Then reinstert plunger, remove the needle, and add needle end to water-filled vial.

c. Click on the Auto Zero button to zero the data system signal.

d. Push the syringe pluger slowly to desired volume. Make sure the needle remains under the water. Make at least 5 standards of varying concentration to create a standard curve. Typically a curve of N_2, CH_4 and CO_2 are created with 20% (100 µl), 40%(200 µl), 60%(300 µl), 80%(400 µl) and 100%(500 µl).

e. Pierce the septum in the on-column injector with the syringe

needle. Insert the needle straight into the on-column injector

port; avoid bending the needle. Depress the syringe plunger to

inject the sample, then withdraw the syringe. For the best and

most consistent results, use an easily reproducible injection technique with quick, smooth movements. Hit the computer

keyboard spacebar to start data acquisition.

f. Click on the peak(Retention time of N2, CH4 and CO2 are about 0.52, 0.95 and 2.10 min respectively), then select calibration Nitrogen(for example).

g. Select the concentration from the Recalibration level.

i. Click the accept new button, then save it.

g. Click the file button, click “Save as”.

Note: Manager will calibration every month. If you want to have your own calibration, you can do it by yourself.

5 Data Analysis

Click the results button, click “Copy”, then plaste whereever you want.

6 Shutting Down

a. Close the “Peak393-32bit CO2 N2” program on the computer.

b. Open the GC cover, turn off the TCD filament current control switch.

c. Once the detector temperate has cooled to at least 45℃, turn off the GC.

d. Turn off the helium, hydrogen and compressed air cylinders only if none of the other GCs are running.

Protocol 6: SOP for Gow-Mac GC with Peak Simple computer interface in B45

Person in Charge: Hanno Richter (Cornell-ID HR95; cell: 413 658 7652)

Channel 2 GC Analytes: Carbon monoxide, Carbon dioxide, Methane, Nitrogen
set up with one Supelco column, 6' x 1/8"; 80/100 mesh HayeSep Q packing material.
Carrier gas: Helium

Channel 3 GC
Analytes: Hydrogen
set up with one Supelco column, 15' x 1/8"; 60/80 Carboxen-1000 packing material.
Carrier gas: Nitrogen, high purity.

Instrument-Preparation:
Make sure gases are open and adjust flow rate to~50 mL/min with flow adjust knobs. Make sure that both A and B lines are flushed, and that the detector current is off, otherwise the detector can fry !
Turn the main power (red button) on, it can be on the rear side.
Temperatures (for biogas measurements) are set, you do not have to adjust them, and please do not remove the yellow tapes:
Injection port: 50 °C
Detector: 115 °C
Column: 25 °C
After warm-up (15 min): turn detector current switch to on. The current is set to 150 mA on the meter. Do not change the setting. If you have to adjust current, then do it by slowly turning the knob.

Sample operation: Open Peak Simple software on computer. Make sure, control file is loaded (Path: C:/Windows8_OS/Users/AngenentGC/Dropbox/Hanno Richter/DEFAULT)
In Main menu, click the "1234"-Icon. Check "active", "display", and "integrate" boxes of the channel you want to use.
Inject sample (500 µL) into port B of either instrument
Press the yellow traffic-light icon for the corresponding time-base to start recording
After run, integrate or save your results

When done, follow the shut-down procedure:
switch off Detector current and then GC main power;
wait 3 hours for cooling down (otherwise you may fry the detector);
then turn off gas-supply on the gas-tank, do not change flow with the valves on the GC itself.

Protocol 7: Extraction Techniques

RNA extraction

1. Gather one 2.0-mL and one 1.5-mL nuclease-free centrifuge tube per sample
2. Use only nuclease-free pipette tips
3. Carefully add 0.75-mL TRI-LS (contains phenol) to the 2.0-mL centrifuge tube
4. Add 0.25-mL of the sample
5. Mix in Pipette
6. Vortex at 5 for 30 seconds
7. Incubate at room temperature for 10 minutes
8. Add 0.2-mL of Chloroform
9. Shake for 15 seconds
10. Incubate at room temperature for 15 minutes
11. Centrifuge for 15 minutes at 12,000 RPM at 4ºC
12. Carefully take off top aqueous layer of RNA using 200-µL Pipetter collect in 1.5-mL centrifuge tube
    - Top- RNA
    - Middle- DNA
    - Bottom- fatty acids
13. Precipitate RNA with 0.5-mL Isopropanol
14. Incubate at room temperature for 10 minutes
15. Centrifuge for 8 minutes at 12,000 RPM at 4ºC
16. remove supernant into a beaker positioned by the centrifuge
17. stand tubes on kimwipe and allow to air dry for a few moments
18. Wash with 100-µL of 75% ethanol
19. Centrifuge for 10 minutes at 12,000 RPM at 4ºC
20. Decant and air dry tube (about 5-10 minutes)
21. Add 5-µL TE buffer
22. gently tap to mix
23. Store at -20ºC

Bead Beating DNA Extraction

1. place beads in 400°C oven overnight
2. Add 0.5g of beads in 2ml O-ring centrifuge tube
3. Add 500µl of Buffer A
4. Add 200µl of 20% SDS
5. Add 200ul of sample
6. Add 500µl 24:24:1 Phenol: Chloroform: Isoamyl alcohol
   Note: Phenol: Chloroform: Isoamyl alcohol mix will melt polystyrene… mix in glass or polypropylene
7. Beat on High for 2 minutes
8. Centrifuge at 8kpm 4°C for 3 minutes
9. Remove top aqueous layer into new vial
10. Add 600µl -20°C Isopropanol (equal volume)
11. Add 60µl (1/10 vol) 3M Sodium acetate
12. Mix by inversion
13. Place in -80°C freezer for 20 minutes
14. Centrifuge at 13kpm 4°C for 20 minutes
15. Decant liquid
16. Add 500µl cold 100% Ethanol
17. Immediately spin at 12kpm 4°C for 5 minutes

18. Decant
19. Dry for about 10 minutes in hood
20. Suspend in ~100µl TE

** TE volume varies with concentration of sample **

TE Buffer Solution

1. 10mM TrisCl (pH 8.0) 1mL of 1M TrisCl
2. 1mM EDTA (pH 8.0) 0.2mL of 0.5M EDTA
3. Mol Bio Water 98.8mL H_2O
4. Store at -4°C

** adjust pH with TrisCl**

2X Buffer A

1. 200mM NaCl 0.58g/50mL
2. 200mM Tris HCl 1.21g/50mL
3. 20mM EDTA 10ml of 0.5M EDTA
4. Mol Bio Water 40ml H_2O
5. Correct pH to 8.0 – use pH strips and ultra-clean HCl
6. Filter sterilize through 0.2µm filters
7. UV sterilize for 20minutes
8. Wrap in foil
9. Store at -20°C

0.5M EDTA Solution (pH 8.0)

EDTA MW – 292.25g/mol

1. Mix 7.306g EDTA
2. 45ml Sterile DI water
3. 1 g NaOH pellets
4. Mix and Add Heat in Microwave
5. Adjust pH to 8.0 with 1N or 10N NaOH or HCl if needed
6. Filter sterilize through 0.2µm filters
7. UV Sterilize for 15minutes
8. Wrap in foil
9. Store at room temperature

Ultra Clean 20% SDS

1. 5.0g SDS
2. 25.0ml Mol Bio Water
3. Filter sterilize through 0.2µm filters
4. Store at room temperature

Ultra Clean 3M Sodium Acetate

1. 6.15225g Mol-Bio Sodium Acetate
2. ~22ml Mol Bio Water
3. Bring pH to 5.2 with Mol Bio Hydrochloric Acid
4. Add Mol Bio Water to 25.0ml
5. Filter sterilize through 0.2µm filters
6. Store at room temperature

Protocol 8: PCR – polymerase chain reactions

Before assembling a PCR reaction the microbial hood and all pipettes required must be Ethanol sterilized and UV sterilized for 15 minutes. Thaw all components on ice and keep the solutions on ice while working with the components. Mix all solutions well before use.

1. Setting up the PCR Master mix
    a. Determine the number of individual reactions that need to be conducted.
    b. Add at least two additional reactions for control positive and a control negative reaction tubes – control positive should be E.coli, control negative should be master mix only
    c. Insert the number of reactions into the PCR excel worksheet.
    d. The program will calculate the total amount of each component that is needed for the number of reactions being conducted +1 to account for mixing losses
    e. Mix each component in the order listed in the program
    f. BSA is an additive that can be used to chelat metals
    g. Acetamide can be used for quenching inhibitor compounds
    h. Betaine can be used to assist annealing of the primers to the cDNA
    i. Make the master mix carefully with maximum mixing and minimum bubbles

No of Rxns 10

Master Mix	[stock]	ul per rxn	conc per rxn		
dd Water		25.75			283.25
5X buffer		10.0			110.0
Promega GoTaq	5 U/ul	0.25	1.25	U/ 50ul	2.75
27F/1391R Primer mix	20 uM ea	1.0	0.4	pmol/ul	11.0
dNTP	10mM/ea	1.0	0.0002	M/ea dNTP	11.0
BSA - A7030	10mg/ml	4.0	0.8	mg/ml	44.0
$MgCl_2$	25mM	6.0	0.002 (total)	M Mg	66.0
Acetamide	50mg/ml	0 (2)	2	mg/ml	0.0
Betaine	5M	0 (5)	5		0.0
Master mix volume/ tube		48.0			
Template DNA		2			
Total rxn volume		50.0			
	ul additives (not water)	22.3		Total Mix Vol	528.0

2. Setting up individual reactions
    a. Aliquot the Master mix into the individual PCR tubes (0.2ml) being careful NOT to introduce bubbles into the tubes
    b. Carefully add 2ul of cDNA from a sample under the surface of the Master Mix in each tube. Use the pipette tip to then mix the cDNA into the Master mix without introducing bubbles.
    c. IF bubbles occur. Close the lid and tap the tube until the bubbles pop
    d. Centrifuge down the filled PCR reaction tubes at 5kprm for 20sec
    e. Place into the smaller holes in the thermocycler
    f. Close the lid and lock it into place
    g. Each set of primers will have a specified thermocycler program. For universal 16S rRNA primers 27F (8F) and 1391R the program is as follows:

Thermocycler Program "16S"

Initial Denaturing	94	2:00
Denaturing	92	0:30
Annealing	45	1:30
Extension	72	1:30
	19	
Final Extension	72	15:00
	30 Cycles	

27 Forward (8F) 5' to 3' AGAGTTTGATCCTGGCTCAG

1391 Reverse 5' to 3' GACGGGCGGTGWGTRCA

    h. The program takes approximate 2.5hr

3. Running an Electrophoresis Gel to check PCR product
    a. Dilute 20X Boric Acid Buffer to 1X for the tank buffer (20X boric acid buffer – 8g NaOH, 47g Boric Acid, 1L DI Water)
    b. Electrophoresis Gel (between 1% and 0.7% agarose)
        i. Add 0.7g Agarose to 100ml of 1X boric acid buffer
        ii. Slowly (10-20 sec intervals) melt agarose in the microwave
        iii. Allow to cool to touchable temperature
        iv. Add 10mg/ml Ethidium Bromide to a concentration of 5ug/ml (5ul per 100ml gel)
        v. Mix carefully and pour into a gel mold with well combs in place
            1. Gel molds can be formed by taping across both sides of a gel plate
        vi. Allow the gel to set
        vii. Remove well combs and tape
        viii. Place the gel and gel plate in the filled buffer tank
        ix. Mix 5ul PCR product with 1ul Loading Dye – add entire sample to a single well
        x. Be sure to always include a Marker Ladder to ensure the electrophoresis was valid and determine the length of the PCR products
        xi. Run PCR products for ~40 minutes at 95 volts – DNA runs from Black to Red
    c. Viewing an Electrophoresis Gel

i. Stop the electrophoresis source
ii. Carefully remove the Gel and Gel Plate from the tank and place on the UV light source
iii. Use the Face Shield to view the bands (UV on high)
iv. Close door and take a picture with the camera set on an extended exposure time of 1 sec

4. Cleaning product for the Genome Sequencing Center
    a. Combine duplicate 50ul PCR reactions (5 total) into a single 2ml tube ~250ul
    b. Add 650ul water and mix well
    c. Aliquot ~450ul into the top, purple portion of two Montage PCR clean-up set-ups (Millipore UFC7PCR50)
    d. Close the caps and Centrifuge with the cap strap toward the center of the rotor at 1000g for 15 minutes.
    e. Check to be sure all the liquid has passed through the filter – IF it has not centrifuge again for 10 minutes with the cap strap towards the outside
    f. Check and repeat centrifuging as needed – BUT DO NOT overdry the filter (leave slight amount of liquid on filter ~1-2ul)
    g. Remove the purple filter and place into a new tube. Keep the filtrate until the final product has been checked.
    h. Add 25ul of water to the filter reservoir
    i. Invert the filter in the new tube
    j. Centrifuge again at 1000g for 2 minutes
    k. Combine like cleaned products.
    l. Run another gel to check the cleaned product. Mix 1ul cleaned product with 1ul of loading dye and 3-4ul 1X sodium borate tank buffer. The band should be bright and distinct.
    m. The ~50ul positively checked sample is ready to be submitted to the GSC

Hints for PCR-

- Bubbles in a PCR tube will prevent the reaction from occurring!!!
- If your PCR does not work:
    - Were there bubbles
    - Mix the Master mix and the reaction tubes well
    - Try diluting the cDNA to dilute out any inhibitory compounds
    - Try a different combination of additives; BSA, Acetamide, Betaine, PVP
    - Reclean an extracted sample – phenol, choroform and ethanol can all inhibit a PCR reaction
- If your control negative is positive:
    - Replace the water
    - Get ALL new chemicals
    - Clean the pipettes with bleach, ethanol and UV
    - Buy new PCR tubes
    - Bleach the microbial hood
    - Bleach your lab coat

Protocol 9: 16S and ITS Illumina MiSeq analysis using Qiita

Angenent Lab edition

Written by Mytien Nguyen (mtn29), 3.5.2015

Updated, Mytien (mtn29), 6.29.2015

http://qiita.ucsd.edu or http://qiita.microbio.me

- Create an account under "New User"

BEFORE YOU BEGIN

Definitions

Sample template: a tab-delimited txt file containing information about your samples, including environmental and other important information about them. If you collected 100 samples, you will need 100 rows in your sample template describing each of them, including blanks. A template of this file is in the Angenent Lab Google drive.

Prep template: a tab-delimited txt file containing basic information about wet lab work on all or a subset of the samples. In your 100 samples, if you prepare 95 of them for 16S and 50 of them for ITS, you will need 2 prep templates: one with 95 rows describing the preparation for 16S, and another one with 50 to describing the ITS. A template of this file is in the Angenent Lab Google drive.

Pre-processing: includes the first steps in sequencing analysis, including demultiplexing and quality filtering. This step outputs quality filtered joined reads.

Processing: includes clustering, OTU picking, and assigning taxonomies, and outputs a biom OTU table.

About studies in Qiita

Studies can contain one set of samples or multiple sets of raw data, each of which can have a different preparation. The number of sample template and prep template you will need depends on the number of datasets you have. For example imagine a study with 100 samples in which:

- Scenario 1: all of the samples were prepped for 16S and sequenced in a single MiSeq run
- Scenario 2: all of the samples were prepped for 16S and sequenced in two MiSeq runs
- Scenario 3: all of the samples were prepped for 16S, and 50 were also prepped for ITS. All 16S and ITS samples were sequenced in a single MiSeq run
- Scenario 4: all of the samples were prepped for 16S and sequenced in a single MiSeq run, and samples are from two separate studies (50 from study 1, 50 from study 2)

To represent this project in Qiita, you will need to create a single study with a single sample template that contains all 100 of the samples. Separately, you will need to create 4 prep templates that describe the preparations for the corresponding samples. All raw data uploaded will need to correspond to a specific

prep template. For instance, the data sets described above would require the following data and template information:

Scenario 1:

- 1 prep template describing the MiSeq run where the 100 samples are represented
- The 3 fastq raw data files without demultiplexing from the sequencing center (i.e., the forward-R1, reverse-R2, and barcodes-Index)

Scenario 2:

- 1 prep template describing the two MiSeq runs (use the run_prefix column to differentiate between the two MiSeq runs, corresponding to the file names) where the 100 samples are represented
- The 6 fastq raw data files without demultiplexing from the sequencing center (i.e., 2 files for forward-R1, 2 files for reverse-R2, and 2 files for barcodes-Index)

Scenario 3:

- 2 prep templates, one describing the 16S preparations and the other describing the ITS preparations
- The 3 fastq raw data files without demultiplexing from the sequencing center (i.e., the forward-R1, reverse-R2, and barcodes-Index)

Scenario 4:

- 2 prep templates, one for each study describing the MiSeq run where the study's 50 samples are represented
- The 3 fastq raw data files without demultiplexing from the sequencing center (i.e., the forward-R1, reverse-R2, and barcodes-Index)

Study status

Sandbox: When a study is in this status, all the required metadata columns must be present in the metadata files (sample and prep), but the values don't have to be filled in or finalized yet. The purpose of this status is so that users can quickly upload their sequence files and some (possibly incomplete) metadata in order to have a preliminary look at their data.

Private: Moving from sandbox to private status requires the user to correct and finalize their metadata. On the each study overview page, there is a button that the user can use to request approval. Approval must be provided by a Qiita admin, who will validate and finalize the metadata. After a study moves from sandbox to private status, very little can be changed about the study without reverting the study to sandbox.

Public: Once a study is made administrator-approved and becomes private, the user can choose when to make it public. Making a study public means that it will be available to anyone with a Qiita user account (e.g., for data downloads and meta-analyses).

Creating a study

1. To create a study, click on the "Study" menu and then on "Create Study". This will take you to a new page that will gather some basic information to create your study.
2. Enter a unique "Study Title", and select the appropriate principal investigator(s) from the list. If the PI is not in this list, you can choose to add a new one. Note: Lars is on the list.

3. (Optional) select the environmental package appropriate to your study. Different packages will request different specific information about your samples.
4. Select the kind of time series you have. The main options are:
    - No time series: the samples do not represent a time series.
    - Single intervention: the study has only one intervention, the classic before/after design. This can be also selected if you are only following individuals/environments over time without an actual intervention.
    - Multiple interventions: the study includes multiple interventions, such as 2-3 antibiotic (ABX) interventions.
    - Combo: the samples are a combination of those having single and multiple interventions.

    Additionally, there is a distinction between real, pseudo or mixed interventions:

        - Real: the study follows the same individuals over time, so there are multiple samples from the same individuals.
        - Pseudo: the study has time information from diverse individuals; for example, it includes samples from individuals from 3 to 60 years of age but has only one sample per individual.
        - Mixed: the study is a combination of real and pseudo.

Adding sample template

When you click on a study, you'll be taken to the study description page. Here you will be able to edit the study info, upload files, and manage all other aspects of your study.

5. To upload your sample template, prep template, and sequence files, click on the "Upload" button. Drag-and-drop files into the grey area or simply click on "select from your computer" to select the fastq, fastq.gz or txt files you want to upload.
   Note: uploads can be paused at any time and restarted again, as long as you do not refresh or navigate away from the page, or log out of the system from another page.

6. Once your file(s) have been uploaded, from the upload tool, click on "Go to study description" and click on the "Sample template" tab. Select your sample template from the dropdown menu, then click "Process sample template". If it is processed successfully, a green message will appear; if processing is unsuccessful, a red message describing the errors will appear. In this case, fix the described issues, re-upload your sample template file, and then re-attempt processing.
7. You can download the processed sample template under the "Sample template" tab once it has been successfully processed.

Adding raw data

8. Once the sample template is successfully processed, you will be able to use the "Raw data" tab. In the "Add raw data" tab, select FASTQ and click "Add raw data". A new tab entitled "FASTQ (ID: ###)". Click on this tab, and select our prepping template under (1) and the corresponding data type under (2). Click "Add prepping template". If you have more than one prepping templates, repeat this for the rest of your prepping templates. Each prepping file will have their own subtab with a unique ID, i.e.) 16S (ID: ###) or ITS (ID: ###)
9. Once you've successfully added your prepping template(s), you can download your prepping template, a summary of your prepping template, and a QIIME-compatible mapping file, which is a combination of your sample template and prepping template.

10. On the right side of the "FASTQ (ID: ###)" tab, you will have a list of all the updated files. Before pre-processing your data, you need to link these files to the appropriate reads by selecting which files are the forward, reverse, and barcodes reads. Once the selections are made, click on "Link raw files for: xxx". This action will take you to a new page with the linking status, but you can move out of there whenever you want. Note that from that moment until the job is finished, you will see a "Linking files" message under the "FASTQ (ID: ###)" tab. Once linking is completed, check the linked files. You can also unlink the file, and re-link them.

Preprocessing and processing your raw data

11. Once you have linked files to your raw data and your prep template has been processed, you can then proceed to preprocessing your data for each preparation by clicking "Preprocess data" under its subtab. A popup will appear requesting you to select the type of barcode. Select the appropriate barcode. For example, if you have 16S 515F/806R Golay sequences, select the *Golay 12bp, reverse complement mapping file barcodes* option, with the following parameters:
    max_barcode_errors: 1.5
    sequence_max_n: 0
    max_bad_run_length: 3
    rev_comp: False
    phred_quality_threshold: 3
    rev_comp_barcode: False
    rev_comp_mapping_barcodes: True
    min_per_read_length_fraction: 0.75
    barcode_type: golay_12
12. Pre-processing may take a couple of hours to complete, and you can logout and do whatever in the meantime. The status is reported under the preparation subtab. Once completed, the message will say: "Preprocessed data generated: ###" where ### is the unique ID for your pre-processed data.
13. Once the preprocessing is finished, a new tab will be created under the "Preprocessed data" tab with a unique ID. You will have 4 new files:
    *_seqs.fna: demultiplexed sequences in fasta format

    *_seqs.fastq: demultiplexed sequences in fastq format

    *_seqs.demux: demultiplexed sequences in an HDF5 format

    *_split_library_log: the classic QIIME split libraries log that summarizes the demultiplexing process

14. If you are happy with the results, click on "Process" below your files to process your data. Check the processing parameters in the popup, then click OK. Processing will take around 24 hours, so you should let it run overnight. You do not need to be logged in.
15. The processing status is reported under the "Pre-processed data" tab. Once completed, the message will say: "Processed data generated: ###" where ### is the unique ID for your processed data.
16. Once the processing is completed, a new tab will be created under the "Processed data" tab with a unique ID. You will have 3 new files:
    Biom – an OTU biom file of your data, in HD5 format (compatible with QIIME 1.9.0 and later)

* Currently, there's a bug with MacQIIME 1.9 (maybe QIIME 1.9 virtualbox also), and you have to convert this biom table to hdf5 again in your local QIIME before using it

Directory – (not sure what this is)

Log – a log file that summarizes the clustering, OTU picking, and taxonomic assignment processes ran in QIIME

17. If you have other prep templates, repeat steps 11-16 for each of them.
18. Complete your microbiome analysis in your local QIIME with the biom OTU table(s) and QIIME mapping file(s) from step 9

Analyzing your data with Qiita

19. Once your sequences have completed processing, you can conduct preliminary microbiome analysis on Qiita. Go to Study > View Studies and select the study(ies) you'd like to add to the analysis. Click Add to Analysis next to each study. Once you've successfully selected your samples, the Selected link on the top right corner should be green.
20. Select Analysis > Create from Selected samples. A list of your selected study will be visible. Here, you can remove samples and/or studies (samples list can be expanded by clicking Show/Hide Samples) you want to exclude from the analysis. Once you have your samples list, click Create Analysis.
21. Specify your rarefaction depth (you can leave it blank for no rarefying), and select any/all of the analysis types. Click Start Processing.
22. All analyses are listed under Analysis > See Previous Analyses.

REFERENCES

1. Agler, M., Spirito, C., Usack, J., Werner, J. and Angenent, L. (2014) 'Development of a highly specific and productive process for *n*-caproic acid production: applying lessons from methanogenic microbiomes', *Water Science & Technology,* 69(1), pp. 62-68.
2. Agler, M. T., Spirito, C. M., Usack, J. G., Werner, J. J. and Angenent, L. T. (2012a) 'Chain elongation with reactor microbiomes: upgrading dilute ethanol to medium-chain carboxylates', *Energy & Environmental Science,* 5(8), pp. 8189-8192.
3. Agler, M. T., Werner, J. J., Iten, L. B., Dekker, A., Cotta, M. A., Dien, B. S. and Angenent, L. T. (2012b) 'Shaping reactor microbiomes to produce the fuel precursor *n*-butyrate from pretreated cellulosic hydrolysates', *Environmental science & technology,* 46(18), pp. 10229-10238.
4. Agler, M. T., Wrenn, B. A., Zinder, S. H. and Angenent, L. T. (2011) 'Waste to bioproduct conversion with undefined mixed cultures: the carboxylate platform', *Trends in biotechnology,* 29(2), pp. 70-78.
5. Angenent, L. T., Karim, K., Al-Dahhan, M. H., Wrenn, B. A. and Domíguez-Espinosa, R. (2004) 'Production of bioenergy and biochemicals from industrial and agricultural wastewater', *TRENDS in Biotechnology,* 22(9), pp. 477-485.
6. Angenent, L. T. and Kleerebezem, R. (2011) 'Bioproducts from undefined mixed cultures: electron pushing', *Microbial Biotechnology,* 4(2), pp. 109-137.
7. Arslan, D., Steinbusch, K., Diels, L., De Wever, H., Hamelers, H. and Buisman, C. (2013) 'Selective carboxylate production by controlling hydrogen, carbon dioxide and substrate concentrations in mixed culture fermentation', *Bioresource technology,* 136, pp. 452-460.
8. Bhat, J. and Barker, H. (1947) '*Clostridium lacto-acetophilum* nov. spec. and the role of acetic acid in the butyric acid fermentation of lactate', *Journal of bacteriology,* 54(3), pp. 381.
9. Bond, J. Q., Upadhye, A. A., Olcay, H., Tompsett, G. A., Jae, J., Xing, R., Alonso, D. M., Wang, D., Zhang, T. and Kumar, R. (2014) 'Production of renewable jet fuel range alkanes and commodity chemicals from integrated catalytic processing of biomass', *Energy & Environmental Science,* 7(4), pp. 1500-1523.
10. Bornstein, B. and Barker, H. (1948) 'The energy metabolism of *Clostridium kluyveri* and the synthesis of fatty acids', *J. biol. Chem,* 172(659.1948).
11. Buffiere, P., Loisel, D., Bernet, N. and Delgenes, J. (2006) 'Towards new indicators for the prediction of solid waste anaerobic digestion properties', *Water Science & Technology,* 53(8), pp. 233-241.

12. Caporaso, J. G., Kuczynski, J., Stombaugh, J., Bittinger, K., Bushman, F. D., Costello, E. K., Fierer, N., Pena, A. G., Goodrich, J. K., Gordon, J. I., Huttley, G. A., Kelley, S. T., Knights, D., Koenig, J. E., Ley, R. E., Lozupone, C. A., McDonald, D., Muegge, B. D., Pirrung, M., Reeder, J., Sevinsky, J. R., Turnbaugh, P. J., Walters, W. A., Widmann, J., Yatsunenko, T., Zaneveld, J. and Knight, R. (2010) 'QIIME allows analysis of high-throughput community sequencing data', *Nat Meth,* 7(5), pp. 335-336.

13. Chen, H. and Jin, S. (2006) 'Effect of ethanol and yeast on cellulase activity and hydrolysis of crystalline cellulose', *Enzyme and Microbial Technology,* 39(7), pp. 1430-1432.

14. Choi, K., Jeon, B. S., Kim, B.-C., Oh, M.-K., Um, Y. and Sang, B.-I. (2013) 'In situ biphasic extractive fermentation for hexanoic acid production from sucrose by *Megasphaera elsdenii* NCIMB 702410', *Applied biochemistry and biotechnology,* 171(5), pp. 1094-1107.

15. Chu, S. and Majumdar, A. (2012) 'Opportunities and challenges for a sustainable energy future', *nature,* 488(7411), pp. 294-303.

16. Counotte, G. H. and Prins, R. (1981) 'Regulation of lactate metabolism in the rumen', *Veterinary research communications,* 5(1), pp. 101-115.

17. Desbois, A. P. (2012) 'Potential applications of antimicrobial fatty acids in medicine, agriculture and other industries', *Recent patents on anti-infective drug discovery,* 7(2), pp. 111-122.

18. Diez-Gonzalez, F., Russell, J. B. and Hunter, J. B. (1995) 'The role of an NAD-independent lactate dehydrogenase and acetate in the utilization of lactate by *Clostridium acetobutylicum* strain P262', *Archives of microbiology,* 164(1), pp. 36-42.

19. Ding, H.-B., Tan, G.-Y. A. and Wang, J.-Y. (2010) 'Caproate formation in mixed-culture fermentative hydrogen production', *Bioresource technology,* 101(24), pp. 9550-9559.

20. Elsden, S. and Lewis, D. (1953) 'The production of fatty acids by a gram-negative coccus', *Biochemical Journal,* 55(1), pp. 183.

21. Elsden, S., Volcani, B., Gilchrist, F. and Lewis, D. (1956) 'Properties of a fatty acid forming organism isolated from the rumen of sheep', *Journal of bacteriology,* 72(5), pp. 681.

22. Ge, S., Usack, J., Spirito, C. M. and Angenent, L. T. (2015) 'Long-term *n*-caproic acid production from yeast-fermentation beer in an anaerobic bioreactor with continuous product extraction', *Environmental science & technology,* 49(13), pp. 8012-8021.

23. Gómez, X., Cuetos, M., Prieto, J. and Morán, A. (2009) 'Bio-hydrogen production from waste fermentation: Mixing and static conditions', *Renewable Energy,* 34(4), pp. 970-975.

24. Grootscholten, T., dal Borgo, F. K., Hamelers, H. and Buisman, C. (2013a) 'Promoting chain elongation in mixed culture acidification reactors by addition of ethanol', *Biomass and Bioenergy,* 48, pp. 10-16.

25. Grootscholten, T., Steinbusch, K., Hamelers, H. and Buisman, C. (2013b) 'Chain elongation of acetate and ethanol in an upflow anaerobic filter for high rate MCFA production', *Bioresource technology,* 135, pp. 440-445.

26. Grootscholten, T., Steinbusch, K., Hamelers, H. and Buisman, C. (2013c) 'High rate heptanoate production from propionate and ethanol using chain elongation', *Bioresource technology,* 136, pp. 715-718.

27. Grootscholten, T., Steinbusch, K., Hamelers, H. and Buisman, C. (2013d) 'Improving medium chain fatty acid productivity using chain elongation by reducing the hydraulic retention time in an upflow anaerobic filter', *Bioresource technology,* 136, pp. 735-738.

28. Guest, J. S., Skerlos, S. J., Barnard, J. L., Beck, M. B., Daigger, G. T., Hilger, H., Jackson, S. J., Karvazy, K., Kelly, L. and Macpherson, L. (2009) 'A new planning and design paradigm to achieve sustainable resource recovery from wastewater 1', *Environmental Science & Technology,* 43(16), pp. 6126-6130.

29. Gutierrez, J., Davis, R., Lindahl, I. and Warwick, E. (1959) 'Bacterial changes in the rumen during the onset of feed-lot bloat of cattle and characteristics of *Peptostreptococcus elsdenii* n. sp.', *Applied microbiology,* 7(1), pp. 16-22.

30. Harvey, B. G. and Meylemans, H. A. (2014) '1-Hexene: a renewable C_6 platform for full-performance jet and diesel fuels', *Green Chemistry,* 16(2), pp. 770-776.

31. Hetzel, M., Brock, M., Selmer, T., Pierik, A. J., Golding, B. T. and Buckel, W. (2003) 'Acryloyl-CoA reductase from *Clostridium propionicum*', *European Journal of Biochemistry,* 270(5), pp. 902-910.

32. Hill, J., Nelson, E., Tilman, D., Polasky, S. and Tiffany, D. (2006) 'Environmental, economic, and energetic costs and benefits of biodiesel and ethanol biofuels', *Proceedings of the National Academy of Sciences,* 103(30), pp. 11206-11210.

33. Hino, T. and Kuroda, S. (1993) 'Presence of lactate dehydrogenase and lactate racemase in *Megasphaera elsdenii* grown on glucose or lactate', *Applied and environmental microbiology,* 59(1), pp. 255-259.

34. Hino, T., Shimada, K. and Maruyama, T. (1994) 'Substrate preference in a strain of *Megasphaera elsdenii*, a ruminal bacterium, and its implications in propionate production and growth competition', *Applied and environmental microbiology,* 60(6), pp. 1827-1831.

35. Hospodsky, D., Yamamoto, N. and Peccia, J. (2010) 'Accuracy, Precision, and Method Detection Limits of Quantitative PCR for Airborne Bacteria and Fungi', *Applied and Environmental Microbiology,* 76(21), pp. 7004-7012.

36. Jeon, B. S., Moon, C., Kim, B.-C., Kim, H., Um, Y. and Sang, B.-I. (2013) 'In situ extractive fermentation for the production of hexanoic acid from galactitol by *Clostridium* sp. BS-1', *Enzyme and microbial technology,* 53(3), pp. 143-151.

37. Jung, K.-W., Kim, D.-H. and Shin, H.-S. (2011) 'A simple method to reduce the start-up period in a H_2-producing UASB reactor', *international journal of hydrogen energy,* 36(2), pp. 1466-1473.

38. Kenealy, W., Cao, Y. and Weimer, P. (1995) 'Production of caproic acid by cocultures of ruminal cellulolytic bacteria and *Clostridium kluyveri* grown on cellulose and ethanol', *Applied microbiology and biotechnology,* 44(3-4), pp. 507-513.

39. Kenealy, W. R. and Waselefsky, D. M. (1985) 'Studies on the substrate range of *Clostridium kluyveri*; the use of propanol and succinate', *Archives of Microbiology,* 141(3), pp. 187-194.

40. Kleerebezem, R. and van Loosdrecht, M. C. (2007) 'Mixed culture biotechnology for bioenergy production', *Current opinion in biotechnology,* 18(3), pp. 207-212.

41. Köpke, M., Mihalcea, C., Bromley, J. C. and Simpson, S. D. (2011) 'Fermentative production of ethanol from carbon monoxide', *Current Opinion in Biotechnology,* 22(3), pp. 320-325.

42. Ladd, J. (1959) 'The fermentation of lactic acid by a gram-negative coccus', *Biochemical Journal,* 71(1), pp. 16.

43. Ladd, J. and Walker, D. (1959) 'The fermentation of lactate and acrylate by the rumen micro-organism LC', *Biochemical Journal,* 71(2), pp. 364.

44. Laird, D. A., Brown, R. C., Amonette, J. E. and Lehmann, J. (2009) 'Review of the pyrolysis platform for coproducing bio-oil and biochar', *Biofuels, Bioproducts and Biorefining,* 3(5), pp. 547-562.

45. Lettinga, G. (1995) 'Anaerobic digestion and wastewater treatment systems', *Antonie van leeuwenhoek,* 67(1), pp. 3-28.

46. Levy, P., Sanderson, J., Kispert, R. and Wise, D. (1981) 'Biorefining of biomass to liquid fuels and organic chemicals', *Enzyme and Microbial Technology,* 3(3), pp. 207-215.

47. Marounek, M., Fliegrova, K. and Bartos, S. (1989) 'Metabolism and some characteristics of ruminal strains of *Megasphaera elsdenii'*, *Applied and environmental microbiology,* 55(6), pp. 1570-1573.

48. McDonald, D., Price, M. N., Goodrich, J., Nawrocki, E. P., DeSantis, T. Z., Probst, A., Andersen, G. L., Knight, R. and Hugenholtz, P. (2012) 'An improved Greengenes taxonomy with explicit ranks for ecological and evolutionary analyses of bacteria and archaea', *ISME J,* 6(3), pp. 610-618.

49. Prabhu, R., Altman, E. and Eiteman, M. A. (2012) 'Lactate and Acrylate Metabolism by *Megasphaera elsdenii* under Batch and Steady-State Conditions', *Applied and Environmental Microbiology,* 78(24), pp. 8564-8570.

50. Raunkjær, K., Hvitved-Jacobsen, T. and Nielsen, P. H. (1994) 'Measurement of pools of protein, carbohydrate and lipid in domestic wastewater', *Water Research,* 28(2), pp. 251-262.

51. Regueiro, L., Spirito, C. M., Usack, J. G., Hospodsky, D., Werner, J. J. and Angenent, L. T. (2015) 'Comparing the inhibitory thresholds of dairy manure co-digesters after prolonged acclimation periods: Part 2–correlations between microbiomes and environment', *Water research,* (In press).

52. Richter, H., Martin, M. E. and Angenent, L. T. (2013) 'A two-stage continuous fermentation system for conversion of syngas into ethanol', *Energies,* 6(8), pp. 3987-4000.

53. Roddick, F. A. and Britz, M. L. (1997) 'Production of Hexanoic Acid by Free and Immobilised Cells of *Megasphaera elsdenii*: Influence of in-situ Product Removal Using Ion Exchange Resin', *Journal of Chemical Technology and Biotechnology,* 69(3), pp. 383-391.

54. Shannon, C. E. (1948) 'A Mathematical Theory of Communication', *Bell System Technical Journal,* 27(3), pp. 379-423.

55. Skrivanova, E., Marounek, M., Benda, V. and Brezina, P. (2006) 'Susceptibility of *Escherichia coli*, *Salmonella* sp. and *Clostridium perfringens* to organic acids and monolaurin', *VETERINARNI MEDICINA-PRAHA-,* 51(3), pp. 81.

56. Spirito, C. M., Richter, H., Rabaey, K., Stams, A. J. and Angenent, L. T. (2014) 'Chain elongation in anaerobic reactor microbiomes to recover resources from waste', *Current opinion in biotechnology,* 27, pp. 115-122.

57. Steinbusch, K. J., Hamelers, H. V., Plugge, C. M. and Buisman, C. J. (2011) 'Biological formation of caproate and caprylate from acetate: fuel and chemical production from low grade biomass', *Energy & Environmental Science,* 4(1), pp. 216-224.

58. Sträuber, H., Lucas, R. and Kleinsteuber, S. (2015) 'Metabolic and Microbial Community Dynamics during the Anaerobic Digestion of Maize Silage in a Two-Phase Process', *Appl Microbiol Biotechnol.,* (In Press).

59. Sträuber, H., Schröder, M. and Kleinsteuber, S. (2012) 'Metabolic and microbial community dynamics during the hydrolytic and acidogenic fermentation in a leach-bed process', *Energy, Sustainability and Society,* 2(1), pp. 1-10.

60. Tao, Y., Li, J., Rui, J., Xu, Z., Zhou, Y., Hu, X., Wang, X., Liu, M., Li, D. and Li, X. (2014) 'Prokaryotic communities in pit mud from different-aged cellars used for the production of Chinese strong-flavored liquor', *Applied and environmental microbiology,* 80(7), pp. 2254-2260.

61. Team, R. C. 2014. R: a language and environment for statistical computing. Vienna, Austria: R Foundation for Statistical Computing; 2012.

62. Temudo, M. F., Poldermans, R., Kleerebezem, R. and van Loosdrecht, M. (2008) 'Glycerol fermentation by (open) mixed cultures: a chemostat study', *Biotechnology and bioengineering,* 100(6), pp. 1088-1098.

63. Thauer, R. K., Jungermann, K. and Decker, K. (1977) 'Energy conservation in chemotrophic anaerobic bacteria', *Bacteriological reviews,* 41(1), pp. 100.

64. Tuck, C. O., Pérez, E., Horváth, I. T., Sheldon, R. A. and Poliakoff, M. (2012) 'Valorization of biomass: deriving more value from waste', *Science,* 337(6095), pp. 695-699.

65. Usack, J. and Angenent, L. (2015) 'Comparing the inhibitory thresholds of dairy manure co-digesters after prolonged acclimation periods: Part 1–Performance and operating limits', *Water research,* (In press).

66. Van Eerten-Jansen, M. C., Ter Heijne, A., Grootscholten, T. I., Steinbusch, K. J., Sleutels, T. H., Hamelers, H. V. and Buisman, C. J. (2013) 'Bioelectrochemical production of caproate and caprylate from acetate by mixed cultures', *ACS sustainable chemistry & engineering,* 1(5), pp. 513-518.

67. Vasudevan, D., Richter, H. and Angenent, L. T. (2014) 'Upgrading dilute ethanol from syngas fermentation to *n*-caproate with reactor microbiomes', *Bioresource technology,* 151, pp. 378-382.

68. Vennestrøm, P., Osmundsen, C. M., Christensen, C. and Taarning, E. (2011) 'Beyond petrochemicals: the renewable chemicals industry', *Angewandte Chemie International Edition,* 50(45), pp. 10502-10509.

69. Wang, Y., Mu, Y. and Yu, H.-Q. (2007) 'Comparative performance of two upflow anaerobic biohydrogen-producing reactors seeded with different sludges', *International journal of hydrogen energy,* 32(8), pp. 1086-1094.

70. Warnes, G. R., Bolker, B., Bonebakker, L., Gentleman, R., Huber, W., Liaw, A., Lumley, T., Maechler, M., Magnusson, A., Moeller, S., Schwartz, M. and Venables, B. (2015) 'gplots: Various R programming tools for plotting data', *R package version,* 2(17).

71. Wallace, R.J., McKain, N., McEwan, N.R., Miyagawa, E., Chaudhary, L.C., King, T.P., Walker, N.D., Apajalahti, J.H.A. and Newbold, C.J. (2003) '*Eubacterium pyruvativorans* sp. nov., a novel non-saccharolytic anaerobe from the rumen that ferments pyruvate and amino acids, forms caproate and utilizes acetate and propionate', *International journal of systematic and evolutionary microbiology*, *53*(4), pp.965-970.

72. Wallace, R.J., Chaudhary, L.C., Miyagawa, E., McKain, N. and Walker, N.D. (2004) 'Metabolic properties of *Eubacterium pyruvativorans*, a ruminal 'hyper-ammonia-producing'anaerobe with metabolic properties analogous to those of *Clostridium kluyveri'*, *Microbiology*, *150*(9), pp.2921-2930.

73. Weimer, P. and Moen, G. (2013) 'Quantitative analysis of growth and volatile fatty acid production by the anaerobic ruminal bacterium *Megasphaera elsdenii* T81', *Applied microbiology and biotechnology,* 97(9), pp. 4075-4081.

74. Weimer, P. J. and Stevenson, D. M. (2012) 'Isolation, characterization, and quantification of *Clostridium kluyveri* from the bovine rumen', *Applied microbiology and biotechnology,* 94(2), pp. 461-466.

75. Xu, J., Guzman, J. J., Andersen, S. J., Rabaey, K. and Angenent, L. T. (2015) 'In-line and selective phase separation of medium-chain carboxylic acids using membrane electrolysis', *Chemical Communications,* 51(31), pp. 6847-6850.

76. Zhang, F., Ding, J., Zhang, Y., Chen, M., Ding, Z.-W., van Loosdrecht, M. C. and Zeng, R. J. (2013) 'Fatty acids production from hydrogen and carbon dioxide by mixed culture in the membrane biofilm reactor', *Water research,* 47(16), pp. 6122-6129.

77. Zhang, W., Werner, J. J., Agler, M. T. and Angenent, L. T. (2014) 'Substrate type drives variation in reactor microbiomes of anaerobic digesters', *Bioresource technology,* 151, pp. 397-401.

78. Zhang, Z.-P., Tay, J.-H., Show, K.-Y., Yan, R., Liang, D. T., Lee, D.-J. and Jiang, W.-J. (2007) 'Biohydrogen production in a granular activated carbon anaerobic fluidized bed reactor', *International Journal of Hydrogen Energy,* 32(2), pp. 185-191.

79. Zhao, Q.-B., Mu, Y., Wang, Y., Liu, X.-W., Dong, F. and Yu, H.-Q. (2008) 'Response of a biohydrogen-producing reactor to the substrate shift from sucrose to lactose', *Bioresource technology,* 99(17), pp. 8344-8347.

80. Zhu, X., Tao, Y., Liang, C., Li, X., Wei, N., Zhang, W., Zhou, Y., Yang, Y. and Bo, T. (2015) 'The synthesis of *n*-caproate from lactate: a new efficient process for medium-chain carboxylates production', *Scientific reports,* 5.